NASA CONTRACTOR REPORT

NASA CR-920

NASA CR-920

COMBUSTION INSTABILITY PREDICTION USING A NONLINEAR BIPROPELLANT VAPORIZATION MODEL

by R. J. Hoffman, R. O. Wright, and B. P. Breen

Prepared by
DYNAMIC SCIENCE
Monrovia, Calif.
for Lewis Research Center

NATIONAL AERONAUTICS AND SPACE ADMINISTRATION • WASHINGTON, D. C. • JANUARY 1968

NASA CR-920

COMBUSTION INSTABILITY PREDICTION USING A NONLINEAR BIPROPELLANT VAPORIZATION MODEL

By R. J. Hoffman, R. O. Wright, and B. P. Breen

Prepared under Contract No. NAS 7-442 by
DYNAMIC SCIENCE DIVISION
Marshall Industries
Monrovia, Calif.

for Lewis Research Center

NATIONAL AERONAUTICS AND SPACE ADMINISTRATION

For sale by the Clearinghouse for Federal Scientific and Technical Information
Springfield, Virginia 22151 – CFSTI price $3.00

FOREWORD

This report documents the work performed at the Dynamic Science Division of Marshall Industries under NASA Contract NAS 7-442 relating to theoretical prediction of liquid rocket combustion instability. All phases of this contract were monitored by Charles E. Feiler and Richard J. Priem, both of the Chemistry and Energy Conversion Division, NASA Lewis Research Center.

SUMMARY

An extension of the Priem-Guentert nonlinear annular combustion instability model for liquid rocket engines is presented. Additions to the model include: droplet drag effects, propellant spray distributions, and independent heat and mass addition due to a bipropellant system. Results of parametric computer studies are presented which show the effect of these additions to the model on stability limits.

The addition of droplet drag to the transport equations produces a new dimensionless term, β, the drag parameter. Computer results show that droplet drag can produce large attenuations in sensitivity to combustion instability.

Drop sprays are treated by defining a spray distribution function for both the fuel and oxidizer spray entering an annulus. Results of a parametric study of the influence of mean drop size and of standard deviation are presented for the spray distribution model.

In a bipropellant system the amount of heat and mass added to the gas phase, as a result of a disturbance wave, are not proportional. The instability equations were modified to independently calculate mass and heat addition for each propellant and these modifications were included in the computer solution. Generally, the independent addition of mass to the flow produced trends similar to the simultaneous addition of heat and mass. For comparison, a complete engine stability map was generated using both the bipropellant model and the monopropellant model. Significant differences are apparent in the predicted sensitivity to instability.

As a result of these extensions to the instability model, additional dimensionless parameters are required to characterize an annulus. It is therefore difficult to show the interrelationship of these parameters through the use of stability limit plots. A particular combustor, however, may be analyzed for sensitivity towards instability with the computer solution developed under this contract.

CONTENTS

INTRODUCTION

Prediction of combustion instability in liquid rocket engines suffers from the extreme complexity of the combustion and gasdynamic processes involved. A realistic determination of an engine's sensitivity to becoming unstable, as a result of a random disturbance, requires a detailed knowledge of the following processes:

(1) The atomization process

(2) The two-phase flow process during steady-state engine operation including: droplet heatup, droplet drag, droplet shattering and droplet vaporization

(3) The kinetic processes including: combustion of the vaporized gases from the droplet spray, and nonequilibrium gasdynamics of the burned gases.

(4) The unsteady response of each of the above processes to a random gasdynamic disturbance or atomization nonuniformity

(5) The effect of the unsteady responses of each process on all other processes, both steady and unsteady.

In addition, the geometry of a real rocket engine combustor and the nature of the random disturbance wave make the problem three dimensional.

Various simplified theoretical models have been developed, as discussed in Reference 1. Basically, each model assumes that one of the above processes controls the combustion response to a disturbance wave and does not interact with other processes. In this way, the problem is reduced to examining the response of a single process independently as an instability wave driving force. The arguments against decoupling the combustion - gasdynamic processes in this way are valid, since it has been shown that many of the processes do strongly interact; however, more rigorous models will have to evolve from the simpler ones due to the complexity of the problem.

This report extends a nonlinear liquid rocket combustion instability model originally developed by Priem (Ref. 1). The basic model assumes that droplet vaporization is the controlling process and that the response of a vaporizing propellant drop due to a gasdynamic disturbance wave can be related to a steady-state droplet vaporization correlation. The additional phenomenon included in this study are:

(1) Momentum and energy transfer due to droplet drag

(2) Propellant droplet spray distributions

(3) Independent heat and mass addition consistent with a bipropellant system.

Derivations of the equations describing the extended instability model are presented in Appendices, A, B, and C. A knowledge of Priem's nonlinear combustion instability model will be assumed in this report, and therefore a complete derivation of the model will not be given.

Based on the extended model, stability limits have been generated as a function of similarity parameters that appear when the instability equations are nondimensionalized. Numerical integrations of the transport equations were accomplished with a computer program described in a previous report, (Ref. 2). Modifications to the computer program needed for the current extended model are included in this report as Appendix D.

SYMBOLS AND UNITS

A_C	cross-sectional area of combustor, sq in.
A_p	initial amplitude of pressure disturbance, dimensionless
A_t	nozzle-throat area of combustor, sq in.
$\mathcal{A}$	combustor contraction ratio, A_C/A_t, dimensionless
a	speed of sound in gases, in./sec
C_d	concentration of liquid drops, drops/cu in.
C_D	coefficient of drag, dimensionless
c_p	specific heat at constant pressure, Btu/(lb)(°F)
c_v	specific heat at constant volume, Btu/(lb)(°F)
c*	characteristic exhaust velocity, ft/sec
D	molecular diffusion coefficient, sq in./sec
$\mathcal{D}$	drag parameter = $3/8\ C_D \mathcal{F}_p r_{an}/r_d$, dimensionless
$f(\gamma)$	function of gamma, $\sqrt{\left(\frac{2}{\gamma+1}\right)^{\frac{\gamma+1}{\gamma-1}}}$
F_D	drag force exerted by the gas on the droplets, lb_f/in^3.

$\mathfrak{F}_p$	ρ_ℓ/ρ_d, dimensionless
g	acceleration due to gravity, 386.09 in.sec^2
J	mechanical equivalent of heat, 9339.1 in.-lb/Btu
$\mathcal{J}$	viscous-dissipation parameter, $\mu_o c^*/r_{an}\bar{P}_c g$, dimensionless
$\mathcal{L}$	burning-rate parameter, $r_{an}m/\mathcal{A}$,dimensionless
M	molecular weight of gas, lb mass/lb mole
M_ℓ	molecular weight of liquid, lb mass/lb mole
m	burning rate of propellant fraction/in.
$\mathcal{O}/\mathfrak{F}$	vapor phase oxidant-fuel ratio
P	pressure, lb/sq in.
P_v	vapor pressure of liquid, lb/sq in.
q	rate of heat transferred by conduction, Btu/(sec)(sq in.)
R	universal gas constant, 19,510 (in.)(lb force)/($^\circ$R)(lb mole)
Re_d	$2r_d\rho_o a_o/\mu_o$, dimensionless
r	radial distance, in.
r_m	mass-mean drop radius, in.
r_n	number mean drop radius, in.
Sc	Schmidt number, $\mu_o/D\rho_o$, dimensionless
T	gas temperature, $^\circ$R
t	time, sec
U	internal energy, Btu/lb
v	gas velocity, in./sec
Δv	velocity difference between gases and drops in axial direction in./sec
v_ℓ	liquid velocity, in./sec
$\dot{W}$	propellant flow rate, lb_m/sec
α	correction factor for mass transfer, $(P/P_v)\ln[P/(P-P_v)]$, dimensionless
γ	specific-heat ratio c_p/c_v, dimensionless
∇	operator, $(in.)^{-1}$
λ	thermal conductivity of gases, Btu/(in.)(sec)($^\circ$F)
μ	gas viscosity, lb/(in.)(sec)

ρ gas density, $lb_m/cu\ in.$

Φ local instantaneous value of $\sigma/\mathfrak{F}$

ρ_d drop density, $\left(\frac{lb_m}{cu\ in.\ of\ drop\ vol.}\right)$

ρ_ℓ liquid density, (lb_m of liquid/cu in. of two phase mixture)

τ stress tensor $lb_f/(in.)(sec^2)$

ω local instantaneous vaporization rate for various combustion models, $lb_m/(sec)(cu\ in.)$

σ_G geometric standard deviation, dimensionless

Subscripts:

an annulus

c combustion chamber

d drop

f fuel

max maximum

min minimum

o steady state

ox oxidizer

s stoichiometric

t total

Superscripts:

' reduced parameter, defined in Equation (A4)

- average

THEORY

Basic Nonlinear Combustion Instability Model

Transport equations describing unsteady combustion in a liquid rocket motor were derived in Reference 1, and are similar to those given in Appendix A of this report, excluding the droplet drag terms. Although the equations have been derived in general form, numerical solution of the model has been restricted to the one-dimensional case of an annular combustor. The length and width of the annulus are assumed to be small thereby restricting the instability wave to travel in the tangential direction around the annulus. As was the case in Reference 1, it was desired that the numerical solution of this one-dimensional model would indicate the importance of the various engine parameters and similarity groups on stability rather than provide specific quantitative information.

Nondimensionalizing of the unsteady transport equations leads to groups of parameters containing only steady-state terms. These groups, after some further simplification, can be used to characterize the stability of an annular ring within a combustor. In this way, an engine may be investigated for its sensitivity towards tangential combustion instability by determining the steady-state parameters that characterize a series of annuli, and then solving the instability equations with these parameters as known quantities for an assumed random disturbance amplitude. The disturbance form used throughout this study is $P'=1+A_p \sin \theta'$

Basic to the model is the assumption of instantaneous burning upon vaporization of the propellant. It is assumed that the rate of vaporization of a liquid drop varies with the amplitude of the disturbance wave and that the vaporization rate can be related to the gasdynamics of the flow through the Reynolds number of the drop. A steady-state vaporization correlation, derived in Reference 3, is used to determine the vaporization rate under transient conditions for this model. The implication is that the droplet surface temperature responds instantly to the fluctuation in external gas flow but a negligible amount of heat is used to raise the temperature of the drop, and that therefore a steady-state correlation is valid. The propellant vaporization rate is given by:

$$\omega = \frac{C_d D M_\ell S_c \alpha}{2RT r_d} P_V \left[2 + .6 S_c^{1/3} \left(\frac{2 r_d |\vec{v} - \vec{v}_\ell| \rho}{\mu} \right)^{1/2} \right] \qquad (1)$$

If the vapor pressure does not vary with time, the vaporization response can be written as

$$\omega' = \frac{\omega}{\omega_o} = \frac{2 + .6\, S_c^{1/3} \left(2 r_d \left|\vec{v} - \vec{v}_\ell\right| \rho/\mu\right)^{1/2}}{2 + .6\, S_c^{1/3} \left(2 r_d \left|\vec{v}_o - \vec{v}_{\ell,o}\right| \rho_o/\mu_o\right)^{1/2}} \tag{2}$$

Priem, Reference 1, simplifies this expression by assuming large velocity differences between the droplets and the combustion gases, obtaining

$$\omega' = \left(\frac{\rho}{\rho_o}\right)^{1/2} \left(\frac{\left|\vec{v} - \vec{v}_\ell\right|}{\left|\vec{v}_o - \vec{v}_\ell\right|}\right)^{1/2} \tag{3a}$$

or, for the one-dimensional annular model, allowing only constant axial liquid drop velocities, the vaporization response reduces to

$$\omega' = (\rho')^{1/2} \left[1 + \left(\frac{v'_\theta}{\Delta v'}\right)^2\right]^{1/4} \tag{3b}$$

In the current model the velocity differences are not assumed large, and the full expression for ω' is used. A direct substitution of

$$Re_d = \frac{2 r_d \rho_o a_o}{\mu_o} \tag{4}$$

in equation (2) yields

$$\omega' = \frac{2 + .6\, S_c^{1/3} \rho'^{1/2} \left|\vec{v}' - \vec{v}'_\ell\right|^{1/2} Re_d^{1/2}}{2 + .6\, S_c^{1/3} \left|\vec{v}'_o - \vec{v}'_{\ell,o}\right|^{1/2} Re_d^{1/2}} \tag{5a}$$

or, for the one-dimensional annular model,

$$\omega' = \frac{2 + .6\, S_c^{1/3} \rho'^{1/2} \left|(v'_\theta)^2 + (\Delta v')^2\right|^{1/4} Re_d^{1/2}}{2 + .6\, S_c^{1/3} (\Delta v')^{1/2} Re_d^{1/2}} \tag{5b}$$

Figure 1, compares the calculated vaporization response (equivalent to the burning rate response for this model) for equation (3b) and (5b) over a range of realistic values of Re_d. For comparison purposes, the typical values of $S_c = 1$, $v'_\theta = 0.04$, and $\rho' = 1.5$ were assumed. All numerical results in this report are based on the vaporization response of equation (5b).

Droplet Drag Model

A derivation of the nondimensional transport equations for a combustion instability model containing the effects of droplet drag is given in Appendix A. It is assumed that the liquid phase consists of a uniform spray of constant diameter droplets with a velocity in the axial direction only. The concentration of drops does not vary within the annulus. As the burning propellant drops pass through the annulus, they are acted upon by a tangential pressure and/or velocity wave which may occur at random in a real engine. The vector velocity difference between the drop velocity and the gas velocity (including axial and tangential components) produces momentum exchange and kinetic energy dissipation. The effect of this interaction is to produce an attenuating effect on the disturbance wave.

The nondimensional instability equations derived in Appendix A are

Continuity. -

$$\frac{\partial \rho'}{\partial t'} = -\rho'\left(\frac{\partial v'_\theta}{\partial \theta'} + \frac{\partial v'_z}{\partial z'}\right) - v'_\theta \frac{\partial \rho'}{\partial \theta'} - v'_z \frac{\partial \rho'}{\partial z'} + \omega' \mathcal{L} f(\gamma) \tag{6}$$

Momentum (θ-direction). -

$$\rho' \frac{\partial v'_\theta}{\partial t'} = -\rho' v'_\theta \frac{\partial v'_\theta}{\partial \theta'} - \frac{1}{\gamma} \frac{\partial P'}{\partial \theta'} + \mathcal{J} f(\gamma) \frac{4}{3} \frac{\partial^2 v'_\theta}{\partial \theta'^2} - v'_\theta \omega' \mathcal{L} f(\gamma) - \mathcal{B} \rho' \frac{|v'_\theta| (v'_\theta)}{r'_d} \tag{7a}$$

Momentum (z-direction). -

$$0 = -\rho' v'_z \frac{\partial v'_z}{\partial z'} - \left|\frac{1}{\gamma}\right| \frac{\partial p'}{\partial z'} - \mathcal{L} f(\gamma) (v'_z - v'_{\ell,z}) \omega' - \mathcal{B} \rho' \frac{|v'_z - v'_{\ell,z}| (v'_z - v'_{\ell,z})}{r'_d} \tag{7b}$$

Energy. -

$$\rho' \frac{\partial T'}{\partial t'} = -\rho'\left(v'_\theta \frac{\partial T'}{\partial \theta'} + v'_z \frac{\partial T'}{\partial z'}\right) + \mathcal{J} f(\gamma) \frac{\partial^2 T'}{\partial \theta'^2} - |\gamma - 1| P'\left(\frac{\partial v'_\theta}{\partial \theta'} + \frac{\partial v'_z}{\partial z'}\right)$$

$$+ \frac{4}{3} |\gamma(\gamma-1)| \mathcal{J} \left[\left(\frac{\partial v'_\theta}{\partial \theta'}\right)^2 + \left(\frac{\partial v'_z}{\partial z'}\right)^2 - \frac{\partial v'_\theta}{\partial \theta'} \frac{\partial v'_z}{\partial z'}\right] f(\gamma)$$

$$+ \mathcal{L} f(\gamma) \omega' \left\{\gamma - T' + \frac{(\gamma-1)\gamma}{2}\left[v'^2_\theta + (v'_z - v'_{\ell,z})^2\right]\right\}$$

$$+ |\gamma(\gamma-1)| \mathcal{B} \rho' \left[v'^2_\theta + (v'_z - v'_{\ell,z})^2\right]^{3/2} \tag{8}$$

Axial derivatives are determined by integrating the nondimensional equations (6), (7), and (8) in the annular direction (θ direction) and assuming that the total mass, momentum, and energy within the annulus remains constant. The integrated equations are given in Appendix A as equations (A17), (A18), and (A19)

Appearing in the nondimensional transport equations are the following similarity parameters that characterize the stability of an annulus

$$
\begin{aligned}
Re_d &= \frac{2r_d \rho_o a_o}{\mu_o} = && \text{Renolds number of the drop based on speed of sound} \\
\Delta V' &= \frac{|\vec{v} - \vec{v}_\ell|}{a_o} = && \text{Nondimensional relative axial velocity} \\
\mathcal{L} &= \frac{r_{an}\, m}{\mathcal{A}} = && \text{Burning rate parameter} \\
\mathcal{D} &= \frac{3\, C_D\, \mathcal{F}_p\, r_{an}}{8\, r_d} = && \text{Drag number}
\end{aligned}
\qquad (9)
$$

The first three are familiar in that they appear in Priem's original model. The last term, $\mathcal{D}$, the drag parameter, appears as a result of our current modifications to include droplet drag. In addition, the viscous dissipation parameter

$$\mathcal{J} = \frac{\mu c^*}{r_{an}\, P_c\, g}$$

also appears in the nondimensional equations. An order of magnitude analysis, and previous numerical solutions have indicated a negligible effect on stability over a wide range of realistic values of $\mathcal{J}$ for a liquid rocket combustor. Therefore, $\mathcal{J}$, has been excluded from the parametric variation to determine stability limits. The effect of $\mathcal{J}$ on the wave shape is discussed in the Results and Discussion section of this report

Drop Spray Distribution

The amount of mass or heat added to the gas phase as a result of the vaporization response of the propellant spray to the disturbance wave is the driving force to sustain a wave. When heat or mass is added in phase with the wave, the effect may be to amplify the wave (Rayleigh's Criteria) depending on the magnitude of the addition and other damping factors which may be present.

Variations in propellant drop size produced by the atomization process require that a distribution of drop sizes be considered in the instability analysis, rather than the assumption of a single drop size as was done in the original model. The need to consider a distribution of sizes can be inferred from Figure 1, which shows the variation of vaporization response as a function of drop size (Re_d is directly proportional to drop size). As part of a program to improve upon the assumptions of the original instability model, a drop spray distribution has been included in the current formulation.

Appendix B discusses the model modification in detail. The resulting expression for the vaporization response (burning response, except for the bipropellant model) is

$$\omega' = \frac{\int_0^\infty \frac{1}{r}\left[2+0.6\,S_c^{1/3}(\rho')^{1/2}\left|(v'_\theta)^2+\Delta v'(r)^2\right|^{1/4}Re_d(r)^{1/2}\right]f(r)dr}{\int_0^\infty \frac{1}{r}\left[2+0.6\,S_c^{1/3}\Delta v'(r)^{1/2}\right]f(r)dr} \qquad (10)$$

where f(r) is the distribution function describing the drop size variation within the spray entering the annulus. In the bipropellant model, discussed in the next section, a distribution function is required for both the fuel and the oxidizer sprays.

For the numerical calculations, a logarithmiconormal distribution of drops was assumed, given by

$$f(r) = \frac{dN}{dr} = \frac{a}{r}\exp\left\{-\frac{1}{2}\left[\frac{\ell n\left(\frac{r}{\bar{r}_n}\right)}{\ell n\,\sigma_G}\right]^2\right\} \qquad (11)$$

where $a = \dfrac{1}{\sqrt{2\pi}\,\ell n\,\sigma_G}$

A logarithmiconormal distribution was chosen as a matter of convenience. Our steady-state combustion program, which is required to define the steady-state gasdynamic and combustion parameters at the annulus being investigated, assumes a logarithmiconormal distribution at the injector. It was determined that although the mean drop size and geometric standard deviation of the spray changes between the injector and the axial position of the annulus, the distribution is still nearly logarithmiconormal. Since no valid criterion for choosing the best distribution has been established, the logarithmiconormal distribution was a natural choice for our numerical studies; however, any distribution of drops may be substituted in the model for future investigations.

Bipropellant Instability Model

In determining the response of a bipropellant system to a random disturbance the vaporization response of both propellants may be important. Since the disturbance wave may not produce the same vaporization response for both the fuel and oxidizer sprays, the local instantaneous amount of vapor phase fuel and oxidizer present may not be the same as under steady-state conditions. Priem's model assumes that the response of both propellants is the same, in that the amount of heat added to the flow is proportional to the amount of mass vaporized of the controlling propellant.

In our current model, the amount of mass added to the system through fuel and oxidizer vaporization response to a disturbance is considered independently. The amount of heat added to the system, is based on the instantaneous vapor phase O/F.

A derivation of the instability equations for a bipropellant system is presented in Appendix C. The resulting nondimensional transport equations for an annular model are,

Continuity. -

$$\frac{\partial \rho'}{\partial t'} = -\rho\left(\frac{\partial v'_\theta}{\partial \theta'} + \frac{\partial v'_z}{\partial z'}\right) - v'_\theta \frac{\partial \rho'}{\partial \theta'} - v'_z \frac{\partial \rho'}{\partial z'} + \mathcal{L}_f \omega'_f f(\gamma) + \mathcal{L}_{ox} \omega'_{ox} f(\gamma) \tag{12}$$

Momentum (θ-direction). -

$$\rho' \frac{\partial v'_\theta}{\partial t'} = -\rho' v'_\theta \frac{\partial v'_\theta}{\partial \theta'} + \mathcal{J} f(\gamma) \frac{4}{3} \frac{\partial^2 v'_\theta}{\partial \theta'^2} - v'_\theta \left[\omega'_f \mathcal{L}_f + \omega'_{ox} \mathcal{L}_{ox}\right] f(\gamma)$$

$$- \left(\frac{\mathcal{B}_f}{r'_{d,f}} + \frac{\mathcal{B}_o}{r'_{d,ox}}\right) \rho' |v'_\theta| (v'_\theta) \tag{13}$$

Momentum (z-direction). -

$$0 = -\rho' v'_z \frac{\partial v'_z}{\partial z'} - \left|\frac{1}{\gamma}\right| \frac{\partial P'}{\partial z'} - f(\gamma)(v'_z - v'_{f,z}) \mathcal{L}_f \omega'_f - f(\gamma)(v'_z - v'_{ox,z}) \mathcal{L}_{ox} \omega'_{ox}$$

$$- \mathcal{B}_f \rho' \frac{|v'_z - v'_{f,z}| (v'_z - v'_{f,z})}{r'_{d,f}} - \mathcal{B}_{ox} \rho' \frac{|v'_z - v'_{ox,z}| (v'_z - v'_{ox,z})}{r'_{d,ox}} \tag{14}$$

Energy. -

$$\rho' \frac{\partial T'}{\partial t'} = -\rho' \left(v'_\theta \frac{\partial T'}{\partial \theta'} + v'_z \frac{\partial T'}{\partial z'} \right) + \mathcal{J} f(\gamma) \frac{\partial^2 T'}{\partial \theta'^2} - |\gamma - 1| P' \left(\frac{\partial v'_\theta}{\partial \theta'} + \frac{\partial v'_z}{\partial z'} \right)$$

$$+ \frac{4}{3} |\gamma(\gamma-1)| \mathcal{J} \left[\left(\frac{\partial v'_\theta}{\partial \theta'} \right)^2 + \left(\frac{\partial v'_z}{\partial z'} \right)^2 - \frac{\partial v'_\theta}{\partial \theta'} \frac{\partial v'_z}{\partial z'} \right] f(\gamma)$$

$$+ \mathcal{L}_t \omega'_c f(\gamma) \gamma - (\mathcal{L}_{ox} \omega'_{ox} + \mathcal{L}_f \omega'_f) f(\gamma) T'$$

$$+ \frac{(\gamma-1)\gamma}{2} f(\gamma) \left\{ \mathcal{L}_f \omega'_f \left[v_\theta^2 + (v'_z - v'_{f,z})^2 \right] + \mathcal{L}_{ox} \omega'_{ox} \left[v'^2_\theta + (v'_z - v'_{ox,z})^2 \right] \right\}$$

$$+ \gamma(\gamma-1) \rho' \left\{ \mathcal{B}_f \frac{\left[v'^2_\theta + (v'_z - v'_{f,z})^2 \right]^{3/2}}{r'_{d,f}} + \mathcal{B}_{ox} \frac{\left[v'^2_\theta + (v'_z - v'_{z,ox})^2 \right]^{3/2}}{r'_{d,ox}} \right\}$$

Although the equations appear similar to those of Reference 1, a burning rate parameter for both the fuel and the oxidizer spray, as well as independent vaporization response terms, ω'_f, ω'_{ox} are present in the bipropellant equations. The droplet velocity Re_d parameter and drag parameter are also considered independently for both propellants. The appearance of these additional "stability parameters" make it more difficult to map the stability limits since several additional dimensions must now be considered.

RESULTS AND DISCUSSIONS

Numerical Methods

The Dynamic Science combustion instability program uses a predictor-corrector scheme to obtain the solution of the nonlinear system of equations defined in (A-11) to (A-13) and (A-17) to (A-19). The numerical scheme combines a first order explicit scheme with a variable iteration first order implicit scheme in the t direction. The spatial derivatives are approximated with a first order central difference scheme. The variable iteration of the implicit scheme is controlled by an error criteria, requiring a given significant figure agreement or a maximum number of iterations, whichever occurs first. In the final report for NASA Contract NAS7-366(Ref.2), a complete discussion of this numerical method can be found. Appendix D contains a discussion and current listing of the bipropellant combustion instability program containing the droplet drag effects.

The proper choice of the ratio of the time interval divided by space interval, $\Delta t/\Delta\theta$, and the magnitude of each remains difficult. Attempts to relate numerical stability criteria derived for linearized instability equations to numerical stability of the nonlinear equations has been only marginally successful. While no known stability criteria has been developed for Priem's nonlinear instability equations, a good estimate of the integration step size requirements can be made by examining the physical phenomenon. Recent numerical experiments with the Dynamic Science combustion instability program gave definite encouragement to this physical approach to the problem of numerical stability and numerical accuracy. Cases have been computed using 20, 40, 80, and 160 nodes under identical operating parameters. The results indicate the damping effect of too few nodes. In effect, too few nodes prevent the wave from steepening into a shock wave, and therefore neglects the important nonlinear phenomenon. Our results indicate that at least 80 nodes and possibly as many as 160 are required in the numerical integration.

It is essential when making accuracy checks with the combustion instability program that the mesh ratio of $\Delta t/\Delta\theta$ remain constant while reducing the independent, Δt and spatial step $\Delta\theta$. Most of the existing results were computed with 40 theta nodes and an independent step of .0625. Accuracy checks have been made by comparing 40 node runs with the results obtained from 80 nodes and a Δt of .03125. However, each step reduction multiplies the machine time by a factor of four, thus making long runs with very small steps prohibitive.

At this point, we feel that the problem of adequately describing the nonlinear combustion instability wave in Priem's one-dimensional model is well in hand. The physical approach, rather than an analytical extension of linear stability theory has been more successful.

Nonlinear Nature of Instability Wave. - An interesting result of the numerical integration of both Priem's model and the current extension is presented in the accompanying figure. An initially sinusoidal pressure disturbance of amplitude equal to 25% of the steady-state pressure rapidly develops into a steep fronted wave. In the accompanying figure the wave form around the entire annulus (2 π radians) is followed through a series of integrations in time. The abscissa represents the position around the annulus (0.0 and 6.283...radians are the same point) and the ordinate represents the non-dimensional pressure, P/P_o, around the annulus. The expected wave form for this type of disturbance is a standing wave with zero pressure nodes 90 degrees around from the maximum pressure node, in both directions.

The disturbance propagates around the annulus in both directions producing an alternating high and low pressure at both the maximum and minimum initial pressure locations. In the sequence of three figures at the right the wave seems first to decay, for nondimensional time between t = 0.0 and 1.5, and then to build up on the opposite side of the annulus at t = 3.5, as would be expected. The nondimensional time of 3.14 (π) radians represents the time it would take for a disturbance to propagate half way around the annulus if it travelled at the sound speed.

The nonlinear effects of the model appear almost immediately in the wave form. Following the disturbance further, in time, the nonlinear nature becomes more evident as the disturbance continues to travel around the annulus in both directions. At t = 8.5 the steep fronted nature of the wave is evident. Several recent experimental studies have confirmed the steep fronted nature of an instability wave traveling around a combuster (Hefner, Ref. 4, Clayton, Ref. 5).

The ability of the computer solution to allow a linear disturbance to develop into a steep fronted wave is dependent upon the number of points taken around

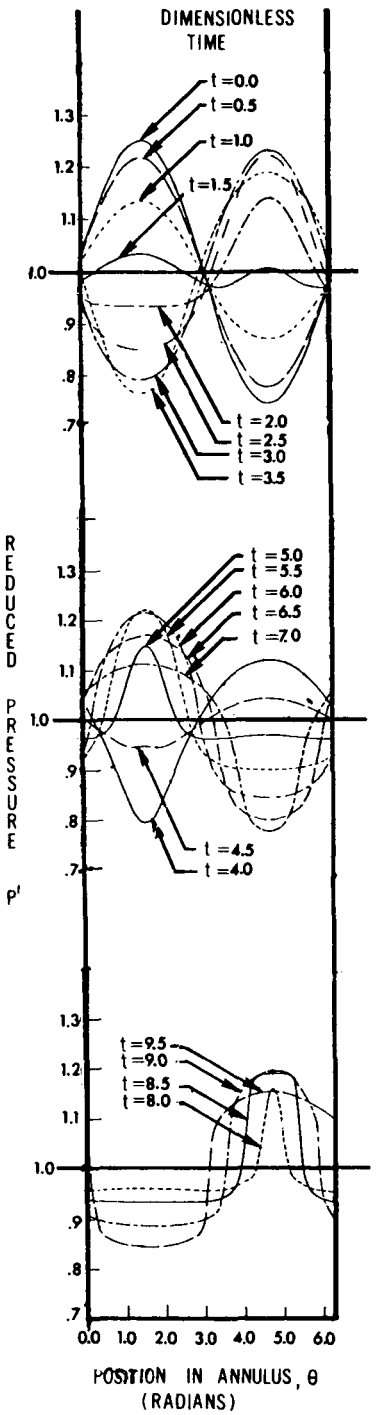

Development of a Steep Fronted Wave

the annulus in the integration. An insufficient number of points tend to "hold down"the wave and not allow the nonlinear effects to develop.

The figure below indicates the nonlinear nature of the solution.

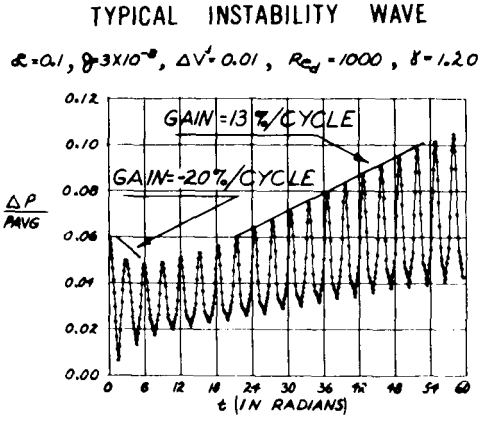

Following the amplitude of the disturbance for increasing nondimensional time, t , the wave first damps at a rate of approximately 20%/cycle*. After one or two cycles, shown previously to be the time it takes for a steep fronted disturbance to develop, the damping is arrested and the wave amplifies, at a rate of about 13%/cycle. Eventually (t>20 cycles) the disturbance reaches an equilibrium amplitude (not shown on figure).

Viscous Damping. - The effect of viscous damping on the final shape of the "steep fronted" wave has been examined. Figure 2a shows the velocity profile in the annular direction for a typical instability case with 80 nodes taken around the annulus. The effect of the viscous dissipation term, $\mathcal{J}$, on the slope of the final velocity profile is shown for values of

$\mathcal{J} = 3\text{x}10^{-2}$

$\mathcal{J} = 3\text{x}10^{-3}$

$\mathcal{J} = 3\text{x}10^{-8}$ (realistic value)

*One cycle is the time it takes for a disturbance to travel entirely around the annulus and return to the same position. For a disturbance traveling at the sound speed this is equal to 2π radians of nondimensional time. Once the disturbance has developed into a steep fronted wave, the disturbance travels faster than the speed of sound.

Figure 2b shows the profile of the velocity derivative for various values of $\mathcal{J}$.

It is evident that viscous damping tends to smooth (hold down) the wave shape and that there is a critical value of $\mathcal{J}$ below which secondary wavelets form. These wavelets represent numerical error which, because of the non-linear nature of the solution, may grow into an instability and therefore should be eliminated by the addition of more nodes in the annular direction.

Droplet Drag

The annular combustion instability equations derived in Appendix A have been programmed and a limited parametric study has been conducted. The addition of a new nondimensional variable, the Drag Parameter, $\mathcal{B}$, to the original set of stability parameters, $\mathcal{L}$, $\mathcal{J}$, ΔV, Re_d, and $\Delta P/P_c$ makes a full parametric variation impractical. Instead, typical values of the original stability parameters were chosen and the drag parameter was varied independently. Realistic values of $\mathcal{B}$, between 0.1 and 100, were used. The component of the droplet velocity in the annular direction was considered to be negligible since the droplets must be assumed to enter the thin annulus axially in this one dimensional model and can not respond to the disturbance wave due to their inertia. The coefficient of drag, C_D, was assumed constant and was computed as a function of the Reynolds number of the drop based on the mean drop diameter and the average value of the relative velocity.

Determination of the Drag Parameter corresponding to a particular annular position involves the evaluation of the liquid concentration at the annular location, since

$$\mathcal{B} = \frac{3}{8} \frac{C_D \mathcal{F}_p r_{an}}{r_d}$$

where $$\mathcal{F}_p = \frac{\rho_\ell}{\rho_d} ,$$

and

$$\rho_\ell = \text{liquid concentration} = \left[\frac{\text{lb}_m \text{ liquid}}{\text{unit volume of two-phase mixture}} \right]$$

$$\rho_d = \text{drop density} = \left[\frac{\text{lb}_m}{\text{unit volume of drop}} \right]$$

Relating ρ_ℓ to operating parameters

$$\rho_\ell = \frac{\dot{W}}{Av_\ell} = \frac{\left[\begin{array}{l}\text{Liquid propellant flow rate} \\ \text{at annular section, } \frac{lb_{prop}}{sec}\end{array}\right]}{\left[\begin{array}{l}\text{Area of chamber} \\ \text{at annular section, } ft^2\end{array}\right]\left[\begin{array}{l}\text{Velocity of liquid at} \\ \text{annular section, ft/sec}\end{array}\right]} = \left[\frac{lb_{prop}}{ft^3}\right]$$

The propellant flow rate at the annular section, $\dot{W}$, and the average liquid velocity in the annulus are obtained from our steady-state combustion computer program and used as input to the instability program.

The variation in the drag parameter may be seen in Table I below

TABLE I - REALISTIC VALUES OF $\mathcal{B}$

(Injection velocity = 1000 in./sec, $\rho_d = 50 (lb_m ft^3)$, $r_d = 3$ mils, $C_D = 1.2$)

Injection Flow Rate $\dot{W}_{Inj}$ $\left[\frac{lb\ prop}{lb\ sec}\right]$	Chamber Diameter (in.)	Percent Vaporized at Annular plane	ρ_ℓ $\left[\frac{lb_m, liquid}{ft^3\ mixture}\right]$	$\mathcal{J}_p$	$\mathcal{B}$
6000	40	10	7.5	.147	440
25.48	11.91	10	.356	.0071	6
0.345	2.0	10	.17	.0033	0.5

Typical results of the parametric droplet drag study are shown in Figures 3 and 4. Figure 3 shows the time variation in dimensionless pressure, P', at the maximum pressure node for a parametric variation in the drag parameter, $\mathcal{B}$, between O and 100. The initial disturbance amplitude A_p, was 0.03 for all cases. The other stability parameters characterizing this typical case were: $\Delta v' = 0.01$, $\mathcal{J} = 3 \times 10^{-8}$, $\mathcal{L} = 0.1$, $Re_d = 1000$. With the drag parameter set to zero, this condition produces a marginal instability. Increasing the drag parameter increases the damping effect of the droplets and with $\mathcal{B}$ set to 100, the wave damps quickly.

A composite stability limit curve has been generated for the variation in critical peak to peak disturbance pressure $\Delta P/P_o$ as a function of the burning rate parameter, $\mathcal{L}$. The drag parameter has been varied parametrically with the

other stability parameters characterizing the flow held constant at $\Delta v'=0.01$, $Re_d = 1000$, and $\mathcal{J}=3\times10^{-8}$. The results are presented in Figure 4. Other values of $\Delta v'$ and Re_d were also used, in a parametric variation of $\mathcal{L}$ and $\mathcal{D}$ and showed the same trends as Figure 4.

The inclusion of droplet drag in the instability model greatly affects the stability limits for values of $\mathcal{L} < 4$ and values of $\mathcal{D}>1$. Although $\mathcal{L}$ and $\mathcal{D}$ both depend upon the droplet size, geometry of the combustor, and concentration of propellants, and therefore can't be varied independently, the stability limit curves presented in Figure 4 do show the effect of droplet drag for realistic combinations of $\mathcal{L}$ and $\mathcal{D}$. At high values of $\mathcal{L}$, damping of the disturbance wave due to droplet drag is overshadowed by the large amount of heat added to the wave. It was shown in both References 1 and 2, that a disturbance either amplifies or damps within a fraction of a cycle for large values of $\mathcal{L}$.

For engines operating below $\mathcal{L}=1$, a small change in the drag parameter can produce a large change in the disturbance amplitude required to trigger an instability. Increases in the drag parameter can even produce an unconditionally stable annulus that previously would have been triggered spontaneously.

Unfortunately, methods of increasing $\mathcal{D}$ without affecting the other stability parameters, are not known. The drag parameter may be increased by decreasing drop size, increasing the propellant flow rate, or decreasing the drop velocity. To meet a specific thrust requirement, the propellant flow rate must be held nearly constant. Changes in drop size or drop velocity will effect the burning rate parameter at the annulus under consideration. The complexity of the relationship between the instability parameters and the engine operating parameters makes general conclusions difficult. Specific engine systems, however, can be analyzed based on their specific geometry and operating variables.

Droplet Spray Distribution

A series of numerical solutions were generated using Equation (10) for the vaporization response and Equation (11) for the drop size distribution function. The mass-mean drop radius, r_m was varied from 1 to 10 mils and the geometric standard deviation was varied from 1.5 to 3.5. Values for r_n were computed from

$$r_n = r_m e^{-3(\ln \sigma_G)^2}$$

For each combination of r_m and σ_G used in the instability solution, the corresponding values of $\Delta v'$ and Re_d were obtained as functions of drop size from the results of the steady-state combustion program, and entered as data in the instability solution. The burning rate parameter, $\mathfrak{L}$, was obtained also from the steady-state solution at the annular position under investigation, and was based on a drop size corresponding to the number mean drop.

Figure 5 indicates the effect of changing the mass-mean drop radius and the geometric standard deviation of the droplet spray, for a particular set of initial instability parameters. Increasing σ_G with r_m held constant decreased the number mean drop radius, r_n. A decrease in r_n corresponds to a decrease in the average Re_d for the spray, which, as shown in Figure 1, decreases the burning response of the spray and therefore makes the system more stable. A decrease in r_m, for a constant value of σ_G has the same affect on stability.

Generalizations are difficult because changes in the drop size or distribution also produce changes in the other stability parameters, such as $\mathfrak{L}$, $\mathfrak{D}$, and $\Delta v'$. Specific numerical solution should be obtained for each engine condition and geometry of interest, rather than relying on an interpretation of general trends.

Bipropellant System

The model developed in Appendix C to account for the response of both propellants to a tangential disturbance wave has been programmed and several cases run. The first series of runs were made to determine general trends produced by the independent addition of mass and heat to the gas phase and are summarized in Table II below.

TABLE II: COMPUTER RUNS - GENERAL TRENDS

Run Number	Burning Rate Parameter		Relative Velocity		Re_d Parameter		Controlling Propellant
	Fuel $\mathcal{L}_f$	Oxidizer $\mathcal{L}_{ox}$	Fuel $\Delta V'_f$	Oxidizer $\Delta V'_{ox}$	Fuel $Re_{d,f}$	Oxidizer $Re_{d,ox}$	
1	.05	.05	.01	.01	1000	1000	Fuel
2	.05	.10	.01	.01	1000	1000	Fuel
3	.05	.50	.01	.01	1000	1000	Fuel
4	.05	1.00	.01	.01	1000	1000	Fuel
5	.05	2.00	.01	.01	1000	1000	Fuel
6	.05	10.00	.01	.01	1000	1000	Fuel
7	.05	.05	.01	.01	1000	100,000	Fuel
8	.05	.05	.01	.1	1000	1000	Fuel

With reference to the NO DRAG STABILITY LIMIT CURVE of Figure 4, which was generated with the monopropellant model discussed in Appendix A, a comparison with the bipropellant model of Table II is possible. Increasing the burning rate parameter of the noncontrolling propellant has the effect of increasing the rate of mass addition to the system while maintaining the rate of heat addition constant. The results of runs 1-6 of Table II indicate the same trends as would have been predicted by the monopropellant model, assuming that

$$\mathcal{L}_{t_{\left(\begin{smallmatrix}\text{monopropellant}\\ \text{model}\end{smallmatrix}\right)}} = \left(\mathcal{L}_f + \mathcal{L}_{ox}\right)_{\left(\begin{smallmatrix}\text{bipropellant}\\ \text{model}\end{smallmatrix}\right)}$$

Run number (1) produced a marginally stable wave in response to an initial $\frac{\Delta P}{P_{avg}} = .03$ corresponding to $\mathcal{L}_t = .05 + .05 = .1$ which is on the left side of of the NO DRAG stability limit curve of Figure 4. Increasing the total burning rate parameter, $\mathcal{L}_t$, through mass addition rather than heat addition as was done in runs 2 and 3, produced marginal stability in response to a lower value of $\frac{\Delta P}{P_{avg}}$. Run 3 corresponding to $\mathcal{L}_t = .55$ is close to the minimum $\frac{\Delta P}{P_{avg}}$ point of Figure 4. Further increases in $\mathcal{L}_t$, as is the case in runs 4-6, produced increased stability, as would have been predicted from Figure 4. In general then, adding mass to the system without added heat produced the same trends as adding both mass and heat simultaneously.

Runs 7 and 8 were made to determine the effect of changes in $Re_{d,ox}$ and $\Delta v'_{ox}$ independent of the corresponding "fuel" values. Increasing $Re_{d,ox}$ from 1000 to 100,000 helped to stabilize the instability slightly. It is felt that a similar increase on the low end of the scale, say from 100-1000 would have produced a much greater stabilizing effect. The effect of increasing $\Delta v'_{ox}$ from .01 to .1, as was done in run 8, had no effect on the instability wave.

In addition to the general effects discussed above, the results of a stability analysis on a real engine using both the monopropellant and bipropellant model is presented in the "Application to Engines" section which follows.

Application to Engines

To determine the effect of independent mass and heat addition on the stability analysis of an engine, both the monopropellant model of Appendix A and the bipropellant model of Appendix C were used to numerically predict the "stability map" of a real engine. Only one engine geometry and set of operating conditions could be chosen because of the number of computer runs, and hence the expense of analyzing an engine. For this reason the results cannot indicate the similarity or difference between the two models at other engine operating parameters.

The basic engine parameters used in the study are:

PROPELLANTS - RP1 - LOX

FLOW RATES: $\dot{W}_{f(RP1)} = 1800\ lb_m/sec$

$\dot{W}_{ox(LOX)} = 4320\ lb_m/sec$

MEAN DROP SIZE: $r_m = 3.0$ mils

Geometric Standard Deviation $\sigma_G = 2.30$

ENGINE GEOMETRY AND OPERATING CONDITIONS

Chamber Pressure, $P_c = 700$ psia

Chamber Area, $A_c = 1250\ in^2$

Throat Area, $A_t = 118\ in^2$

$\mathcal{A} = 10.5$

Initial $\Delta v'_f = 0.0425$

$\Delta v'_{ox} = 0.0168$

Based on the above parameters, the Dynamic Science Steady-State Combustion Computer Program (ref. 2) was used to analyze the steady-state burning of both liquid propellants as they vaporize and burn while moving

axially in the combustion chamber. From these results, the nondimensional stability parameters needed to characterize several similar positions within the combustor were obtained. At each of five axial positions within the combustor both instability models were used to obtain the initial pressure amplitude required to trigger an instability. For simplicity, it was assumed that the drag parameter was zero, however, if results were required for a real engine, this would not have been neglected.

The stability parameters as well as the resulting threshold $\frac{\Delta P}{P_{avg}}$ are presented in Table III below.

TABLE III: INSTABILITY ANALYSIS

	$\frac{\Delta P}{P_{avg}}$ Threshold								
x Position	Bipropellant Model	Monopropellant Model	$\mathfrak{L}_f$	$\mathfrak{L}_{ox}$	$Re_{d,f}$	$Re_{d,ox}$	Δv_f	Δv_{ox}	v_z
0.02	0.026	.024	.17	.8	2100	2300	.013	.038	.05
0.05	0.025	.023	.28	1.7	2200	2100	.01	.025	.05
0.10	0.037	.041	.61	.94	2100	1900	.015	.01	.05
0.125	0.055	.058	.67	.54	2000	1800	.019	.01	.05
0.20	0.30	.350	.61	1.4	1600	1300	.03	.025	.05

The monopropellant model cases were run by assuming $\mathfrak{L}_t = \mathfrak{L}_f + \mathfrak{L}_{ox}$ and $\Delta v = \Delta v_f$, $Re_d = Re_{d,f}$. The results are plotted in Figure 6 in terms of the threshold pressure disturbance as a function of axial position of the annulus. In addition, Figure 7 shows the time response of the system to various disturbances close to the threshold disturbance value for three of the axial positions (x = 0.02, 0.05, 0.10).

The results of this particular engine analysis indicate that the bipropellant model predicted the same general trends as did the monopropellant model. Although the threshold pressure disturbances are not identical, the additional mass added to the gas phase through excess noncontrolling propellant vaporization did not shift the equilibrium stability point greatly.

These results are not general. Other analysis using the bipropellant model at different operating conditions did not produce the same agreement between models. These results were not complete at the time of publication of this report.

The process of parametrically varying one of the stability parameters while holding the others constant can lead to some false conclusions about how to fix an unstable engine. In a physical situation, changing one of the parameters usually changes several others also. For example, in Figure 8, the affect on stability of changing the mass-mean drop size or the geometric standard deviations of the propellant spray, for a particular engine (particular stability parameters) is shown. Rather than hold each of the other stability parameters constant ($\mathfrak{L}$, $\mathcal{D}$, Re_d, Δv, σ_G) they were recomputed with our steady-state combustion program based on the value of mass-mean drop radius chosen. Point 1 on Figure 8 represents the base engine, which is marginally stable. Changing r_m from 3.0 mils to 2.0 mils (Point 2) produces the corresponding changes in $\mathfrak{L}$, $\mathcal{D}$, and Re_d indicated on the figure. The dashed line represents the new stability limit based on the values of Re_d and $\mathcal{D}$ at Point 2. In this case, making the drops smaller produced negligible affect on stability through changes in Re_d and $\mathcal{D}$. However, the change in $\mathfrak{L}$ shifted the engine operating point into the very stable region. Examples of increasing the drop size can be seen at Points 3 and 4. Point 5 shows the effect of choosing the wrong value for the standard deviation of the spray. A change in σ_G from 2.3 to 3.5 changes the engine stability from neutral (marginally unstable to the specified disturbance level) to unconditionally stable to all disturbances. While this example serves as a caution not to over-simplify the relationship between parameters, any particular engine may be analyzed by specifying the stability parameters and then letting the numerical solution predict stability, within the validity of the model.

GENERALIZED RESULTS AND CONCLUDING REMARKS

A nonlinear combustion instability model has been developed and solved numerically for an annular combustor of small thickness and length. Following Priem's assumption (Ref. 1) the vaporization rate of the propellant spray was assumed to respond instantaneously to a gasdynamic disturbance wave traveling around the annulus. The following results were indicated by the numerical solutions.

1. A finite disturbance is required to trigger an instability.

2. The minimum amplitude disturbance that will amplify into an instability is a function of:

   a. The burning rate parameter of both propellants, $\mathfrak{L}_f$ and $\mathfrak{L}_{ox}$.

   b. The velocity difference between the propellant drops and the combustion gases, considering both propellant sprays.

   c. The drag parameter, $\mathcal{D}$, indicative of the amount of momentum and energy transfer between the drop spray and the combustion gases.

   d. The size and distribution of droplets of both fuel and oxidizer.

   e. The characteristics of the particular propellant or combustor, only as they affect the determination of the above parameters.

3. As was found by Priem, gas phase viscous damping, associated with the viscous dissipation parameter, $\mathcal{J}$, had negligible affect on the stability limits.

4. For values of the burning rate parameter $\mathfrak{L}$ less than 4, droplet drag can be very effective in attenuating a disturbance. In this region inclusion of the effect of droplet drag in the solution produced radically different stability limits for values of the drag parameter, $\mathcal{D}$, greater than about 10. At higher values of $\mathfrak{L}$ the combustion process dominates the stability solution and overshadows any damping effects of droplet drag.

5. An accurate description of the droplet size distribution produced by the atomization process, as well as how this distribution changes during its history within a combustor is vital to a meaningful prediction of combustion instability.

6. Considering the heat addition and mass addition to the system independently (bipropellant model, Appendix C) produced significantly different numerical results when compared with the linear heat and mass addition model (monopropellant model, Appendix A). The addition of mass without heat produced the same trends as the addition of both heat and mass.

REFERENCES

1. Priem, R. J. and Guentert, D. C.: Combustion Instability Limits Determined by a Nonlinear Theory and a One-Dimensional Model. Lewis Research Center, Cleveland, Ohio, NASA TN-1409, October 1962.

2. Dynamic Science: Combustion Stability Limits Calculated Utilizing a Nonlinear Model. Final Report on NASA Contract NAS7-366, 10 Aug.1966.

3. Ranz, W. E. and Marshall, W. R., Jr.: Evaporation from Drops. Pt. I, Eng. Prog., Vol. 48, No. 3, Mar. 1952, pp 141-146.

4. Hefner, R. J.: Diagnosis of High Frequency Combustion Stability Characteristics from Pressure Measurements. Aerojet-General Corporation, presented at the 3rd ICRPG Combustion Conf., Cape Kennedy, Oct. 1966.

5. Clayton, R.M.: Recent Experimental Results from a Study of Resonant Combustion. Jet Propulsion Laboratory, presented at the 3rd ICRPG Combustion Conf., Cape Kennedy, Oct. 1966.

6. Bird, R. B., Stewart, W. E., and Lightfoot, E. N.; Transport Phenomena John Wiley & Sons, Inc., New York, 1965.

7. Williams, F. A.: Combustion Theory, Chapter 11, Addison Wesley, Palo Alto, California 1965.

8. Priem, R. J. and Heidmann, M. F.: Propellant Vaporization as a Design Criterion for Rocket-Engine Combustion Chambers, NASA Tech.Rept. R-67, 1960.

APPENDIX A

ANNULAR COMBUSTION INSTABILITY MODEL INCLUDING DROPLET DRAG

The transport equations for an annular combustion instability model which includes the effects of aerodynamic droplet drag are developed in this appendix. The derivation follows closely the original instability model of Priem (Ref. 1) with the addition of momentum and energy transfer between the liquid propellant droplets and the bulk combustion gases due to aerodynamic drag. The nomenclature used is that of Bird (Ref. 2) also used by Priem. In developing the droplet drag addition, Priem's derivation (Ref. 1) of the annular model was carefully rederived. A full derivation will not be repeated here, however, the important steps leading to the drag terms will be reviewed. The model will be generalized to a droplet spray distribution and a bipropellant system in the following appendices, however, only a constant drop size of a single (controlling) propellant will be considered in this appendix for simplicity.

General Equations

Continuity. - Assuming that the volume occupied by the liquid drops within the annulus is negligible, the mass balance equation (continuity) for a stationary elementary unit volume may be written in the usual manner

$$\text{Gas} \qquad \frac{\partial \rho}{\partial t} = - \nabla \cdot \rho \vec{v} + \omega \tag{A-1a}$$

$$\text{Liquid} \qquad \frac{\partial \rho_\ell}{\partial t} = - \nabla \cdot \rho_\ell \vec{v}_\ell - \omega \tag{A-1b}$$

where ω is the local instantaneous vaporization rate; equal to the rate of disappearance of liquid propellant.

Momentum. - A momentum-balance applied to a stationary unit volume through which both gases and liquid propellants are passing leads to the vectorial equation:

$$\frac{\partial}{\partial t} \rho \vec{v} = - \nabla \cdot \rho \vec{v}\vec{v} - \nabla \cdot \rho_\ell \vec{v}_\ell \vec{v}_\ell - g \nabla P - \nabla \cdot \tau \tag{A-2a}$$

The divergence of liquid momentum from the unit volume can be rewritten as

$$\nabla \cdot \rho_\ell \vec{v}_\ell \vec{v}_\ell = \vec{v}_\ell \nabla \cdot \rho_\ell \vec{v}_\ell + \rho_\ell (\vec{v}_\ell \cdot \nabla) \vec{v}_\ell \tag{A-2b}$$

From the liquid continuity equation

$$\nabla \cdot \rho_\ell \vec{v}_\ell = - \frac{\partial \rho_\ell}{\partial t} - \omega$$

A change in liquid density within the annulus with time $\partial \rho_\ell / \partial t$, requires a change in the liquid velocity entering the annulus, since the drop flux remains constant. For the one-dimensional model change in flow properties entering the annulus is assumed to be zero, and therefore there cannot be any buildup of liquid within the annulus.

Hence, $\nabla \rho_\ell \vec{v}_\ell = - \omega$ and equation (A-2b) reduces to

$$\nabla \cdot \rho_\ell \vec{v}_\ell \vec{v}_\ell = - \vec{v}_\ell \omega + \rho_\ell (\vec{v}_\ell \cdot \nabla) \vec{v}_\ell \qquad \text{(A-2c)}$$

In Priem's original model, the last term above is assumed to be zero based on the assumption of constant liquid velocity, $(\vec{v}_\ell \cdot \nabla)\vec{v}_\ell = 0$.

Actually, if the same assumption as was made for the gas phase; (i.e., constant axial velocity due to the thin annulus while allowing for an axial derivative,) is made for the liquid phase, then the effect of droplet drag forces on the gas phase shows up.

Written in terms of the drag coefficient

$$\rho_\ell (\vec{v}_\ell \cdot \nabla)\vec{v}_\ell = \rho_\ell \frac{Dv_\ell}{Dt} \quad \left(\text{since } \frac{\partial \rho_\ell}{\partial t} = 0\right)$$

$$\vec{F}_D = \frac{1}{g} \rho_\ell \frac{D\vec{v}_\ell}{Dt} = \frac{1}{g} \frac{3}{8} C_D \frac{\rho_\ell}{\rho_d} \rho \frac{(\vec{v}-\vec{v}_\ell)\,|\vec{v}-\vec{v}_\ell|}{r_d}$$

$$\vec{F}_D = \frac{1}{g} \frac{3}{8} C_D \mathfrak{F}_P \rho \frac{(\vec{v}-\vec{v}_\ell)\,|\vec{v}-\vec{v}_\ell|}{r_d}$$

where $\vec{F}_D$ is the drag force exerted by the gas on the droplets, and $\mathfrak{F}_P$ is a "packing fraction" representing the volume occupied by drops, in a unit volume of gas-drop mixture.

The divergence of liquid momentum is then

$$\nabla \cdot \rho_\ell \vec{v}_\ell \vec{v}_\ell = - \vec{v}_\ell \omega + g \vec{F}_D \qquad \text{(A-2d)}$$

The momentum equation can be written as

$$\frac{\partial}{\partial t}(\rho\vec{v}) = -\nabla\cdot\rho\vec{v}\vec{v} + \vec{v}_\ell\omega - g\vec{F}_D - g\nabla P - \nabla\cdot\tau$$

or after expanding the first two terms and using the gas continuity equation (A-1a)

$$\rho\frac{\partial\vec{v}}{\partial t} = -\rho(\vec{v}\cdot\nabla)\vec{v} - (\vec{v}-\vec{v}_\ell)\omega - g\vec{F}_D - g\nabla P - \nabla\cdot\tau \qquad \text{(A-2)}$$

Energy. - Following Priem, (Ref. 1), the energy balance equation for two phase flow passing through a stationary unit volume written as

$$\frac{\partial}{\partial t}(\rho C_v T + \frac{1}{2gJ}\rho v^2) = -\nabla\cdot\rho\vec{v}(C_v T + \frac{1}{2gJ}v^2) - \nabla\cdot\rho_\ell\vec{v}_\ell(U_\ell + \frac{1}{2gJ}v_\ell^2)$$
$$- \nabla\cdot\vec{q} - \frac{1}{J}\nabla\cdot P\vec{v} - \frac{1}{gJ}\nabla\cdot(\tau\cdot\vec{v})$$

The divergence of total energy (internal + kinetic energy) from the liquid phase is given as

$$\nabla\cdot\rho_\ell\vec{v}_\ell(U_\ell + \frac{1}{2gJ}v_\ell^2) = \rho_\ell\vec{v}_\ell\cdot\nabla(U_\ell + \frac{1}{2gJ}v_\ell^2) + (U_\ell + \frac{1}{2gJ}v_\ell^2)\nabla\cdot\rho_\ell\vec{v}_\ell \qquad \text{(A-3a)}$$

where again

$$\nabla\cdot\rho_\ell\vec{v}_\ell = -\omega$$

Assuming a constant liquid temperature ($\nabla U_\ell = 0$) but allowing for acceleration of the liquid due to gas-liquid drag, the first term on the right hand side of Equation A-3a, representing the loss of energy by the liquid due to changes in liquid internal energy and liquid velocity, reduces to

$$\rho_\ell\vec{v}_\ell\cdot\nabla(U_\ell + \frac{1}{2gJ}v_\ell^2) = \rho_\ell\vec{v}_\ell\cdot\nabla\frac{1}{2gJ}v_\ell^2$$
$$= \frac{1}{gJ}\rho_\ell\vec{v}_\ell\cdot\left[(\vec{v}_\ell\cdot\nabla)\vec{v}_\ell\right]$$
$$= \frac{1}{gJ}\rho_\ell\vec{v}_\ell\cdot\frac{D\vec{v}_\ell}{Dt}$$

In terms of the drag force

$$\frac{1}{gJ}\ \rho_\ell \vec{v}_\ell \cdot \frac{D\vec{v}_\ell}{Dt} = \frac{1}{J}\ \vec{F}_D \cdot \vec{v}_\ell$$

and therefore the divergence of energy from the liquid phase is

$$\nabla \cdot \rho_\ell \vec{v}_\ell (U_\ell + \frac{1}{2gJ}\ v_\ell^2) = \frac{1}{J}\ \vec{F}_D \cdot \vec{v}_\ell\ -(U_\ell + \frac{1}{2gJ}\ v_\ell^2)\ \omega \qquad \text{(A-3b)}$$

and the energy equation therefore is

$$\frac{\partial}{\partial t}\ (\rho C_v T + \frac{1}{2gJ}\ \rho v^2) = -\nabla \cdot \rho \vec{v}(C_v T + \frac{1}{2gJ}\ v^2)\ -\frac{1}{J}\ \vec{F}_D \cdot \vec{v}_\ell$$

$$+ (U_\ell + \frac{1}{2gJ}\ v_\ell^2)\ \omega\ -\ \nabla \cdot \vec{q}$$

$$-\frac{1}{J}\ \nabla \cdot P\vec{v} - \frac{1}{gJ}\ \nabla \cdot (\tau \cdot \vec{v}) \qquad \text{(A-3c)}$$

Expanding and rearranging with

$$\nabla \cdot \vec{q} = -\lambda \nabla^2 T,$$

$$\vec{v} \cdot \nabla v^2 = \vec{v} \cdot \left[2(\vec{v} \cdot \nabla)\ \vec{v} \right]$$

the energy equation can written

$$\rho C_v \frac{\partial T}{\partial t} = -\rho C_v (\vec{v} \cdot \nabla)\ T + \lambda \nabla^2 T - \frac{1}{J}\ \nabla \cdot P\vec{v}\ -\frac{1}{gJ}\ \nabla \cdot (\tau \cdot \vec{v})$$

$$-\frac{1}{J}\vec{F}_D \cdot \vec{v}_\ell + \left(U_\ell - \frac{1}{2gJ}(v^2 - v_\ell^2) - C_v T \right) \omega$$

$$-\frac{1}{2gJ}\ \rho \left[\frac{\partial (v)^2}{\partial t}\ + \vec{v} \cdot \nabla\ (v^2) \right] \qquad \text{(A-3d)}$$

Now, dotting the momentum equation, (A- 2) with the gas velocity, $\vec{v}$, and dividing by gJ we get

$$\frac{1}{gJ}\rho\vec{v}\cdot\frac{\partial\vec{v}}{\partial t} = -\frac{1}{gJ}\rho\vec{v}\cdot(\vec{v}\cdot\nabla)\vec{v} - \frac{1}{gJ}\vec{v}\cdot(\vec{v}-\vec{v}_\ell)\,\omega$$

$$-\frac{1}{J}\vec{v}\cdot\vec{F}_D - \frac{1}{J}\vec{v}\cdot\nabla P - \frac{1}{gJ}\vec{v}\cdot(\nabla\cdot\tau)$$

Substracting the momentum equation (dotted with $\vec{v}$) from the energy equation (A-3d) we get

$$\rho C_v\frac{\partial T}{\partial t} = -\rho C_v(\vec{v}\cdot\nabla)T + \lambda\nabla^2 T - \frac{P}{J}\nabla\cdot\vec{v} - \frac{1}{gJ}\tau:\nabla\vec{v}$$

$$+\frac{1}{J}\vec{F}_D\cdot(\vec{v}-\vec{v}_\ell) + \left[U_\ell - \frac{1}{2gJ}(v^2-v_\ell^2) - C_vT + \frac{1}{gJ}\vec{v}\cdot(\vec{v}-\vec{v}_\ell)\right]\omega \qquad \text{(A-3e)}$$

Combining velocity terms, the last expression is

$$\left[U_\ell - C_vT + \frac{1}{2gJ}(v_\ell^2 - v^2 + 2v^2 - 2\vec{v}\cdot\vec{v}_\ell)\right]\omega$$

$$= \left[U_\ell - C_vT + \frac{1}{2gJ}(\vec{v}-\vec{v}_\ell)\cdot(\vec{v}-\vec{v}_\ell)\right]\omega$$

therefore, the final energy equation, with drag is

$$\rho C_v\frac{\partial T}{\partial t} = -\rho C_v(\vec{v}\cdot\nabla)T + \lambda\nabla^2 T - \frac{P}{J}\nabla\cdot\vec{v} - \frac{1}{gJ}\tau:\nabla\vec{v}$$

$$+\frac{1}{J}\vec{F}_D\cdot(\vec{v}-\vec{v}_\ell) + \omega\left[U_\ell - C_vT + \frac{1}{2gJ}(\vec{v}-\vec{v}_\ell)\cdot(\vec{v}-\vec{v}_\ell)\right] \qquad \text{(A-3)}$$

Nondimensionalized Equations

Following the transformations of reference 1

$$
\begin{aligned}
t' &= ta_o/r_{an} & p' &= P/P_o & r'_d &= \frac{r_d}{r_{an}} \\
\nabla' &= r_{an}\nabla & \tau' &= \tau r_{an}/\mu_o a_o & & \\
\omega' &= \omega/\omega_o & T' &= T/T_o & & \\
\rho' &= \rho/\rho_o & v' &= v/a_o & &
\end{aligned}
\tag{A-4}
$$

the nondimensionalized transport equations are:

Continuity. -

$$
\frac{\partial \rho'}{\partial t'} = - \nabla' \cdot \rho' v' + \left| \frac{r_{an}\omega_o}{\rho_o a_o} \right| \omega' \tag{A-5}
$$

Momentum. -

$$
\rho' \frac{\partial \vec{v}}{\partial t'} = - \rho' (\vec{v}' \cdot \nabla') v' - \left| \frac{g \bar{P}_c}{\rho_o a_o} \right| \nabla' P' - \left| \frac{\mu}{r_{an} \rho_o a_o} \right| \nabla' \tau'
$$

$$
- \left| \frac{r_{an}\omega_o}{\rho_o a_o} \right| (\vec{v}' - \vec{v}'_\ell)\, \omega' - \left| \frac{3\, C_o \mathfrak{F}_p r_{an}}{8 \quad r_d} \right| \rho' \frac{(\vec{v}' - \vec{v}'_\ell) \left| \vec{v}' - \vec{v}'_\ell \right|}{r'_d} \tag{A-6}
$$

Energy. -

$$
\rho' \frac{\partial T'}{\partial t'} = - \rho' (v' \cdot \nabla')\, T' + \left| \frac{\lambda}{r_{an} \rho_o C_v a_o} \right| \nabla'^2 T' - \left| \frac{\bar{P}_c}{\rho_o C_v T_o J} \right| P' \nabla' \cdot \vec{v}'
$$

$$
- \left| \frac{a_o \mu}{r_{an} \rho_o C_v T_o g J} \right| \tau' : \nabla' \vec{v}' + \left| \frac{\omega_o r_{an}}{\rho_o a_o} \right| \omega' \left[\frac{U_\ell}{C_v T_o} - T' + \left(\frac{a_o^2}{2 g J c_v T_o} \right) \left| (\vec{v}' - \vec{v}'_\ell) \right|^2 \right]
$$

$$
+ \left| \frac{3\, \mathfrak{F}_p C_D r_{an}\, a_o^2}{8\, g J C_v T_o\, r_d} \right| \rho' \frac{(\vec{v}' - \vec{v}'_\ell) \left| \vec{v}' - \vec{v}'_\ell \right|}{r'_d} \cdot (\vec{v}' - \vec{v}'_\ell) \tag{A-7}
$$

Following Priem's assumptions and substitutions and with the addition

$$\mathcal{B} = \frac{3\, C_D\, \mathcal{F}_p\, r_{an}}{8\, r_d} \quad \text{and} \quad \frac{a_o^2}{C_v\, T_o\, g\mathcal{J}} = \gamma\,(\gamma-1)$$

we get final transport equations

Continuity. -

$$\frac{\partial \rho'}{\partial t'} = -\nabla' \cdot \rho' \vec{v}' + \boldsymbol{\omega}'\, \mathcal{L}\, f\,(\gamma) \tag{A-8}$$

Momentum. -

$$\rho' \frac{\partial \vec{v}'}{\partial t'} = -\rho' (\vec{v}' \cdot \nabla')\, \vec{v}' - \frac{1}{\gamma}\, \nabla' P' - \mathcal{J} f(\gamma)\, \nabla' \cdot \tau'$$

$$-(\vec{v}' - \vec{v}_\ell')\, \boldsymbol{\omega}'\, \mathcal{L} f(\gamma) - \mathcal{B} \rho' \frac{(\vec{v}' - \vec{v}_\ell')\, |\vec{v}' - \vec{v}_\ell'|}{r_d'} \tag{A-9}$$

Energy. -

$$\rho' \frac{\partial T'}{\partial t'} = -\rho' (\vec{v} \cdot \nabla')\, T' + \nabla'^2 T\, \mathcal{J} f(\gamma) - |\gamma - 1|\, P' \nabla' \cdot \vec{v}'$$

$$-|\gamma(\gamma-1)|\, \mathcal{J} f(\gamma)\, \tau' : (\nabla' \vec{v}') + \mathcal{L} f(\gamma)\, \boldsymbol{\omega}' \left[\gamma - T' + \frac{(\gamma-1)\gamma}{2} |\vec{v}' + \vec{v}_\ell'|^2 \right]$$

$$+|\gamma(\gamma-1)|\, \mathcal{B} \rho' \frac{|\vec{v}' - \vec{v}_\ell'|\, (\vec{v}' - \vec{v}_\ell')}{r_d'} \cdot (\vec{v}' - \vec{v}_\ell') \tag{A-10}$$

Annular Model

Transport Equations. - Assuming

1) No radial velocity or derivatives $v_r = 0$, $\partial v_r / \partial r = 0$, etc.
2) No variation of axial velocity around the annulus $\partial v_z / \partial \theta = 0$
3) No second derivatives in the axial direction, $\partial^2 (\,) / \partial z^2 = 0$.
4) $r_c = r_{an}$ $r' = 1$,

the nondimensional transport equations for the annular model, including drag are:

Continuity. -

$$\frac{\partial \rho'}{\partial t'} = -\rho'\left(\frac{\partial v'_\theta}{\partial \theta'} + \frac{\partial v'_z}{\partial z'}\right) - v'_\theta \frac{\partial \rho'}{\partial \theta'} - v'_z \frac{\partial \rho'}{\partial z'} + \omega' \mathcal{L} f(\gamma) \tag{A-11}$$

Momentum (θ-direction). -

$$\rho' \frac{\partial v'_\theta}{\partial t'} = -\rho' v'_\theta \frac{\partial v'_\theta}{\partial \theta'} - \frac{1}{\gamma} \frac{\partial P'}{\partial \theta'} + \mathcal{J} f(\gamma) \frac{4}{3} \frac{\partial^2 v'_\theta}{\partial \theta'^2}$$

$$- v'_\theta \omega' \mathcal{L} f(\gamma) - \mathcal{B} \rho' \frac{|v'_\theta| (v'_\theta)}{r'_d} \tag{A-12a}$$

Momentum (z-direction). -

$$0 = -\rho' v'_z \frac{\partial v'_z}{\partial z'} - \left|\frac{1}{\gamma}\right| \frac{\partial p'}{\partial z'} - \mathcal{L} f(\gamma) (v_z' - v'_{\ell,z}) \omega'$$

$$- \mathcal{B} \rho' \frac{|v'_z - v'_{\ell,z}| (v'_z - v'_{\ell,z})}{r'_d} \tag{A-12b}$$

Energy. -

$$\rho' \frac{\partial T'}{\partial t'} = -\rho' \left(v'_\theta \frac{\partial T'}{\partial \theta'} + v'_z \frac{\partial T'}{\partial z'}\right) + \mathcal{J} f(\gamma) \frac{\partial^2 T'}{\partial \theta'^2} - |\gamma - 1| P' \left(\frac{\partial v'_\theta}{\partial \theta'} + \frac{\partial v'_z}{\partial z'}\right)$$

$$+ \frac{4}{3} |\gamma(\gamma-1)| \mathcal{J} \left[\left(\frac{\partial v'_\theta}{\partial \theta'}\right)^2 + \left(\frac{\partial v'_z}{\partial z'}\right)^2 - \frac{\partial v'_\theta}{\partial \theta'} \frac{\partial v'_z}{\partial z'}\right] f(\gamma)$$

$$+ \mathcal{L} f(\gamma) \omega' \left\{\gamma - T' + \frac{(\gamma-1)\gamma}{2}\left[v''^2_\theta + (v'_z - v'_{\ell,z})^2\right]\right\}$$

$$+ |\gamma(\gamma-1)| \mathcal{B} \rho' \left[v'^2_\theta + (v'_z - v'_{\ell,z})^2\right]^{3/2} \tag{A-13}$$

z Derivatives (Integrated Equations). -

To determine the derivatives in the axial direction, the conservation equations are integrated over the volume of the annulus. Since there is no variation in the axial and radial direction, the equations only have to be integrated in the θ-direction to apply the conservation equations to the entire system.

Continuity. -

$$\int_0^{2\pi} \frac{\partial \rho'}{\partial t'}\, d\theta' = \int_0^{2\pi} \left[-\rho' \left(\frac{\partial v'_\theta}{\partial \theta'} + \frac{\partial v'_z}{\partial z'} \right) - v'_\theta \frac{\partial \rho'}{\partial z'} - v'_z \frac{\partial \rho'}{\partial z'} + \omega' \mathcal{L} f(\gamma) \right] d\theta' \tag{A-14}$$

Momentum (z-direction). -

$$0 = -\int_0^{2\pi} \left[\rho' v'_z \frac{\partial v'_z}{\partial z'} + \frac{1}{\gamma} \frac{\partial P'}{\partial z'} + \mathcal{L} f(\gamma) (v'_z - v'_{\ell,z}) \omega' + \mathcal{B} \rho' \frac{|v'_z - v'_{\ell,z}| (v'_z - v'_{\ell,z})}{r'_d} \right] d\theta' \tag{A-15}$$

Energy. -

$$\begin{aligned} \int_0^{2\pi} \rho' \frac{\partial T'}{\partial t'} = \int_0^{2\pi} \Bigg(& -\rho' \left(v'_\theta \frac{\partial T'}{\partial \theta'} + v'_z \frac{\partial T'}{\partial z'} \right) + \frac{\partial^2 T'}{\partial \theta'^2} \mathcal{J} f(\gamma) - (\gamma - 1) P' \left(\frac{\partial v'_\theta}{\partial \theta'} + \frac{\partial v'_z}{\partial z'} \right) \\ & + \frac{4}{3} \gamma (\gamma - 1) f(\gamma) \mathcal{J} \left[\left(\frac{\partial v'_\theta}{\partial \theta'} \right)^2 + \left(\frac{\partial v'_z}{\partial z'} \right)^2 - \frac{\partial v'_\theta}{\partial \theta'} \frac{\partial v'_z}{\partial z'} \right] \\ & + \omega' \mathcal{L} f(\gamma) \left\{ \gamma - T' + \frac{(\gamma - 1)\gamma}{2} \left[v'^2_\theta + (v'_z - v'_{\ell,z})^2 \right] \right. \\ & \left. + |\gamma (\gamma - 1)| \mathcal{B} \rho' \frac{\left[v'^2_\theta + (v'_z - v'_{\ell,z})^2 \right]^{3/2}}{r'_d} \right) \Bigg\} d\theta' \end{aligned} \tag{A-16}$$

Based on a theoretical order of magnitude analysis as well as confirmation in the numerical results, both terms containing the viscous dissipation parameter, $\mathcal{J}$, were found to be negligible (approximately five orders of magnitude less than the terms retained) when $\mathcal{J}$ is given a practical value of 3×10^{-8}. Noting that

$$\int \rho' d\theta' = \text{constant} = 2\pi \text{ and assuming no variation of mass,}$$

momentum or energy within the annulus with time and no variation in the small

distances, $\Delta r'_c$ and $\Delta z'$ as well as assuming that the axial derivatives of the flow properties do not vary around the annulus, we get the final integral equations for the z derivatives.

Continuity. -

$$0 = -2\pi \left[\frac{\partial v'_z}{\partial z'} + v'_z \frac{\partial \rho'}{\partial z'} \right] + \mathfrak{Sf}(\gamma) \int_0^{2\pi} \omega' d\theta' \tag{A-17}$$

Momentum - z direction. -

$$0 = 2\pi \frac{\partial v'_z}{\partial z'} v'_z + 2\pi \frac{1}{\gamma} \frac{\partial p'}{\partial z'}$$

$$+ \mathfrak{Sf}(\gamma) (v'_z - v'_{\ell,z}) \int_0^{2\pi} \omega' d\theta' + 2\pi \mathfrak{D} \frac{|v'_z - v'_{\ell,z}| (v'_z - v'_{\ell,z})}{r'_d} \tag{A-18}$$

Energy. -

$$0 = -2\pi \frac{\partial T'}{\partial z'} v'_z \int_0^{2\pi} \rho' v'_\theta \frac{\partial T'}{\partial \theta'} d\theta' - (\gamma-1) \frac{\partial v'_z}{\partial z'} \int_0^{2\pi} P' d\theta'$$

$$- (\gamma-1) \int_0^{2\pi} P' \frac{\partial v'_\theta}{\partial \theta'} d\theta' + \mathfrak{Sf}(\gamma) \int_0^{2\pi} \omega' \left\{ \gamma - T' + (\gamma-1) \frac{\gamma}{2} \left[v'^2_z + (v'_z - v'_{\ell,z})^2 \right] \right\} d\theta'$$

$$+ |\gamma(\gamma-1)| \mathfrak{D} \frac{1}{r'_d} \int_0^{2\pi} \rho' \left[v'^2_\theta + (v'_z - v'_{\ell,z})^2 \right]^{3/2} \tag{A-19}$$

APPENDIX B

DROP SPRAY DISTRIBUTION IN COMBUSTION INSTABILITY MODEL

Priem's original Annular Instability Model requires the selection of a single "representative" drop size and "representative" relative velocity at the position in the combustion chamber at which an annulus is to be examined. This selection is very difficult and is eliminated in the current modifications through the use of a drop size distribution. The Dynamic Science steady-state combustion computer program described in Reference (2) is used to analyze the change in an assumed initial drop distribution at the injector face as the drops travel through the chamber to the point of interest (the position of the annulus).

In treating a drop size distribution in the instability equations, the first question raised was whether to use an analytical expression for the distribution function or to use a summation over a number of drop groups. The advantages of an analytical expression are many:

An analytical distribution rather than a summation of drop groups is mathematically more appealing.

The computer time usage is not increased significantly over a single drop formulation, whereas if a summation over many drop groups was used, computer time usage would be increased several times.

Use of a distribution function assures that a uniquely important combination of variables such as size and velocity, which might not be evident in choosing particular drop groups, will not be omitted in the analysis.

The effect of changing parameters in the distribution function (mean drop radius, variance) as well as changing the form of the distribution function, can be determined easily.

The disadvantage of an analytical distribution is:

Formulation and integration of the various parameters containing the distribution function are more difficult than with a summation process.

The development of a drop size spray distribution model is presented in this appendix.

Distribution Function. - Simplified Functional Dependence (see Williams, Reference (7), for basic concepts.)

A spray of liquid drops in a combustion chamber (fuel and oxidizer) will have a distribution of drop sizes, drop velocities, and drop positions at any time. In general, then, the number of drops within a size range, dr, about $\vec{r}$, and within a spatial position range $d\vec{x}$ about $\vec{x}$, and velocity range, $d\vec{v}$, about $\vec{v}$, at a time t, will be given by the general distribution function.

$$dN = f_j(\vec{r},\vec{x},\vec{v},t)\,dr\,d\vec{x}\,d\vec{v}, \text{ where } j = o(\text{oxidizer}),\ f(\text{fuel})$$

and $$dN = \text{number of drops in } dr, d\vec{x}, d\vec{v}, \text{ at } t \qquad \text{(B-1)}$$

The distribution function, f_j, must be simplified for our model, since a general distribution for drop sprays is not known.

The first assumption will be that the drop velocity is dependent on drop size. In other words, a unique value of velocity will be assigned to a drop size at a position $\vec{x}$ and time, t, instead of a velocity distribution. This velocity then will be the average velocity $(\vec{v})$ of particles at x and r for a time t.

$$(\vec{v})_j = \frac{\int_o^\infty \vec{v} f_j d\vec{v}}{G_j} \qquad \text{(B-2)}$$

where $G_j = \int_o^\infty f_j\, d\vec{v}$ = number of drops in spatial range $d\vec{x}$ around $\vec{x}$ and radius range dr around r at time t.

For the one-dimensional annular model, the change in the drop spray distribution as a function of position within the annulus may be neglected. This is in keeping with the assumption of constant gas and liquid velocities across the annulus (axial). The proper distribution function is determined to correspond to specific values of $\vec{x}$ for a given annulus.

$$dN_j = f_j\,(r,t)\,dr\,dt \quad \text{at a given } \vec{x} \qquad \text{(B-3)}$$

The Dynamic Science steady-state combustion program is used to determine the change in an assumed distribution function between the injector face and the position of the annulus in question

The dependence of f_j on time may be very important in the ultimate solution of combustion instability problems. To account for this dependence, however, more than a one-dimensional annular model is required. Since the value of f_j must be specified at a particular annulus in question and held

constant across the annulus (very thin) the change in f_j with time must come from a nonsteady-state change in f_j between the injector face and the annulus in question. This is consistent with assuming that the annulus represents a portion (slice) of a wider region containing the total instability.

Inclusion of the time dependence of f_j will require a two-dimensional model (very wide annulus) or, at least, a cascade of thin annuli. For this reason, the change of f_j with time was neglected in our current one-dimensional model modification while realizing the importance of the assumption. Essentially, the assumption allows determination of the sensitivity of the annulus while the engine is operating at steady-state. This sensitivity changes, however, with a finite disturbance in engine operation.

The dependence of f_j reduces therefore to a single variable, size (given by radius r).

$$dN_j = f_j(r)\,dr \quad \text{at a specified value of } \vec{x} \tag{B-4}$$

Examining the transport equations derived in Appendix A (Equations A-8, A-9, A-10) the three variables assumed to represent the liquid spray are ω', $\mathcal{D}$, and v'_ℓ. Inclusion of a spray distribution in the model requires that these variables be specified as a function of the drop size distribution. The liquid velocity distribution of the spray, at the annulus under examination, is determined by the steady-state combustion program and is considered to be input to the instability model, that is

$$v_\ell = v_\ell(r) \text{ in equations A-8, A-9, A-10.}$$

Determination of $\mathcal{D}$ for the spray distribution is accomplished simply by noting that (subscript j is omitted for clarity)

$$\mathcal{D} = \frac{3}{8}\, C_D\, r_{an} \int_0^\infty \frac{d\mathcal{F}_p(r)}{r} \tag{B-5}$$

where

$$\mathcal{F}_p = \frac{\rho_\ell}{\rho_d} = \frac{\int_0^{N_0} \frac{4}{3}\pi r^3 \rho_d\, dN}{\rho_d} = \frac{4}{3}\pi \int_0^{N_0} r^3\, dN = \frac{4}{3}\pi \int_0^\infty r^3 f(r)\, dr$$

and

$$d\mathcal{F}_p(r) = \frac{4}{3}\pi r^3 f(r)\, dr$$

Therefore

$$\mathcal{D} = \frac{3}{8} C_D r_{an} \int_0^\infty \frac{4}{3} \pi r^2 f(r) dr$$

$$= \frac{1}{2} \pi C_D r_{an} \int_0^\infty r^2 f(r) dr \qquad \text{(B-6)}$$

Here again, $\mathcal{D}$ is determined independently of the flow disturbance since the spray distribution function is assumed to remain constant. Once a distribution function has been chosen, the drag parameter is computed with equation (B-6) and is used as input to the numerical solution.

The burning rate response function, ω', must be evaluated at each mesh point during the numerical solution, and is dependent on the drop size. In terms of the distribution function

$$\omega' = \frac{\int_0^\infty w(r) f(r) dr}{\int_0^\infty w_o(r) f(r) dr} \qquad \text{(B-7)}$$

where w is the burning w is the burning rate of a drop of size r and determined, as in References (1) and (8), as

$$w = K \frac{1}{r} \left[2 + 0.6 S_c^{1/3} \left(\frac{2r |\vec{v} - \vec{v}_\ell| \rho}{\mu} \right)^{1/2} \right] \qquad \text{(B-8)}$$

and

$$w_o = K \frac{1}{r} \left[2 + 0.6 S_c^{1/3} \left(\frac{2r |\vec{v}_o - \vec{v}_{\ell,o}| \rho}{\mu} \right)^{1/2} \right] \qquad \text{(B-9)}$$

where

$$K = \frac{D M_\ell S_{dr} \alpha}{2RT} P_v = \text{constant}$$

or in terms of an annular model, and with

$$Re_d = \frac{2r \rho_o a_o}{\mu}$$

the burning rate for a drop is

$$w = K\frac{1}{r}\left[2+0.6\,S_c^{1/3}(\rho')^{1/2}\left|(v'_\theta)^2+\Delta v'(r)^2\right|^{1/4}\mathrm{Re}_d(r)^{1/2}\right] \tag{B-10}$$

and

$$w_o = K\frac{1}{r}\left[2+0.6\,S_c^{1/3}\,\Delta v'(r)^{1/2}\,\mathrm{Re}_d(r)^{1/2}\right] \tag{B-11}$$

therefore, substituting into equation (B-7), the total burning response for the spray is

$$\omega' = \frac{\int_o^\infty \frac{1}{r}\left[2+0.6\,S_c^{1/3}(\rho')^{1/2}\left|(v'_\theta)^2+\Delta v'(r)^2\right|^{1/4}\mathrm{Re}_d(r)^{1/2}\right]f(r)\,dr}{\int_o^\infty \frac{1}{r}\left[2+0.6\,S_c^{1/3}\Delta v'(r)^{1/2}\,\mathrm{Re}_d(r)^{1/2}\right]f(r)\,dr} \tag{B-12}$$

For the numerical solution of the instability equations a logarithmiconormal distribution function was chosen such that

$$f(r) = \frac{dN}{dr} = \frac{a}{r}\exp\left\{-\frac{1}{2}\left[\frac{\ell n\left(\frac{r}{r_n}\right)}{\ell n\,\sigma_G}\right]^2\right\}$$

where $a = \dfrac{1}{\sqrt{2\pi}\;\ell n\,\sigma_G}$

A logarithmiconormal distribution was chosen because our steady-state combustion program, which is used to supply the instability parameters at a particular annular position in a real engine, is based on a logarithmiconormal distribution of drops at the injector face. It was determined that the distribution of drop sizes remained nearly logarithmiconormal at typical sensitive annular positions, although the number mean drop radius and geometric standard deviation had changed. It was therefore a convenience, rather than an experimental reality, that led us led us to use a logarithmiconormal distribution. Any other mathematical expression for the size distribution could have been used; however, no criterion for choosing the best one has been established.

APPENDIX C

BIPROPELLANT ANNULAR COMBUSTION INSTABILITY MODEL

A derivation is presented in this appendix for the transport equations describing unsteady combustion of a bipropellant system. The vaporization response of both propellants is considered in determining the amount of mass and heat added to the gas system. With this formulation, it is not necessary to assume that all of the mass of liquid propellant vaporized, in response to a disturbance, is burned. Aerodynamic droplet drag has been included in the equations in a manner similar to that of Appendix A.

In defining the dependent variables of the equations it is possible to interpret the mass and energy transport in several ways. In Priem's equations, the mass entering a unit volume consists of burned material (gas) and unburned material (liquid or gas) as defined in Reference 1, with the subscript "ℓ" representing unburned material. In deriving the equations, however, it is necessary to assume that the velocity of the unburned material is constant as well as the temperature of the unburned material. Also, the terms representing the rate of accumulation of mass, momentum, or energy contain only product gases (burned material) and exclude unburned gases as well as liquid propellants.

Since the velocity and temperature of the unburned gases will be identical to the velocity and temperature of the burned gases, it is difficult to justify the above assumptions. For this reason, and others, which are related directly to the bipropellant formulations, we have chosen to consider a division of mass entering a unit volume as consisting of gases (burned and unburned) and liquid propellants. With this in mind the derivation of the transport equations follow.

Transport Equations for a Bipropellant Model

Equation of Continuity. - A mass balance equation may be easily written for two phase reacting flow through a stationary unit volume as,

$$\left(\begin{array}{c}\text{Rate of mass}\\ \text{accumulation}\end{array}\right) = \left(\begin{array}{c}\text{Net rate}\\ \text{of mass in}\end{array}\right)$$

where the rate of accumulation of mass within the volume is

$$\frac{\partial}{\partial t}\left[\rho + \rho_f + \rho_{ox}\right]$$

$$\rho = \text{gas density}\left[\frac{\#\ \text{gas}}{\text{unit volume of mixture}}\right]$$

$$\rho_f = \underline{\text{liquid}} \text{ fuel density } \left[\frac{\#\text{ fuel}}{\text{unit volume of mixture}}\right]$$

$$\rho_{ox} = \underline{\text{liquid}} \text{ oxidizer density } \left[\frac{\#\text{ oxidizer}}{\text{unit volume of mixture}}\right]$$

Since it is reasonable to assume that the velocity of the liquid fuel and liquid oxidizer does not change within the volume, and that the flux of liquid propellant drops into the volume is a constant, there is no net accumulation of liquid propellant within the volume, hence

$$\left(\begin{matrix}\text{Rate of mass} \\ \text{accumulation}\end{matrix}\right) = \frac{\partial \rho}{\partial t}$$

The net rate of mass into the volume by convection is

$$-\nabla \cdot \rho \vec{v} - \nabla \cdot \rho_f \vec{v}_f - \nabla \cdot \rho_{ox} \vec{v}_{ox}$$

Therefore the continuity equation can be written as

$$\frac{\partial \rho}{\partial t} = -\nabla \cdot \rho \vec{v} - \nabla \cdot \rho_f \vec{v}_f - \nabla \cdot \rho_{ox} \vec{v}_{ox}$$

The last two terms represent the divergence of liquid fuel and liquid oxidizer from the unit volume, and will be called the vaporization rate (not the burning rate) for our model, ω_f and ω_{ox}.

The continuity equation is therefore written as

$$\frac{\partial \rho}{\partial t} = -\nabla \cdot \rho \vec{v} + \omega_f + \omega_{ox} \qquad \text{(C-1)}$$

where ω_f = vaporization rate of liquid fuel $\left[\frac{\#}{\text{sec in}^3}\right]$

ω_{ox} = vaporization rate of liquid oxidizer $\left[\frac{\#}{\text{sec in}^3}\right]$

Equation of Motion. -

$$\left(\begin{matrix}\text{Rate of} \\ \text{momentum} \\ \text{accumulation}\end{matrix}\right) = \left(\begin{matrix}\text{Net rate} \\ \text{of momen-} \\ \text{tum in}\end{matrix}\right) + \left(\begin{matrix}\text{Sum of forces} \\ \text{acting on} \\ \text{system}\end{matrix}\right)$$

The rate of accumulation of momentum is given by $\partial(\rho \vec{v})/\partial t$ where, again, the liquid velocity change is considered to be zero, and hence, the accumulations of momentum in the liquid phase is zero.

Considering the liquid fuel and liquid oxidizer separately, the influx of momentum is given by

$$\begin{pmatrix}\text{Net rate of}\\ \text{momentum in}\end{pmatrix} = -\nabla\cdot\rho\vec{v}\vec{v} - \nabla\cdot\rho_f\vec{v}_f\vec{v}_f - \nabla\cdot\rho_{ox}\vec{v}_{ox}\vec{v}_{ox}$$

The pressure forces and viscous forces remain the same as in equation (A-2a) of Appendix A, and therefore

$$\frac{\partial}{\partial t}(\rho\vec{v}) = -\nabla\cdot\rho\vec{v}\vec{v} - \nabla\cdot\rho_f\vec{v}_f\vec{v}_f - \nabla\cdot\rho_{ox}\vec{v}_{ox}\vec{v}_{ox} - g\nabla P - \nabla\cdot\tau \qquad \text{(C-2a)}$$

Since

$$\nabla\cdot\rho_f\vec{v}_f\vec{v}_f = \vec{v}_f\nabla\cdot\rho_f\vec{v}_f + \rho_f(\vec{v}_f\cdot\nabla)\vec{v}_f$$

in a manner similar to that of Appendix A. The divergence of momentum from the fuel is

$$\nabla\cdot\rho_f\vec{v}_f\vec{v}_f = -\vec{v}_f\omega + g\vec{F}_{D,f} \qquad \text{(C-2b)}$$

Similarly for the oxidizer

$$\nabla\cdot\rho_{ox}\vec{v}_{ox}\vec{v}_{ox} = \vec{v}_{ox}\nabla\cdot\rho_{ox}\vec{v}_{ox} = -\vec{v}_{ox}\omega_{ox} + g\vec{F}_{D,ox} \qquad \text{(C-2c)}$$

and therefore the momentum equation is

$$\frac{\partial\rho\vec{v}}{\partial t} = -\nabla\cdot\rho\vec{v}\vec{v} + \vec{v}_f\omega_f + \vec{v}_{ox}\omega_{ox} - g\vec{F}_{D,f} - g\vec{F}_{D,ox} - g\nabla P - \nabla\cdot\tau \qquad \text{(C-2d)}$$

Expanding the first two terms of the above equation and using the continuity equation we get

$$\rho\frac{\partial\vec{v}}{\partial t} = -\rho(\vec{v}\cdot\nabla)\vec{v} - (\vec{v}-\vec{v}_f)\omega_f - (\vec{v}-\vec{v}_{ox})\omega_{ox} - g\vec{F}_{D\,f} - g\vec{F}_{D,ox} - g\nabla P - \nabla\cdot\tau \qquad \text{(C-2)}$$

Energy Equation. -

$$\begin{pmatrix}\text{Rate of accumulation}\\ \text{of internal and kinetic}\\ \text{energy}\end{pmatrix} = \begin{pmatrix}\text{Net rate of internal and}\\ \text{kinetic energy in}\\ \text{by convection}\end{pmatrix}$$

$$+\begin{pmatrix}\text{Net rate of heat}\\ \text{addition}\\ \text{by conduction}\end{pmatrix} - \begin{pmatrix}\text{Net rate of work}\\ \text{done by system on}\\ \text{surroundings}\end{pmatrix}$$

Neglecting liquid accumulation, the rate of accumulation of internal and kinetic energy is given by

$$\left(\begin{array}{l}\text{Rate of accumulation}\\ \text{of internal and}\\ \text{kinetic energy}\end{array}\right) = \frac{\partial}{\partial t}\left(\rho c_v T + (1/2gJ)\rho v^2\right)$$

Energy is convected into and out of the stationary unit volume in the form of internal and kinetic energy of both the liquid and gas phases. The expression for the net convection into the volume of internal and kinetic energy is given by

$$\left(\begin{array}{l}\text{Net rate of internal and kinetic}\\ \text{energy in by convection}\end{array}\right) = -\nabla\cdot\rho\vec{v}\left(c_v T + \frac{1}{2gJ}v^2\right) - \nabla\cdot\rho_f\vec{v}_f\left(U_f + \frac{1}{2gJ}v_f^2\right)$$

$$- \nabla\cdot\rho_{ox}\vec{v}_{ox}\left(U_{ox} + \frac{1}{2gJ}v_{ox}^2\right)$$

Heat addition by conduction as well as work done by pressure and viscous forces (neglecting gas particle drag) results in an energy equation of the form

$$\frac{\partial}{\partial t}\left(\rho c_v T + \frac{1}{2gJ}\rho v^2\right) = -\nabla\cdot\rho\vec{v}\left(c_v T + \frac{1}{2gJ}v^2\right) - \nabla\cdot\rho_f\vec{v}_f\left(U_f + \frac{1}{2gJ}v_f^2\right)$$

$$-\nabla\cdot\rho_{ox}\vec{v}_{ox}\left(U_{ox} + \frac{1}{2gJ}v_{ox}^2\right) - \nabla\cdot\vec{q} \qquad \text{(C-3)}$$

$$-\frac{1}{J}\nabla\cdot P\vec{v} - \frac{1}{gJ}\nabla\cdot(\tau\cdot\vec{v})$$

The divergence of total energy (internal + kinetic energy) from the liquid fuel phase is

$$\nabla\cdot\rho_f\vec{v}_f\left(U_f + \frac{1}{2gJ}v_f^2\right) = \rho_f\vec{v}_f\cdot\nabla\left(U_f + \frac{1}{2gJ}v_f^2\right) + \left(U_f + \frac{1}{2gJ}v_f^2\right)\nabla\cdot\rho_f\vec{v}_f \qquad \text{(C-4)}$$

since

$$\nabla\cdot\rho_f\vec{v}_f = -\omega_f$$

and for constant temperature but allowing for droplet drag

$$\nabla \quad U_f \qquad = 0$$

the divergence of energy from the liquid fuel phase is

$$\nabla \cdot \rho_f \vec{v}_f \left(U_f + \frac{1}{2gJ} v_f^2 \right) = - \left(U_f + \frac{1}{2gJ} v_f^2 \right) \omega_f + \frac{1}{J} \vec{F}_{D,f} \cdot \vec{v}_f \qquad \text{(C-5a)}$$

and similarly for the oxidizer

$$\nabla \cdot \rho_{ox} \vec{v}_{ox} \left(U_{ox} + \frac{1}{2gJ} v_{ox}^2 \right) = - \left(U_{ox} + \frac{1}{2gJ} v_{ox}^2 \right) \omega_{ox} + \frac{1}{J} \vec{F}_{D,ox} \cdot \vec{v}_{ox} \qquad \text{(C-5b)}$$

Substituting for the liquid phase divergence and letting

$$\nabla \cdot \vec{q} \; = \; - \lambda \, \nabla^2 T$$

the energy equation may be written as

$$\frac{\partial}{\partial t} \left(\rho C_v T + \frac{1}{2gJ} \rho v^2 \right) = - \nabla \cdot \rho \vec{v} \left(C_v T + \frac{1}{2gJ} v^2 \right) + \lambda \nabla^2 T - \frac{1}{J} \nabla \cdot P \vec{v} - \frac{1}{gJ} \nabla \cdot (\tau \cdot \vec{v})$$

$$+ \omega_t U_t + \frac{1}{2gJ} \left(\omega_f v_f^2 + \omega_{ox} v_{ox}^2 \right) - \frac{1}{J} \left(F_{D,f} \cdot \vec{v}_f + F_{D\,ox} \cdot \vec{v}_{ox} \right) \qquad \text{(C-6)}$$

where $\omega_t U_t = \omega_f U_f + \omega_{ox} U_{ox}$

Combining equation (C-6) with the continuity and momentum equations, (C-1, C-2) we get

$$\rho C_v \frac{\partial T}{\partial t} = - \rho C_v \left(\vec{v} \cdot \nabla \right) T + \lambda \nabla^2 T - \frac{P}{J} \nabla \cdot \vec{v} \; - \; \frac{1}{gJ} \; \tau : \nabla \vec{v} + \omega_t (U_t - C_v T) + \frac{1}{J} \vec{F}_{D,f} \cdot (\vec{v} - \vec{v}_f)$$

$$+ \frac{1}{J} F_{D,ox} \cdot (\vec{v} - \vec{v}_{ox}) + \frac{1}{2gJ} \left[\omega_f (\vec{v}_f - \vec{v}) \; (\vec{v}_f - \vec{v}) + \omega_{ox} (\vec{v}_{ox} - \vec{v}) \cdot (\vec{v}_{ox} - \vec{v}) \right] \qquad \text{(C-7)}$$

The specific internal energy of each propellant is given by

$$U_f \quad = \quad C_{v,f} T_f + \Delta H_f$$

$$U_{ox} \quad = \quad C_{v,ox} T_{ox}$$

for a fuel controlled system, and by

$$U_f = C_{v,f} T_f$$

$$U_{ox} = C_{v,ox} T_{ox} + 1/\Phi_s \, \Delta H_f \, , \quad \Phi_s = (\mathcal{O}/\mathcal{F})_{\text{stoichiometric}}$$

for an oxidizer controlled system where

U_f = specific interval energy of the fuel including the thermal energy given by $C_{v,f} T_f$, and <u>if the fuel is the controlling propellant</u>, the chemical energy released when the fuel reacts with the oxidizer at stoichiometric portions.

U_{ox} = specific internal energy of the oxidizer including the thermal energy given by $C_{v,ox} T_{ox}$, and <u>if the oxidizer is the controlling propellant</u>, the chemical energy released when one pound of oxidizer reacts with a stoichiometric portion of fuel.

An explanation of the above definitions of the internal energies of the liquid propellants is needed. Consider first a system controlled by the vaporization rate of the fuel. In this case each pound of fuel vaporized is instantly burned with a stoichiometric amount of oxidizer which is present in abundance. The energy released to the gas phase by the vaporization of fuel consists, therefore, of the internal thermal energy ($C_{v,f} T_f$) and the chemical energy release when one pound of fuel is burned, ΔH_f. Vaporization of the oxidizer, however, contributes only thermal energy ($C_{v,ox} T_{ox}$) to the gas phase, since the chemical energy of combustion has already been considered.

If the oxidizer is the controlling propellant then for each pound of oxidizer that is vaporized, the energy added to the gas phase will be $c_{v,ox} T_{ox}$ plus the energy released when one pound of oxidizer burns with a stoichiometric amount of fuel. Vaporization of the fuel produces only thermal energy addition to the gas phase since the amount of fuel that can burn is limited by the amount of oxidizer vaporizing. Any fuel present in the gas phase, as unburned propellant also does not contribute to the chemical energy release, except as dictated by the oxidizer vaporization.

While the specific internal energy of both propellants remains constant, the specific internal energy of the propellant combination is dependent on the local instantaneous vaporization rate of both propellants, and is given by

$$U_t = \frac{\omega_f}{\omega_t} U_f + \frac{\omega_{ox}}{\omega_t} U_{ox} = U_f \left(\frac{1}{1+\Phi}\right) + U_{ox} \left(\frac{\Phi}{1+\Phi}\right) \qquad \text{(C-8)}$$

where Φ is the local instantaneous $\mathcal{O}/\mathcal{F}$.

With the above definitions for U_f and U_{ox} one of the two terms on the left side of Equation (C-8) is negligible in that most of the energy added to the flow is chemical energy, therefor

$$U_t \approx \frac{\omega_f}{\omega_t} U_f = U_f \left(\frac{1}{1+\Phi}\right) \text{ for fuel controlling}$$

and (C-9)

$$U_t \approx \frac{\omega_{ox}}{\omega_t} U_{ox} = U_{ox} \left(\frac{\Phi}{1+\Phi}\right) \text{ for oxidizer controlling}$$

Assuming a calorically perfect gas, the local instantaneous temperature of the bulk combustion gases may be expressed as a function of the energy released by the propellant combination as

$$U_t = C_p T = U_c \frac{\omega_c}{\omega_t}, \text{ where } c = \begin{cases} f & \text{for fuel controlling} \\ ox & \text{for oxidizer controlling} \end{cases}$$

Under steady-state conditions

$$U_{t,o} = C_p T_o = U_c \frac{\omega_{c,o}}{\omega_{t,o}}$$

therefore

$$U_t = U_{t,o} \left(\frac{\omega_c / \omega_{c,o}}{\omega_t / \omega_{t,o}}\right) = C_p T_o \left(\frac{\omega_c / \omega_{c,o}}{\omega_t / \omega_{t,o}}\right) \quad \text{(C-10)}$$

Nondimensional Equations

Using the same transformations as in Appendix A and with the above definition of U_t, we obtain the following transport equations

Continuity. -

$$\frac{\partial \rho'}{\partial t'} = - \nabla' \cdot \rho' \vec{v}' + \left|\frac{r_{an} \omega_{f,o}}{\rho_o a_o}\right| \omega'_f + \left|\frac{r_{an} \omega_{ox,o}}{\rho_o a_o}\right| \omega'_{ox} \quad \text{(C-11)}$$

Motion . -

$$\rho' \frac{\partial \vec{v}'}{\partial t'} = - \rho' (\vec{v}' \cdot \nabla') \vec{v}' - \left|\frac{g \bar{P}_c}{\rho_o a_o}\right| \nabla' p' - \left|\frac{\mu}{r_{an} \rho_o a_o}\right| \nabla' \cdot \tau'$$

$$- \left|\frac{r_{an} \omega_{f,o}}{\rho_o a_o}\right| \omega'_f (\vec{v}' - \vec{v}'_f) - \left|\frac{r_{an} \omega_{ox,o}}{\rho_o a_o}\right| \omega'_{ox} (\vec{v}' - \vec{v}'_{ox}) \quad \text{(C-12)}$$

$$- \left|\frac{3}{8} \frac{C_D \mathfrak{F}_{p,f} r_{an}}{r_{d,f}}\right| \rho' \frac{(\vec{v}' - \vec{v}'_f)|\vec{v}' - \vec{v}'_f|}{r'_{d,f}} - \left|\frac{3}{8} \frac{C_D \mathfrak{F}_{p,ox} r_{an}}{r_{d,ox}}\right| \rho' \frac{(\vec{v}' - \vec{v}'_{ox})|\vec{v}' - \vec{v}'_{ox}|}{r'_{d,ox}}$$

Energy. -

$$\rho' \frac{\partial T'}{\partial t'} = -\rho'(v' \cdot \nabla')\, T' + \left| \frac{\lambda}{r_{an} \rho_o c_v a_o} \right| \nabla'^2 T' - \left| \frac{\bar{P}_c}{\rho_o c_v T_o J} \right| P' \nabla' \cdot \vec{v}'$$

$$- \left| \frac{a_o}{r_{an} \rho_o c_v T_o g J} \right| \tau' : \nabla' \vec{v}' + \left| \frac{\omega_{t,o} r_{an}}{\rho_o a} \right| \omega'_t \left(\gamma \frac{\omega'_c}{\omega'_t} - T' \right)$$

$$+ \left(\frac{a_o^2}{2gJc_v T_o} \right) \left[\left| \frac{\omega_{f,o} r_{an}}{\rho_o a_o} \right| \omega'_f (\vec{v}'_f - \vec{v}')^2 + \left| \frac{\omega_{ox,o} r_{an}}{\rho_o a_o} \right| \omega'_{ox} (\vec{v}'_{ox} - \vec{v}')^2 \right]$$

$$+ \left| \frac{3}{8} \frac{\mathfrak{F}_{p,f} C_D r_{an} a_o^2}{gJ C_v T_o r_{d,f}} \right| \rho' \frac{(\vec{v}' - \vec{v}'_f) |\vec{v}' - \vec{v}'_f|}{r'_{d,f}} \cdot (\vec{v} - \vec{v}'_f)$$

$$+ \left| \frac{3}{8} \frac{\mathfrak{F}_{p,ox} C_D r_{an} a_o^2}{gJ C_v T_o r_{d,ox}} \right| \rho' \frac{(\vec{v}' - \vec{v}_{ox}) |\vec{v}' - \vec{v}'_{ox}|}{r'_{d,ox}} \cdot (\vec{v}' - \vec{v}'_{ox}) \qquad \text{(C-13)}$$

Following the approximations of Reference (1) and noting that

$$\left| \frac{\omega_{f,o} r_{an}}{\rho_o a_o} \right| \approx \left| \frac{m_f \dot{W}_f r_{an}}{\mathcal{A} \dot{W}_t} \right| f(\gamma) = \left| \frac{m_f r_{an}}{\mathcal{A}} \frac{1}{1+\Phi_I} \right| f(\gamma) \equiv \mathfrak{L}_f f(\gamma)$$

$$\left| \frac{\omega_{ox,o} r_{an}}{\rho_o a_o} \right| \approx \left| \frac{m_{ox} \dot{W}_{ox} r_{an}}{\mathcal{A} \dot{W}_t} \right| f(\gamma) = \left| \frac{m_{ox} r_{an}}{\mathcal{A}} \frac{\Phi_I}{1+\Phi_I} \right| f(\gamma) \equiv \mathfrak{L}_{ox} f(\gamma)$$

$$\mathfrak{L}_t = \mathfrak{L}_f + \mathfrak{L}_{ox}$$

the final nondimensional transport equations are

Continuity. -

$$\frac{\partial \rho'}{\partial t'} = -\nabla' \cdot \rho' \vec{v}' + \mathfrak{L}_t f(\gamma) \omega'_t \qquad \text{(C-14)}$$

Motion. -

$$\rho' \frac{\partial \vec{v}'}{\partial t'} = - \rho' (\vec{v}' \cdot \nabla') \vec{v}' - \frac{1}{\gamma} \nabla' P' - \mathcal{J} f(\gamma) \nabla' \cdot \tau'$$

$$- (\vec{v}' - \vec{v}_f') \omega_f' \mathcal{L}_f f(\gamma) - (\vec{v}' - \vec{v}_{ox}') \omega_{ox}' \mathcal{L}_{ox} f(\gamma) \qquad \text{(C-15)}$$

$$- \mathcal{B}_f \rho' \frac{(\vec{v}' - \vec{v}_f') \left| \vec{v}' - \vec{v}_f' \right|}{r_{d,f}'}$$

$$- \mathcal{B}_{ox} \rho' \frac{(\vec{v}' - \vec{v}_{ox}') \left| \vec{v}' - \vec{v}_{ox}' \right|}{r_{d,ox}'}$$

Energy. -

$$\rho' \frac{\partial T'}{\partial t'} = - \rho' (\vec{v}' \cdot \nabla') T' + \mathcal{J} \nabla'^2 T' f(\gamma) - |\gamma - 1| P' \nabla' \cdot \vec{v}'$$

$$- |\gamma(\gamma - 1)| \mathcal{J} f(\gamma) \tau' : (\nabla' \vec{v}') + \mathcal{L}_t f(\gamma) \omega_t' (\gamma \frac{\omega_c'}{\omega_t'} - T')$$

$$+ \frac{(\gamma - 1)\gamma}{2} f(\gamma) \left[\mathcal{L}_f \omega_f' (\vec{v}_f' - \vec{v}')^2 + \mathcal{L}_{ox} \omega_{ox}' (\vec{v}_{ox} - \vec{v}')^2 \right] \qquad \text{(C-16)}$$

$$+ \gamma(\gamma - 1) \left\{ \mathcal{B}_f \rho' \frac{\left| \vec{v}' - \vec{v}_f' \right| (\vec{v}' - \vec{v}_f')}{r_{d,f}'} \cdot (\vec{v}' - \vec{v}_f') \right.$$

$$\left. + \mathcal{B}_{ox} \rho' \frac{\left| \vec{v}' - \vec{v}_{ox}' \right| (\vec{v}' - \vec{v}_{ox}')}{r_{d,ox}'} \cdot (\vec{v}' - \vec{v}_{ox}') \right\}$$

Equation C-16 assumes that the steady state and instantaneous $\mathcal{O}/\mathcal{F}$ values are both on the same side of $\mathcal{O}/\mathcal{F}$ stoichiometric.

Annular Model

The transport equations for the bipropellant annular model, following the assumptions of Appendix A, are

Continuity. -

$$\frac{\partial \rho'}{\partial t'} = -\rho\left(\frac{\partial v'_\theta}{\partial \theta'} + \frac{\partial v'_z}{\partial z'}\right) - v'_\theta \frac{\partial \rho'}{\partial \theta'} - v'_z \frac{\partial \rho'}{\partial z'} + \mathcal{L}_{ox}\omega'_{ox} f(\gamma) + \mathcal{L}_f \omega'_f f(\gamma) \qquad \text{(C-17)}$$

Momentum (θ-direction). -

$$\rho' \frac{\partial v'_\theta}{\partial t'} = -\rho' v'_\theta \frac{\partial v'_\theta}{\partial \theta'} - \frac{1}{\gamma}\frac{\partial P'}{\partial \theta'} + \mathcal{J} f(\gamma)\frac{4}{3}\frac{\partial^2 v'_\theta}{\partial \theta'^2} \qquad \text{(C-18a)}$$

$$- v'_\theta\left[\omega'_f \mathcal{L}_f + \omega'_{ox}\mathcal{L}_{ox}\right] f(\gamma) - \left(\frac{\mathcal{D}_f}{r'_{d,f}} + \frac{\mathcal{D}_{ox}}{r'_{d,ox}}\right)\rho' |v'_\theta| v'_\theta$$

Momentum (z-direction). -

$$0 = -\rho' v'_z \frac{\partial v'_z}{\partial z'} - \left|\frac{1}{\gamma}\right| \frac{\partial P'}{\partial z'} - f(\gamma)(v'_z - v'_{f,z})\mathcal{L}_f \omega'_f - f(\gamma)(v'_z - v'_{ox,z})\mathcal{L}_{ox}\omega'_{ox}$$

$$-\mathcal{D}_f \rho' \frac{|v'_z - v'_{f,z}|(v'_z - v'_{f,z})}{r'_{d,f}} - \mathcal{D}_{ox}\rho' \frac{|v'_z - v'_{ox,z}|(v'_z - v'_{ox,z})}{r'_{d,ox}} \qquad \text{(C-18b)}$$

Energy. -

$$\rho' \frac{\partial T'}{\partial t'} = -\rho'\left(v'_\theta \frac{\partial T'}{\partial \theta'} + v'_z \frac{\partial T'}{\partial z'}\right) + \mathcal{J} f(\gamma)\frac{\partial^2 T'}{\partial \theta'^2} - |\gamma - 1| P'\left(\frac{\partial v'_\theta}{\partial \theta'} + \frac{\partial v'_z}{\partial z'}\right)$$

$$+ \frac{4}{3}|\gamma(\gamma-1)|\mathcal{J}\left[\left(\frac{\partial v'_\theta}{\partial \theta'}\right)^2 + \left(\frac{\partial v'_z}{\partial z'}\right)^2 - \frac{\partial v'_\theta}{\partial \theta'}\frac{\partial v'_z}{\partial z'}\right] f(\gamma)$$

$$+ \mathcal{L}_t \omega'_c f(\gamma)\gamma - (\mathcal{L}_{ox}\omega'_{ox} + \mathcal{L}_f \omega'_f) f(\gamma) T'$$

$$+ \frac{(\gamma-1)\gamma}{2} f(\gamma)\left\{\mathcal{L}_f \omega'_f\left[v'^2_\theta + (v'_z - v'_{f,z})^2\right] + \mathcal{L}_{ox}\omega'_{ox}\left[v'^2_\theta + (v'_z - v'_{ox,z})^2\right]\right\}$$

$$+ \gamma(\gamma-1)\rho'\left\{\mathcal{D}_f \frac{\left[v'^2_\theta + (v'_z - v'_{f,z})^2\right]^{3/2}}{r'_{d,f}} + \mathcal{D}_{ox}\frac{\left[v'^2_\theta + (v'_z - v'_{z,ox})^2\right]^{3/2}}{r'_{d,ox}}\right\}$$

(C-19)

z-Derivatives (integrated Equations).- Based on the same assumptions as in Appendix A, the integrated equations are

Continuity

$$0 = 2\pi \left[\frac{\partial v'_z}{\partial z'} + v'_z \frac{\partial \rho'}{\partial z'} \right] + f(\gamma)\mathcal{L}_f \int_0^{2\pi} \omega'_f d\theta + f(\gamma)\mathcal{L}_{ox} \int_0^{2\pi} \omega'_{ox} d\theta' \qquad \text{(C-20)}$$

Momentum - z direction

$$0 = 2\pi \frac{\partial v'_z}{\partial z'} v'_z + 2\pi \frac{1}{\gamma} \frac{\partial p'}{\partial z'}$$

$$+ f(\gamma)(v'_z - v'_{f,z}) \mathcal{L}_f \int_0^{2\pi} \omega'_f \, d\theta' + f(\gamma)(v'_z - v'_{ox,z})\mathcal{L}_{ox} \int_0^{2\pi} \omega'_{ox} d\theta' \qquad \text{(C-21)}$$

$$+ 2\pi \mathcal{B}_f \frac{|v'_z - v'_{f,z}|\,(v'_z - v'_{f,z})}{r'_d} + 2\pi \mathcal{B}_{ox} \frac{|v'_z - v'_{ox,z}|\,(v'_z - v'_{ox,z})}{r'_d}$$

Energy

$$0 = -2\pi \frac{\partial T'}{\partial z'} v'_z - \int_0^{2\pi} \rho' v'_\theta \frac{\partial T'}{\partial \theta'} d\theta' - (\gamma - 1) \frac{\partial v'_z}{\partial z'} \int_0^{2\pi} P' d\theta'$$

$$- (\gamma - 1) \int_0^{2\pi} P' \frac{\partial v'_\theta}{\partial \theta'} d\theta' + \mathcal{L}_t f(\gamma) \gamma \int_0^{2\pi} \omega'_c d\theta$$

$$- f(\gamma) \left[\mathcal{L}_{ox} \int_0^{2\pi} \omega'_{ox} T' d\theta' + \mathcal{L}_f \int_0^{2\pi} \omega'_f T' d\theta' \right]$$

$$+ \frac{(\gamma - 1)\gamma}{2} f(\gamma) \left\{ \mathcal{L}_f \int_0^{2\pi} \omega'_f \left[v'^2_\theta + (v'_z - v'_{f,z})^2 \right] d\theta' \right.$$

$$+ \mathcal{L}_{ox} \int_0^{2\pi} \omega'_{ox} \left[v'^2_\theta + (v'_z - v_{ox,z})^2 \right] d\theta' \qquad \text{(C-22)}$$

$$+ \gamma(\gamma - 1) \left\{ \frac{\mathcal{B}_f}{r_{d,f}} \int_0^{2\pi} \rho' \left[v'^2_\theta + (v'_z - v'_{f,z})^2 \right]^{3/2} d\theta' \right.$$

$$\left. \left. + \frac{\mathcal{B}_{ox}}{r_{d,ox}} \int_0^{2\pi} \rho' \left[v'^2_\theta + (v'_z - v'_{ox,z})^2 \right]^{3/2} d\theta' \right\} \right\}$$

APPENDIX D

COMPUTER PROGRAM DESCRIPTION

The bipropellant combustion instability model developed in Appendix C has been programmed in Fortran IV language and checked out for the CDC 6600 computer. The spray distribution model developed in Appendix B is contained in a separate computer program and has been checked out on the CDC 3600 computer.

The mathematical model, represented by equations (C14), (C15), (C16), is used for the analytical determination of the minimum pressure perturbation required to develop into a standing tangential instability wave within the combustion chamber.

The numerical methods used in the computer program can be illustrated by following the steps of the integration cycle. The first step determines the coefficients of the z derivatives followed by the actual determination of the z derivatives, $\partial v'_z/\partial z'$, $\partial \rho'/\partial z'$, and $\partial T'/\partial z'$. Once these values are known at time t'_n, partial derivatives with respect to t are then determined at t'_n. Employing the first order predictor relation:

$$\rho'_{n+1} = \rho'_n + \Delta t' \left(\frac{\partial \rho'}{\partial t'}\right)_n \tag{D1}$$

the solution is approximated at the next step in time.

Using the approximated values at t'_{n+1} the partial derivatives with respect to theta are then computed with the relation:

$$\left(\frac{\partial \rho'}{\partial \theta'}\right)_{n+1} = \frac{\rho'_{n+1,m+1} - \rho'_{n+1,m-1}}{2\Delta\theta'} \tag{D2}$$

where $\rho'_{n+1,m+1} = \rho'|(n+1)\,\Delta t', (m+1)\,\Delta\theta'|$, at each node around the annulus.

Once the theta derivatives at each node of the annulus at time t'_{n+1} are known, z derivatives and t derivatives to are recalculated and an implicit formula is used to iterate the approximated values at t'_{n+1}. The implicit iteration formula is:

$$\rho'_{n+1,m} = \rho'_{n,m} + \Delta t' \left(\frac{\partial \rho'}{\partial t'}\right)_{n+1,m}, \text{ for } 1 < m < ND \tag{D3}$$

where ND is the number of nodes. With the present Dynamic Science instability program the iterations are continued until convergence is achieved or the maximum number of iterations (4) is exceeded. The computations are then continued to the succeeding step.

The derivatives in the axial direction are determined with the assumption that the total mass, momentum, and energy in the annulus remain constant. Furthermore, it is assumed that these derivatives are independent of r and θ. These assumptions lead to equations (C20), (C21), and (C22), which permit evaluation of the derivatives taken with respect to z at each time step. Equations (C20), (C21), and (C22), may be represented by a system of nonlinear algebraic equations to be solved at each step (Δ t') in time, as follows:

$$a_1x_1 + a_2x_2 = c_1$$

$$a_4x_1 + a_5x_2 + a_6x_3 = c_2$$

$$a_7x_1 + a_8x_3 = c_3$$

where,

$$x_1 = \frac{\partial v_z'}{\partial z'}$$

$$x_2 = \frac{\partial \rho'}{\partial z'}$$

$$x_3 = \frac{\partial T'}{\partial z'}$$

Using the relation

$$2\pi \frac{\partial P'}{\partial z'} = 2\pi \frac{\partial T'}{\partial t'} + \frac{\partial \rho'}{\partial z'} \int_0^{2\pi} T' d\theta'$$

the coefficients are:

$$a_1 = 2\pi$$

$$a_2 = 2\pi v_z'$$

$$a_4 = 2\pi v_z'$$

$$a_5 = \frac{1}{\gamma} \int_0^{2\pi} T' d\theta'$$

$$a_6 = 2\pi/\gamma$$

$$a_7 = (\gamma-1)\int_0^{2\pi} P'\, d\theta'$$

$$a_8 = 2\pi v'_z$$

and;

$$c_1 = f(\gamma)\,\mathfrak{L}_f \int_0^{2\pi} \omega'_f\, d\theta' + f(\gamma)\,\mathfrak{L}_{ox}\int_0^{2\pi} \omega'_{ox}\, d\theta'$$

$$c_2 = -f(\gamma)\,\Delta v'_{f,z}\,\mathfrak{L}_f \int_0^{2\pi} \omega'_f\, d\theta' - f(\gamma)\,\Delta v'_{ox,z}\,\mathfrak{L}_{ox}\int_0^{2\pi} \omega'_{ox}\, d\theta'$$

$$- \frac{2\pi \mathfrak{D}_f |\Delta v'_{f,z}|\,\Delta v'_{f,z}}{r'_{d,f}} - \frac{2\pi \mathfrak{D}_{ox}|\Delta v'_{ox,z}|\,\Delta v'_{ox,z}}{r'_{d,ox}}$$

$$c_3 = -\int_0^{2\pi} \rho' v'_\theta \frac{\partial T'}{\partial \theta'}\, d\theta' - (\gamma-1)\int_0^{2\pi} P' \frac{\partial v'_\theta}{\partial \theta'}\, d\theta'$$

$$+ \mathfrak{L}_t\, f(\gamma)\,\gamma \int_0^{2\pi} \omega'_c\, d\theta'$$

$$- f(\gamma)\left[\mathfrak{L}_{ox}\int_0^{2\pi} \omega'_{ox}\, T'd\theta' + \mathfrak{L}_f \int_0^{2\pi} \omega'_f\, T'd\theta'\right]$$

$$+ \frac{(\gamma-1)}{2}\gamma f(\gamma)\left(\mathfrak{L}_f \int_0^{2\pi} \omega'_f [v'^2_\theta + \Delta v'^2_{f,z}]\, d\theta'\right.$$

$$\left. + \mathfrak{L}_{ox}\int_0^{2\pi} \omega'_{ox}[v'^2_\theta + \Delta v'^2_{ox,z}]\, d\theta'\right)$$

$$+ \gamma(\gamma-1)\left(\frac{\mathfrak{D}_f}{r'_{d,f}}\int_0^{2\pi} \rho[v'^2_\theta + \Delta v'^2_{f,z}]^{3/2}\, d\theta'\right.$$

$$\left. + \frac{\mathfrak{D}_{ox}}{r'_{d,ox}}\int_0^{2\pi} \rho[v'^2_\theta + \Delta v'^2_{ox,z}]^{3/2}\, d\theta'\right)$$

The solution of the above system is:

$$x_1 = \frac{c_2 - \frac{a_5 c_1}{a_2} - \frac{a_6 c_3}{a_8}}{a_4 - \frac{a_5 a_1}{a_2} - \frac{a_6 a_7}{a_8}}$$

$$x_2 = \frac{c_1 - a_1 x_1}{a_2}$$

$$x_3 = \frac{c_3 - a_7 x_1}{a_8}$$

For the droplet distribution modification an additional semi-infinite integral evaluation was necessary to evaluate the vaporization response, ω', as defined by Equation (B7). Since the integrand is an analytic function of r and hence can be evaluated at the roots of the Laguerre polynomials, Laguerre-Gaussian Quadrature formulae were used for the integration. The Laguerre-Gaussian formulae has the following form:

$$\int_0^\infty e^{-x} f(x)dx = \sum_{k=1}^{m} H_k f(x_k) + E. \tag{D4}$$

where x_i is the i^{th} zero of the m^{th} order Laguerre polynomial, L_m, and

$$H_i = \frac{(m!)^2}{L'_m(x_i) L_{m+1}(x_i)}. \tag{D5}$$

and

$$E = \frac{(m!)^2}{(2m!)} f^{(2m)}(\xi), \quad 0 < \xi < \infty. \tag{D6}$$

The Gaussian quadrature formulae require evaluation of the integrand at roots of the Laguerre polynomial as opposed to Simpson's rule which is normally used with equally spaced abscissae. However, since the integrand can be evaluated at the roots of the Laguerre polynomials this method has a $2m^{th}$ order

term while an equally spaced evaluation of the same order has an m^{th} order error. Therefore, greater accuracy can be obtained with fewer points and hence a significant improvement of computational time required to evaluate Equation (B7) can be made. The method is more suited for semi-infinite axis than an equal interval evaluation since the formula is specifically designed for the semi-infinite interval.

Figures D-1 and D-2 illustrate the common locations used in the combustion instability program. Figure D-3 describes the input card format required to run the program. Figure D-4 is a complete listing of the computer program used to generate the results of the drag studies and the bipropellant studies. For a more detailed discussion of the combustion instability program refer to the final report of NASA Contract NAS 7-366, Reference 2.

Following the computer program listing, Figures D-5 and D-6 show a sample case input and output. The complete listing of the output for the given case has not been included due to its length. The several steps of the integration have been included to display the typical step printout, as well as a pressure history summary.

Cell	Description	Cell	Description	Cell	Description
1	Initial Time (TI)	41	v'_z (VZ)	61	(SCR)
2	RKTIME (RKT)	42	$f(\gamma)$ (FGAM)	62	$\gamma(\gamma-1)/2.0$ (SIP)
3	Step Size (H)	43	$a_1 = 2\pi$ (A(1))	63	$\gamma(\gamma-1)$ (SIP2)
4	Step Size/2 (HO)	44	$a_2 = 2\pi v'_z$ (A(2))	64	
5	Min Step (HMIN)	45		65	$\mathcal{J}*f(\gamma)$ (BC)
6	Max Step (HMAX)	46	$a_4 = 2\pi v'_z$ (A(4))	66	$4/3*\mathcal{J}f(\gamma)$ (BZ)
7	Ho/2. (HZD2)	47	$a_5 = \frac{1}{\gamma}\int_0^{2\pi} T'd\theta'$ (A(5))	67	$Re_{d,f}$ (REFO)
8	Min Error (EMIN)	48	$a_6 = 2\pi/\gamma$ (A(6))	68	$Re_{d,ox}$ (REFD)
9	Max Error (EMAX)	49	$a_7 = (\gamma-1)\int_0^{2\pi} p'd\theta'$	69	$(Re_{d,ox})^{\frac{1}{2}}$ (SRD2)
10	Max CY ERR (E1)	50	$a_8 = 2\pi v'_z$	70	2(DTH) (D2)
11	Weight (WT(1))	51	c_1 (C(1))	71	$(DTH)^2$ (DSQ)
30	Weight (WT(20))	52	c_2 (C(2))	72	$(\Delta v'_{ox,z})^2$ (DELIV)
31	Time Stop (TSTOP)	53	c_3 (C(3))	73	
32	$\mathcal{L}=\mathcal{L}_f+\mathcal{L}_{ox}$ (XL)	54	Theta Step (DTH)	74	$\mathcal{L}_f$ (XLF)
33		55	$\partial v'/\partial z$ (X(1))	75	$\mathcal{L}_{ox}$ (XLO)
34	Parameter, $\mathcal{J}$ (XJ)	56	$\partial \rho'/\partial z$ (X(2))	76	$\Delta v'_{f,z}$ (VFZ)
35		57	$\partial T'/\partial z$ (X(3))	77	$\Delta v'_{ox,z}$ (VOZ)
36	γ (GAM)	58		78	$\mathcal{D}_f$ (DRAGF)
37	Init. Pres. Dist.(AP)	59	$(Re_{d,f})^{1/2}$ (SRD)	79	$\mathcal{D}_{ox}$ (DRAGO)
38		60	.6*Sc**1/3 (SCB)	80	(SCRO)
39	Schmidt No. (SC)				
40	$(\Delta v'_{f,z})^2$ (DEL2V)				

FIGURE D-1 - COMMON MAP (FC REGION)

Cell	Variable	Dim.	Description
1	P(1,1)	(2,161)	pressure
323	DPTH(1, 1)	(2,161)	$\partial P'/\partial\theta$
645	DTT (1,1)	(2,161)	$\partial T'/\partial t'$
967	DTTH (1,1)	(2,161)	$\partial T'/\partial\theta'$
1289	D2TTH (1,1)	(2,161)	$\partial^2 T'/\partial\theta'^2$
1611	DRHOT (1,1)	(2,161)	$\partial\rho'/\partial t'$
1933	DRHOTH (1,1)	(2,161)	$\partial\rho'/\partial\theta'$
2255	DVT (1,1)	(2,161)	$\partial v_z'/\partial t'$
2577	DVTH (1,1)	(2,161)	$\partial v_z'/\partial\theta'$
2899	D2VTH (1,1)	(2,161)	$\partial^2 v_z'/\partial\theta'^2$
3221	WZ(1,1)	(2,161)	
3543	W(1,1)	(40,161)	Burning Rate

(BC REGION)

1	T	(3,161)	T', Temperature
484	RHO	(3,161)	ρ', Density
967	V	(3,161)	v_z' Velocity

(BE REGION)

FIGURE D-2. COMMON MAP (BC REGION), (BE REGION)

FORTRAN CODING FORM

PROGRAM | CONTROL DATA CORPORATION | NAME

ROUTINE | DATE | PAGE | OF

TYPE | STATEMENT NO. | CONT. | FORTRAN STATEMENT (0 = ZERO, Ø = ALPHA O; 1 = ONE, I = ALPHA I; 2 = TWO, Z = ALPHA Z) | SERIAL NUMBER

HEADER CARD (Leave Column 1 Blank) — Card #1, 12A6

					Card #2, 6 E12.8
initial pressure disturbance AP	$\mathcal{L}_f$ XLF	$\mathcal{L}_{ox}$ XLO	$Re_{d,f}$ REFD	$Re_{d,ox}$ REOD	$\Delta v'_{f,z} = v'_z - v'_{f,z}$ VFZ
$\Delta v'_{ox,z} = v'_z - v'_{ox,z}$ VOZ	drag, b_f DRAGF	drag, b_{ox} DRAGO	parameter, J XJ	gamma, γ GAM	Schmidt No. SC
axial vel. v'_z VZ	initial time T	step size, $\Delta t'$ HMAX	stop time TSTOP		
burning control para. MP=2 for fuel, 4 for ox. MP	No. θ' nodes+1 ND	print at NO*$\Delta t'$ NO	print every n_j^{th} node NJ		

Card #3, 6E12.8

Card #4, 6E12.8

Card #5, 6I12

FIGURE D-3. INPUT FORMAT

FORM 252 B

```
C      MAIN PROGRAM FOR COMBUSTION INSTABILITY MODEL OF DSC
       DIMENSION FC(80), NM(20), BD(2,361,14),BE(3,361,3),V(3,361)
      1  ,ART(800,3),P(2,361), RHO(3,361), T(3,361), AB(92,10)
      2 , XZX(1086)
       DIMENSION DTT(2,361),DTTH(2,361),DRHOT (2,361),DRHOTH(2,361),
      1  DVT(2,361),DVTH(2,361),W(6,361),WZ(2,361),DPTH(2,361),
      1  D2VTH(2,361), D2TTH(2,361)
            COMMON/E/FC,NM/B/BD,BE
         COMMON ART, AB, XZX
       EQUIVALENCE (BE(1),T), (BE(1084),RHO), (BE(2167), V)
       EQUIVALENCE (BD(1),P), (BD( 723),DPTH),(BD(1445),DTT),
      1 (BD(2167),DTTH),(BD(2889),D2TTH), (BD(3611),DRHOT),
      2(BD(4333),DRHOTH),(BD(5055),DVT),(BD(5777),DVTH),(BD(6499),D2VTH),
      3  (BD(7221),W), (BD(9387), WZ)
       EQUIVALENCE  (FC(1), TI), (FC(31), TSTOP), (NM(4), MGAM),
      1 (FC(3), H), (NM(5), MPTN), (NM(3), MALP), (NM(13), I),
      2 (FC(38), ZIP), (FC(32), XL), (FC(34), XJ), (FC(35), DELV),
      3 (FC(36), GAM) ,(NM(7),NSW), (NM(14), ND), (FC(33), RED)
      4 ,(FC(74),TL), (FC(75), TH), (NM(17), NJ), (FC(39), SC)
C
        IZ = 1
    5   I = 1
       NN = 1
       CALL REED
       CALL RSET
C      SUBROUTINE  ORG INITIALIZES PRINT COUNTERS AND SETS UP THE NECESS
C      ARY  INTEGRATION TERMS
          CALL ORG
C      SET UP COEFFICIENTS TO SOLVE FOR  Z  DERIVATIVES
   10     CALL ASET
C      SUBROUTINE ZDIR SOLVES FOR Z DERIVATIVEO
          CALL  ZDIR
C      NOW SOLVE FOR T DERIVATIVES       P
          CALL TDIR
C      NADM  PERFORMS THE ACTUAL NUMERICAL INTEGRATION
          CALL NADM (DRHOT, RHO, 1)
          CALL NADM (DVT , V, 2)
          CALL NADM (DTT, T,  3)
        CALL THPRED
C      NEXT TEST FOR PRINT POINT
          IF(MPTN) 60, 50, 60
C      BRANCH TO 50 IMPLIES PRINT POINT OBTAINED
   50     CALL  AVGE
       WRITE(6,97) ART(I,1),ART(I,2),NM(1),(FC(JM),JM=55,57 )
 97    FORMAT (6HOTIME=F9.5 ,10X,17H(PMAX-PMIN)/PAVE=F9.5,10X,3HIT=I2
      1 ,//,20X,42HAXIAL DERIVATIVES FOR V,RHO, AND T ..... ,/ ,
      2 ,17X,3E16.7 ,//  ,8X,1HP,17X,3HRHO,15X,1HT,17X
      3 ,7HV THETA,11X,6HW FUEL,12X,5HW OX. ,/)
       WRITE(6,98) (P(1,J),RHO(1,J),T(1,J),V(1,J),W(3,J)
      1 ,W(5,J), J=1,ND,NJ)
 98    FORMAT (F14.5,2F18.5,E22.5,F14.5,F18.5)
       WRITE (6,980)
 980   FORMAT(1H0,///)
   52   I = I+1
C      TEST FOR  TIME STOP.
              IF (TI - TSTOP)  60,  55, 55
C      STORE PRINT POINT FOR  PLOTTING
   55     ZIP  =  ART(1,2)
        I = I-1
       NN = NN-1
        WRITE (6,99) (ART(J,1), ART(J,2), ART(J,3),J =1,I)
```

FIGURE D-4. BIPROPELLANT PROGRAM LISTING

```
 99    FORMAT(1H1,6X,4HTIME,15X,16H(PMAX-PMIN)/PAVE,4X,8HPRESSURE
     1 ,//,(3E20.8))
C      CALL PLOTTING ROUTINES
           GO  TO 5
C      SUBROUTINE  SHIFT  UPDATES TERMS INVOLVED WITH INTEGRATION-
   60     CALL SHIFT
          GO TO 10
C
       END
```

```
      SUBROUTINE REED
C
      DIMENSION FC(80), NM(20), BD(2,361,14),BE(3,361,3),WT(20)
     1 ,BCD(12)
      COMMON  /E/FC,NM /B/BD,BE
      EQUIVALENCE  (FC(1),T), (FC(6),HMAX),(FC(8),EMIN),
     1 (FC(9),EMAX), (FC(11), WT(1)), (FC(31), TSTOP),(FC(32),XL),
     2  (FC(33),RED), (FC(34),XJ), (FC(35),DELV), (FC(36),GAM),
     3 (FC(37),AP), (FC(39),SC), (FC(41), VZ),(FC(54),DTH)
     4 ,(FC(74),XLF),(FC(75),XLO),(NM(17),NJ)
     5 ,(FC(76),VFZ), (FC(77), VOZ),(FC(67),REFD), (FC(68),REOD)
     6 ,(FC(78),DRAGF),(FC(79),DRAGO)
      EQUIVALENCE (NM(7),NSW), (NM(9),MP), (NM(11),NO),(NM(14), ND)
C
      EMIN=.0001
      DO 10 I = 1,20
 10   WT(I) = 1.0
      READ (5,90) (BCD(I),I=1,12)
 90   FORMAT(12A6)
      IF( EOF, 5) 99,1
 1    WRITE (6,91) (BCD(I),I=1,12)
 91   FORMAT (1H1,38X,41HDYNAMIC SCIENCE BIPROPELLANT INSTABILITY
     1 ,7HPROGRAM ,///,12A6 )
      READ (5,92) AP,XLF,XLO,REFD,REOD,VFZ,VOZ,DRAGF,DRAGO
     1 ,XJ,GAM,SC,VZ,T,HMAX,TSTOP
 92   FORMAT(6E12.8)
      READ (5,94) MP,ND,NO,NJ
 94   FORMAT (6I12)
      XL=XLF+XLO
      XND = ND - 1
      DTH = 6.2831853071/XND
      TSTS=HMAX/DTH
      WRITE (6,93) AP,XLF,XLO,REFD,REOD,VFZ,VOZ,DRAGF,DRAGO
     1 ,XJ,GAM,SC,VZ,T,HMAX,TSTOP,DTH,TSTS
 93   FORMAT(//,47HOINITIAL AMPLITUDE OF PRESSURE DISTURBANCE,AP =
     1 ,F9.6,//////,51X,20HSTABILITY PARAMETERS,//,51X,4HFUEL,8X
     2 ,8HOXIDIZER,///,4X,24HBURNING-RATE PARAMETER,L ,21X,F9.3,
     3 ,3X,F9.3,//,4X, 8HRE SUB D,37X,F9.0,3X,F9.0,//
     4 ,4X,26HRELATIVE VELOCITY, DELTA V,19X,F9.4,3X,F9.4,//
     5 ,4X,16HDRAG PARAMETER,D ,29X,F9.2,3X,F9.2 ,//////////
     6 ,13X,3HJ =,E12.5,/,9X,7HGAMMA =,F7.4,/,16H   SCHMIDT NO. =
     7 ,F7.4,/,7X,9HV SUB Z =,F9.6,//////
     8 ,15H INITIAL TIME =,F9.6,20X,12HTIME  STEP =,F9.6,/
     9 ,15H   FINAL TIME =,F9.6,20X,12HTHETA STEP =,F9.6,/
     1 ,34X              ,22HTIME STEP/THETA STEP =,F9.6,//)
C
C         MP=2 FUEL       OR       MP=4 OX.      CONTROLS BURNING
C
      WRITE(6,94) MP,ND,NO,NJ
      WRITE(6,95)
 95   FORMAT(1H1)
      RETURN
C
 99   STOP
      END
```

```
      SUBROUTINE  ASET
C
C     THIS  SUBROUTINE  CALCULATES THE COEFFICIENTS FOR THE AXIAL
C     DERIVATIVE  PACKAGE AND ALSO INITIATES THE W ARRAY AND THE WZ
C     ARRAY.
C
      DIMENSION FC(80), NM(20), BD(2,361,14),BE(3,361,3),V(3,361)
     1  ,ART(800,3),P(2,361), RHO(3,361), T(3,361), AB(92,10)
     2 , XZX(1086)
     2 ,PVD(361),BVD(361),DD(361),BZD(361),AZ(361), A(11), C(3)
      DIMENSION DTT(2,361),DTTH(2,361),DRHOT (2,361),DRHOTH(2,361),
     1  DVT(2,361),DVTH(2,361),W(6,361),WZ(2,361),DPTH(2,361),
     1  D2VTH(2,361), D2TTH(2,361)
           COMMON/E/FC,NM/B/BD,BE
       COMMON ART, AB, XZX
      EQUIVALENCE (BE(1),T), (BE(1084),RHO), (BE(2167), V)
      EQUIVALENCE (BD(1),P), (BD( 723),DPTH),(BD(1445),DTT),
     1 (BD(2167),DTTH),(BD(2889),D2TTH), (BD(3611),DRHOT),
     2(BD(4333),DRHOTH),(BD(5055),DVT),(BD(5777),DVTH),(BD(6499),D2VTH),
     3  (BD(7221),W), (BD(9387), WZ)
      EQUIVALENCE (FC(33), RED), (FC(39), SC), (FC(35), DELV),
     1 (FC(32), XL), (FC(34), XJ),  (FC(40), DEL2V), (FC(41), VZ),
     2  (FC(42), FGAM),  (FC(36),  GAM),  (FC(43),  A), (FC(51), C)
     3 ,(FC(59), SRD), (FC(60),SCB),(FC(61),SCR),(FC(62),SIP),
     4 (FC(38), ZIP) ,(FC(64),BB),(NM(14), ND)
     5,(FC(63),SIP2), (FC(65),BC), (FC(66),BZ)
     6 ,(NM(4),MGAM), (FC(69), SRD2),(NM(9),MP)
     7 ,(FC(74), XLF), (FC(75), XLO), (FC(76),VFZ), (FC(77), VOZ)
     8 ,(FC(78),DRAGF),(FC(79),DRAGO),(FC(67), REFD),(FC(68),REOD)
     9 ,(FC(72), DEL1V), (FC(80), SCRO)
C
      IF(MGAM) 10, 10, 12
10    J = 1
      LL = 3
      LJ = 5
      ML = MP + 1
      K = 1
      GO TO 13
12    J = 2
      LL = 4
      LJ = 6
      ML = MP + 2
      K = 3
C
13    DO 40  I = 1, ND
      BVD(I) = RHO(K,I)*  V(K,I)
      BZD(I) = BVD(I)*DTTH(J,I)
      PVD(I) = P(J,I)*DVTH(J,I)
      IF(RHO(K,I)) 60,20,20
20    W(LL,I) = (2.0 + SCB*SQRT (RHO(K,I))*(V(K,I)**2+ DEL2V)**.250*SRD
     1 )/SCR
      W(LJ,I) = (2.0 + SCB*SQRT (RHO(K,I))*(V(K,I)**2+ DEL1V)**.250*SRD
     12)/SCRO
      W(J,I) = W(ML,I)
      AZ(I) = XLF*W(LL,I) + XLO*W(LJ,I)
      DD(I) = VFZ*XLF*W(LL,I)  + VOZ*XLO*W(LJ,I)
40  WZ(J,I)= XL*GAM*W(J,I) -(XLO*W(LJ,I) + XLF*W(LL,I))*T(K,I) +
     1 SIP*(XLF*(V(K,I)**2+DEL2V)*W(LL,I)+XLO*(V(K,I)**2+DEL1V)*W(LJ,I))
C
      A(5)=WEDD(T(K,1))/GAM
      A(7)=(GAM-1.)*WEDE(P(J,1))
```

```
      C(1) = FGAM*WEDS(AZ)
      C(2)=-FGAM*WEDS(DD)
      C(3)=FGAM*WEDE(WZ(J,1))-(GAM-1.)*WEDS(PVD)-WEDS(BZD)
C
      IF(DRAGF+DRAGO .LT. 1.E-20) RETURN
C         R SUB D,F = R SUB D,OX = 1.
C
      C(2)=C(2)-6.28318531*(DRAGF*ABS(VFZ)*VFZ+DRAGO*ABS(VOZ)*VOZ)
      DO 50 I=1,ND
      PVD(I)=RHO(K,I)*(V(K,I)**2+VFZ**2)**1.5
 50   BZD(I)=RHO(K,I)*(V(K,I)**2+VOZ**2)**1.5
      C(3)=C(3)+SIP2*(DRAGF*WEDS(PVD)+DRAGO*WEDS(BZD))
         RETURN
C
   60 WRITE(6,21)     FC(1),          (P(1,J),RHO(1,J),T(1,J),V(1,J),
     1 W(1,J),WZ(1,J), J=1,ND)
   21 FORMAT(1H0,1E20.8/(6E18.8))
      STOP
      END
```

```
      SUBROUTINE AVGE
      DIMENSION FC(80), NM(20), BD(2,361,14),BE(3,361,3),V(3,361)
     1  ,ART(800,3),P(2,361), RHO(3,361), T(3,361), AB(92,10)
     2 , XZX(1086)
      DIMENSION DTT(2,361),DTTH(2,361),DRHOT (2,361),DRHOTH(2,361),
     1  DVT(2,361),DVTH(2,361),W(6,361),WZ(2,361),DPTH(2,361),
     1  D2VTH(2,361), D2TTH(2,361)
      COMMON/E/FC,NM/B/BD,BE
      COMMON ART, AB, XZX
      EQUIVALENCE (BE(1),T), (BE(1084),RHO), (BE(2167), V)
      EQUIVALENCE (BD(1),P), (BD( 723),DPTH),(BD(1445),DTT),
     1 (BD(2167),DTTH),(BD(2889),D2TTH), (BD(3611),DRHOT),
     2(BD(4333),DRHOTH),(BD(5055),DVT),(BD(5777),DVTH),(BD(6499),D2VTH),
     3  (BD(7221),W), (BD(9387), WZ)
      EQUIVALENCE (FC(1),TI),              (NM(13), IU)
     1 , (NM(14), ND), (NM(15),N1)
C
      XMA = P(1,1)
      XMI =  XMA
      SUM =  XMI
      DO 10 I = 2,N1
      SUM = SUM + P(1,I)
      IF(P(1,I) -  XMA) 5,10,3
 3     XMA = P(1,I)
      GO TO 10
 5     IF(P(1,I)  - XMI)  7, 10, 10
 7     XMI = P(1,I)
10     CONTINUE
      XN = N1
      SUM = SUM/XN
      ART(IU,2) =  (XMA - XMI)/SUM
      ART(IU,1)  =  TI
      NN = N1/4 + 1
      ART(IU,3) = P(1,NN)
C
      RETURN
      END
```

```
      SUBROUTINE NADM(YP,Y,KK)
       DIMENSION YP(722),Y(1083), FC(80),NM(20),WT(20)
      COMMON /E/  FC,NM
      EQUIVALENCE (FC(3),H), (FC(11),WT), (FC(10), E1), (FC(9), EMAX),
     1 (FC(8), EMIN), (NM(2), INDR), (NM(7), NSW), (NM(4), MGAM),
     2 (NM(3), MALP), (NM(20),NOD)
C
C     MGAM=-1,0,1 INDICATES PREDICTOR-RUNGE-KUTTA OR CORRECTORPHASE
C     MALP-INDICATES PERT OF RUNGE KUTTA PHASE
C     NSW- PRINT SWITCH FOR ERROR INDICATION
C     E1 - CONTAINS MAXIMUM ERROR FOR EACH CYCLE
C     YP - ADDRESS OF DERIVATIVE ARRAY
C     Y - ADDRESS  OF THE ORDINATE ARRAY
C     ******************************
      IF (MGAM) 40, 40,  60
C     ***************************
C          PREDICTOR
C     *********************************
   40  DO 42  I = 1,NOD,2
         K = I + I/2
   42    Y(K+2) = Y (K) + H*YP(I)
      GO TO 99
C     ***************************
C          CORRECTOR
C     ************************************
   60   DO 98 I = 1,NOD,2
         K = I + I/2
         Y(K+1) = Y(K) + H*YP(I+1)
         E = ABS (Y(K+1) - Y(K+2))*WT(KK)
         IF(Y(K+1)) 70, 80, 70
   70      E = E/ABS (Y(K+1))
   80  IF( E - EMAX) 85, 95, 95
   85  IF(E - EMIN) 98, 87, 87
C     *********************************
C     RELATIVE ERROR CHECK-BRANCH TO 99 INDICATES ERROR SMALLER THAN
C     ALLOWABLE ERROR-ADDING ONE TO INDR INDICATES VARIABLE WITHIN
C     ERROR ALLOWED
C     *********************************
   87 INDR = INDR  + 1
         GO TO 98
C     *****************************
C     ONE HUNDRED IS SUBTRACTED FOR EACH VARIABLE LARGER THAN THE
C     ERROR LIMITS
C     *********************************
   95  INDR =  INDR - 100
C     ************************************
C     E1 CONTAINS MAXIMUM ERROR OCCURING DURING THE CYCLE
C     *******************************
   98 E1 =AMAX1(E, E1)
  99   RETURN
       END
```

```
      SUBROUTINE ORG
      DIMENSION FC(80), NM(20), W(20)
       COMMON /E/ FC, NM
       EQUIVALENCE (FC(1),T), (FC(2),RKT), (FC(3),H), (FC(4),HO),
     1 (FC(5), HMIN), (FC(6),HMAX), (FC(7),HZD2), (FC(8),EMIN),
     2(FC(9),EMAX), (FC(11),W), (FC(10),E1),
     3 (NM(1),IM), (NM(2),INDR), (NM(3),MALP), (NM(4),MGAM),
     4 (NM(5),MPTN), (NM(6),MPTS), (NM(7),NSW), (NM(8),NCOU),
     5 (NM(9),MP), (NM(10),NV) , (NM(11), NO)
C     ****************************************************************
C          DESCRIPTION OF THE LISTED VARIABLES
C     T - THIS CELL CONTAINS CURRENT INTEGRATION TIME
C     RKT - START TIME OR PREVIUUS BEGINING OF RK TIM5
C     H - CURRENTLY USED STEP SIZE IN COMPUTING
C     HO - STORED STEP SIZE
C     HZD2 - HALF OF STORED STEP SIZE
C     HMIN - MINIMUM STEP SIZE
C     HMAX - MAXIMUM ALLOWABLE STEP
C     EMIN - EMAX MIN AND MAX AOLOWABLE ERROR
C     W - ARRAY OF WEIGHTS TO WEIGHT ERROR CINSIDERATION
C     IM - NO OF GOOD POINTS FROM R.K START
C     INDR - INDICATOR FOR ERROR OUTSIDE OR WITHIN MIN MAX TOLERANCE
C     MALP - COUNTER FOR R.K INTRRMEDIATE POINTS
C     MGAM - PHASE INDICATOR -1,PREDICTOR0,R.K  1, CORRECTOR
C     MPTN - PRINT COUNTER, CURRENT
C     MPTS - TOTAL NO OF POINTS IN PRINT INTERVAL
C     NSW - PRINT INDICATOR IN NADM ROUTINE
C     NCOU - TOTAL NO OF COMPUTED POINTS DURING INTEGRATION CYCLE
C     MP - POWER OF 2 VARIATION FROM HMIN TO HMAX
C     HMAX, MP, NO, NSW, NV AND W(I) MUST EITHER BE READ INTO CORE OR
C     INITIAIZED BY AN ADDITIONAL ROUTINE
C     ****************************************************************
      HMIN = HMAX/2.**MP
      HO = HMIN
      HZD2 = HO/2.0
      H = HO
      RKT = T
       E1 = 0.0
C     ****************************************************************
C      FIXED POINT INITIALIZATIONS
C     ****************************************************************
       IM = 0
       MALP = 4
       MGAM = -1
         MPTN = 0
       MPTS  = NO*2**MP
       INDR = 0
       NCOU = 0
C     ****************************************************************
C      MPTN SET TO ZERO TO PRINT INITIAL CONDITIONS
C     ****************************************************************
       RETURN
       END
```

```
      SUBROUTINE  RSET
     DIMENSION FC(80), NM(20), BD(2,361,14),BE(3,361,3),V(3,361)
    1  ,ART(800,3),P(2,361), RHO(3,361), T(3,361), AB(92,10)
    2 , XZX(1086)
     DIMENSION DTT(2,361),DTTH(2,361),DRHOT (2,361),DRHOTH(2,361),
    1  DVT(2,361),DVTH(2,361),W(6,361),WZ(2,361),DPTH(2,361),
    1  D2VTH(2,361), D2TTH(2,361) , A(11)
          COMMON/E/FC,NM/B/BD,BE
      COMMON ART, AB, XZX
     EQUIVALENCE (BE(1),T), (BE(1084),RHO), (BE(2167), V)
     EQUIVALENCE (BD(1),P), (BD( 723),DPTH),(BD(1445),DTT),
    1 (BD(2167),DTTH),(BD(2889),D2TTH), (BD(3611),DRHOT),
    2(BD(4333),DRHOTH),(BD(5055),DVT),(BD(5777),DVTH),(BD(6499),D2VTH),
    3  (BD(7221),W), (BD(9387), WZ)
    4,(FC(59),SRD), (FC(60),SCB), (FC(61),SCR), (FC(35),DELV),
    5 (FC(40),DEL2V), (FC(64),BB), (FC(65),  BC), (FC(66),BZ),
    6 (FC(33), RED), (FC(39), SC), (FC(32), XL), (FC(34), XJ),
    7  (FC(42), FGAM)  ,(FC(62),SIP),(FC(63),SIP2), (FC(38),ZIP)
    8 , (FC(43), A), (FC(41), VZ) ,(FC(36),GAM), (FC(37),AP)
    9 ,(FC(67), REFD) ,(FC(68),REOD), (FC(69),SRD2),(FC(76),VFZ)
     EQUIVALENCE (NM(14), ND), (NM(15),N1),(NM(20),NOD), (FC(70),D2)
    1, (FC(71), DSQ), (NM(19), NOD1),(NM(20), NOD)
    2 ,(FC(54), DTH), (NM(12), NZ)
    3,(NM(16), NCD),  (FC(80), SCRO) , (FC(72),DEL1V)
    4 ,(FC(77), VOZ)
    5 ,(FC(78),DRAGF),(FC(79),DRAGO)
C
C      SET UP  INITIAL ARRAY
C
      A(1)=6.28318531
      A(2)=A(1)*VZ
      A(4)=A(2)
      A(6)=A(1)/GAM
      A(8)=A(2)
C
         GAM1 = GAM + 1.0
         FGAM = SQRT ((2.0/GAM1)**(GAM1/(GAM-1.0)))
               BC = XJ*FGAM
               BZ = 1.3333333333*BC
         DEL2V = VFZ**2
         DEL1V = VOZ**2
         SIP2=  GAM*(GAM - 1.0)
        SIP = SIP2/2.0
         ZIP =  GAM +  SIP*DEL2V
        SRD =SQRT (REFD)
        SRD2=SQRT (REOD)
         SCB = .6 *SC**.33333333333
          SCR = 2.0 +  SCB*SQRT (VFZ)*SRD
          SCRO= 2.0 +  SCB*SQRT (VOZ)*SRD2
       D2 =  2.0*DTH
       DSQ = D2*DTH/2.0
         NOD = 2*ND
         NOD1 = 3*ND
         NZ = ND + 1
       N1 = ND - 1
         NCD = 0
               CON1 =  1.0/GAM
               CON2 =  1.0 - CON1
          DO 20  I = 1,ND
          XI = I -1
          ZIG  = XI*DTH
```

```
            P(1,I) =  AP*SIN (ZIG) + 1.0
            DPTH(1,I) = AP*COS (ZIG)
            T(1,I) = P(1,I)**CON2
            RHO(1,I)= P(1,I)**CON1
            V(1,I) = 0.0
            DTTH(1,I) =  CON2/RHO(1,I)*DPTH(1,I)
            DVTH(1,I) =  0.0
            DRHOTH(1,I) = CON1/T(1,I)*DPTH(1,I)
            D2VTH(1,I)  = 0.0
   20       D2TTH(1,I)  = CON2/RHO(1,I)*(-CON1/P(1,I)* DPTH(1,I)*DPTH(1,I)
     1      + 1.0 - P(1,I))
C
         RETURN
         END
```

```
      SUBROUTINE SHIFT
     DIMENSION FC(80), NM(20), BD(2,361,14),BE(3,361,3),V(3,361)
    1  ,ART(800,3),P(2,361), RHO(3,361), T(3,361), AB(92,10)
    2 , XZX(1086)
     DIMENSION DTT(2,361),DTTH(2,361),DRHOT (2,361),DRHOTH(2,361),
    1  DVT(2,361),DVTH(2,361),W(6,361),WZ(2,361),DPTH(2,361),
    1  D2VTH(2,361), D2TTH(2,361)
          COMMON/E/FC,NM/B/BD,BE
      COMMON ART, AB, XZX
     EQUIVALENCE (BE(1),T), (BE(1084),RHO), (BE(2167), V)
     EQUIVALENCE (BD(1),P), (BD( 723),DPTH),(BD(1445),DTT),
    2(BD(4333),DRHOTH),(BD(5055),DVT),(BD(5777),DVTH),(BD(6499),D2VTH),
    3  (BD(7221),W), (BD(9387), WZ)
     EQUIVALENCE (NM(5),MPTN),(NM(4),MGAM), (NM(3),MALP),
    1 (NM(1),IM), (FC(3),H), (FC(7),HZD2), (NM(10),NV), (FC(4),HO),
    2 (FC(1),TI),(NM(2), INDR), (FC(10), E1), (NM(8),NCOU),
    3 (FC(6), HMAX), (NM(6),MPTS), (FC(8),EMIN), (FC(9), EMAX),
    4  (FC(2),RKT),(NM(16),NCD),(NM(19),NOD1), (NM(20),NOD)
C       PRINT PREVIOUS POINT IN PREDICTOR CYCLE
C     NO SHIFTING TO OCCUR ON PREDICTOR CYCLE
      IF(MPTN) 20,10,20
10   MPTN = MPTS
20    IF(MGAM) 80, 80, 60
C     IS CORRECTOR CYCLE COMPLETE
60      IF(E1 - EMIN)  72, 68, 68
68    IF(NCD - 3)  69, 69, 72
C     CONTINUE ITERATION (INCREMENT ITERATION COUNTER)
69    DO 70 J = 1,3
      NZ = 1083*(J-1) + 1
      NZZ = NZ + NOD1 -1
        DO 70 I = NZ,NZZ,3
70    BE(I+2) = BE(I+1)
      E1 = 0.0
      NCD = NCD +1
      RETURN
C    TERMINATE CORRECTOR ITERATION
72   MGAM = -1
        MPTN = MPTN - 1
         IM = NCD
        NCD = 0
        FC(58) = E1
        E1 = 0.0
           DO 74 J= 1,14
      NZ = 722*(J-1) + 1
        NZZ = NZ + NOD - 1
             DO 74 I = NZ,NZZ,2
74           BD(I) = BD(I+1)
C      UPDATE NONINTEGRATED VARIABLES ABOVE
C     UPDATE INTEGRATED VARIABLES BELOW
        DO 76  J = 1,3
        NZ = 1083*(J-1) + 1
        NZZ = NZ + NOD1 - 1
             DO 76  I = NZ,NZZ,3
76           BE(I) = BE(I+1)
        RETURN
80      MGAM = +1
        TI = TI + H
        RETURN
     END
```

```
      SUBROUTINE  TDIR
C
      DIMENSION FC(80), NM(20), BD(2,361,14),BE(3,361,3),V(3,361)
C     THIS ROUTINE COMPUTES THE PARTIAL DERIVATIVES WITH RESPECT TO T
     1  ,ART(800,3),P(2,361), RHO(3,361), T(3,361), AB(92,10)  ,X(4)
     2 , XZX(1086)
      DIMENSION DTT(2,361),DTTH(2,361),DRHOT (2,361),DRHOTH(2,361),
     1  DVT(2,361),DVTH(2,361),W(6,361),WZ(2,361),DPTH(2,361),
     1  D2VTH(2,361), D2TTH(2,361)
           COMMON/E/FC,NM/B/BD,BE
       COMMON ART, AB, XZX
      EQUIVALENCE (BE(1),T), (BE(1084),RHO), (BE(2167), V)
      EQUIVALENCE (BD(1),P), (BD( 723),DPTH),(BD(1445),DTT),
     1 (BD(2167),DTTH),(BD(2889),D2TTH), (BD(3611),DRHOT),
     2(BD(4333),DRHOTH),(BD(5055),DVT),(BD(5777),DVTH),(BD(6499),D2VTH),
     3  (BD(7221),W), (BD(9387), WZ)
      EQUIVALENCE (FC(32), XL),(FC(34), XJ), (FC(33), RED),
     1 (FC(41),  VZ),  (FC(42), FGAM), (FC(36), GAM), (FC(55), X)
     2,(FC(64),BB),(FC(65),BC), (FC(66),BZ), (FC(62),SIP),(FC(63),SIP2)
     3 ,(FC(74), XLF), (FC(75), XLO)
     4 ,(NM(14), ND), (NM(4), MGAM) , (NM(9), MP) ,(FC(62), SIP)
     5 ,(FC(40), DEL2V) , (FC(80), DEL1V)
     6 ,(FC(78),DRAGF),(FC(79),DRAGO)
C
        IF(MGAM) 10, 10, 12
   10   J = 1
       KZ = 3
       KZ2= 5
        K = 1
        GO TO 15
   12   J = 2
       KZ = 4
       KZ2= 6
        K = 3
 15    CONTINUE
       BA=VZ*X(2)
       BM=VZ*X(3)
C
C      THE DERIVATIVE OR RHO WITH RESPECT TO T -  THE CONTINUITY EQUATION
C      THE MOMENTUM EQ. - THE ENERGY EQUATION
C
         DO 40 I = 1, ND
       ABBE = FGAM*(XLO*W(KZ2,I) + XLF*W(KZ,I))
          DRHOT(J,I) = -RHO(K,I)*(DVTH(J,I) + X(1))  - V(K,I)*DRHOTH(J,I
     1)- BA + ABBE
         DVT(J,I) = (-(RHO(K,I)*DVTH(J,I) + ABBE)*V(K,I)-  DPTH(J,I)/GAM
     1+BZ*D2VTH(J,I))/RHO(K,I)
       DTT(J,I) =  -V(K,I)*DTTH(J,I) -BM + ((1. -GAM)*P(J,I)*(DVTH(J,
     1 I)+X(1)) +BC*D2TTH(J,I)+ BZ*SIP2*(DVTH(J,I)**2+ X(1)*(X(1)-DVTH(
     2 J,I))) + FGAM*WZ(J,I))/RHO(K,I)
       IF(DRAGF+DRAGO .LT. 1.E-20) GO TO 40
       DVT(J,I)=DVT(J,I)-(DRAGF+DRAGO)*ABS(V(K,I))*V(K,I)
       DTT(J,I)=DTT(J,I)+SIP2*(DRAGF*(V(K,I)**2+VFZ**2)**1.5
     1                      +DRAGO*(V(K,I)**2+VOZ**2)**1.5)
 40    CONTINUE
C
       RETURN
       END
```

```
          SUBROUTINE  THPRED
C      EMPLOYING THE RESULTS OF THE INTEGRATION THIS ROUTINE ATTEMPTS TO
C      COMPUTE THE THETA  DERIVATIVES OF  THE  N+1   ANNULUS
        DIMENSION FC(80), NM(20), BD(2,361,14),BE(3,361,3),V(3,361)
       1 ,ART(800,3) ,P(2,361), RHO(3,361), T(3,361) ,AAA(92,10)
       2  , AA(362), AB(362), AC(362)
        DIMENSION DTT(2,361),DTTH(2,361),DRHOT (2,361),DRHOTH(2,361),
       1  DVT(2,361),DVTH(2,361),W(6,361),WZ(2,361),DPTH(2,361),
       1  D2VTH(2,361), D2TTH(2,361)
              COMMON/E/FC,NM/B/BD,BE
        COMMON ART, AAA, AA, AB, AC
        EQUIVALENCE (BE(1),T), (BE(1084),RHO), (BE(2167), V)
        EQUIVALENCE (BD(1),P), (BD( 723),DPTH),(BD(1445),DTT),
       1 (BD(2167),DTTH),(BD(2889),D2TTH), (BD(3611),DRHOT),
       2(BD(4333),DRHOTH),(BD(5055),DVT),(BD(5777),DVTH),(BD(6499),D2VTH),
       3  (BD(7221),W), (BD(9387), WZ)
       3 ,(NM(12), NZ)     , (FC(54), DTH), (NM(4), MGAM)
       4 ,(NM(14),ND), (NM(15), N1),(FC(70),D2), (FC(71),DSQ)
C
          IF(MGAM) 10,10,12
    10    J = 3
           GO TO 13
    12    J = 2
    13      AA(1) = RHO(J,N1)
           AB(1) = V(J,N1)
          AC(1) = T(J,N1)
              DO 20  I = 2,NZ
           AA(I) = RHO(J,I-1)
            AB(I) = V(J,I-1)
    20     AC(I) = T(J,I-1)
           DO 25  I = 1,N1
            DRHOTH(2,I) = (AA(I+2) - AA(I))/D2
            DVTH(2,I) = (AB(I+2) - AB(I))/D2
            DTTH(2,I) = (AC(I+2) - AC(I))/D2
            D2VTH(2,I) = (AB(I+2) - 2.0*AB(I+1) + AB(I))/DSQ
    25      D2TTH(2,I) = (AC(I+2) - 2.0*AB(I+1) + AB(I))/DSQ
       DVTH(2,ND) = DVTH(2,1)
       DTTH(2,ND)=DTTH(2,1)
       DRHOTH(2,ND) = DRHOTH(2, 1)
       D2TTH(2,ND) =D2TTH(2,1)
         D2VTH(2,ND) = D2VTH(2,1)
           DO 50 I = 1,ND
           P(2,I) = RHO(J,I)*T(J,I)
    50   DPTH(2,I) =DRHOTH(2,I)*T(J,I) +DTTH(2,I)*RHO(J,I)
C
           RETURN
           END
```

```
      FUNCTION  WEDD(A)
C
C     THIS FUNCTION EMPLOYS WEDDLES RULE TO EVALUATE THE INTEGRAL(0,2PI)
C
      DIMENSION A(3,361),B(361), FC(80), NM(20)
      COMMON /E/ FC,NM
      EQUIVALENCE (NM(15), N1),(FC(54),DTH)
C
      DO 10 I = 1,N1
   10 B(I) =  A(1,I)
      SUM = 0.0
      DO 30   I = 1,N1,5
   30 SUM =  SUM +  38.*B(I) +75.*(B(I+1) + B(I+4)) + 50.*(B(I+2) +
     1 B(I+3))
      WEDD = 5.0*DTH/288.*SUM
C
      RETURN
      END
```

```
          FUNCTION  WEDE(A)
C
C     THIS FUNCTION EMPLOYS WEDDLES RULE TO EVALUATE THE INTEGRAL(0,2PI)
C
       DIMENSION A(2,361),B(361), FC(80), NM(20)
      COMMON /E/ FC,NM
      EQUIVALENCE (NM(15), N1),(FC(54),DTH)
C
       DO 10 I = 1,N1
   10     B(I) =  A(1,I)
      SUM = 0.0
          DO 30    I = 1,N1,5
   30     SUM =  SUM +  38.*B(I) +75.*(B(I+1) + B(I+4)) + 50.*(B(I+2) +
     1    B(I+3))
      WEDE = 5.0*DTH/288.*SUM
C
      RETURN
      END
```

```
      FUNCTION  WEDS(B)
C
C     THIS FUNCTION EMPLOYS WEDDLES RULE TO EVALUATE THE INTEGRAL(0,2PI)
C
      DIMENSION          B(361), FC(80), NM(20)
      COMMON /E/ FC,NM
      EQUIVALENCE (NM(15), N1),(FC(54),DTH)
C
      SUM = 0.0
          DO 30    I = 1,N1,5
   30     SUM =  SUM +  38.*B(I) +75.*(B(I+1) + B(I+4)) + 50.*(B(I+2) +
     1    B(I+3))
      WEDS = 5.0*DTH/288.*SUM
C
      RETURN
      END
```

```
      SUBROUTINE  ZDIR
C
      DIMENSION A(8),  C(3), X(4), FC(80), NM(20)
      COMMON /E/ FC,  NM
      EQUIVALENCE (FC(36), GAM), (FC(43), A), (FC(51),  C),
     1 (FC(55), X) , (FC(41), VZ)
C
      X(1)=(C(2)-A(5)*C(1)/A(2)-A(6)*C(3)/A(8))
     1    /(A(4)-A(5)*A(1)/A(2)-A(6)*A(7)/A(8))
      X(2)=(C(1)-A(1)*X(1))/A(2)
      X(3)=(C(3)-A(7)*X(1))/A(8)
C
      RETURN
      END
```

SAMPLE CASE

Figure D-5 shows the input cards required to run the bipropellant combustion instability program with droplet drag. Figure D-6 shows the output obtained from the sample input. The entire printout has not been included. However, the initial conditions are listed along with several successive integration steps as well as the last step (t'=9.5) for this case. The pressure summary is also printed on the last page. The ΔP plot, high pressure node plot and the velocity wave plots have not been included for this case, however, a complete description of the plots and the subroutines that generate the plots may be found in Reference 2.

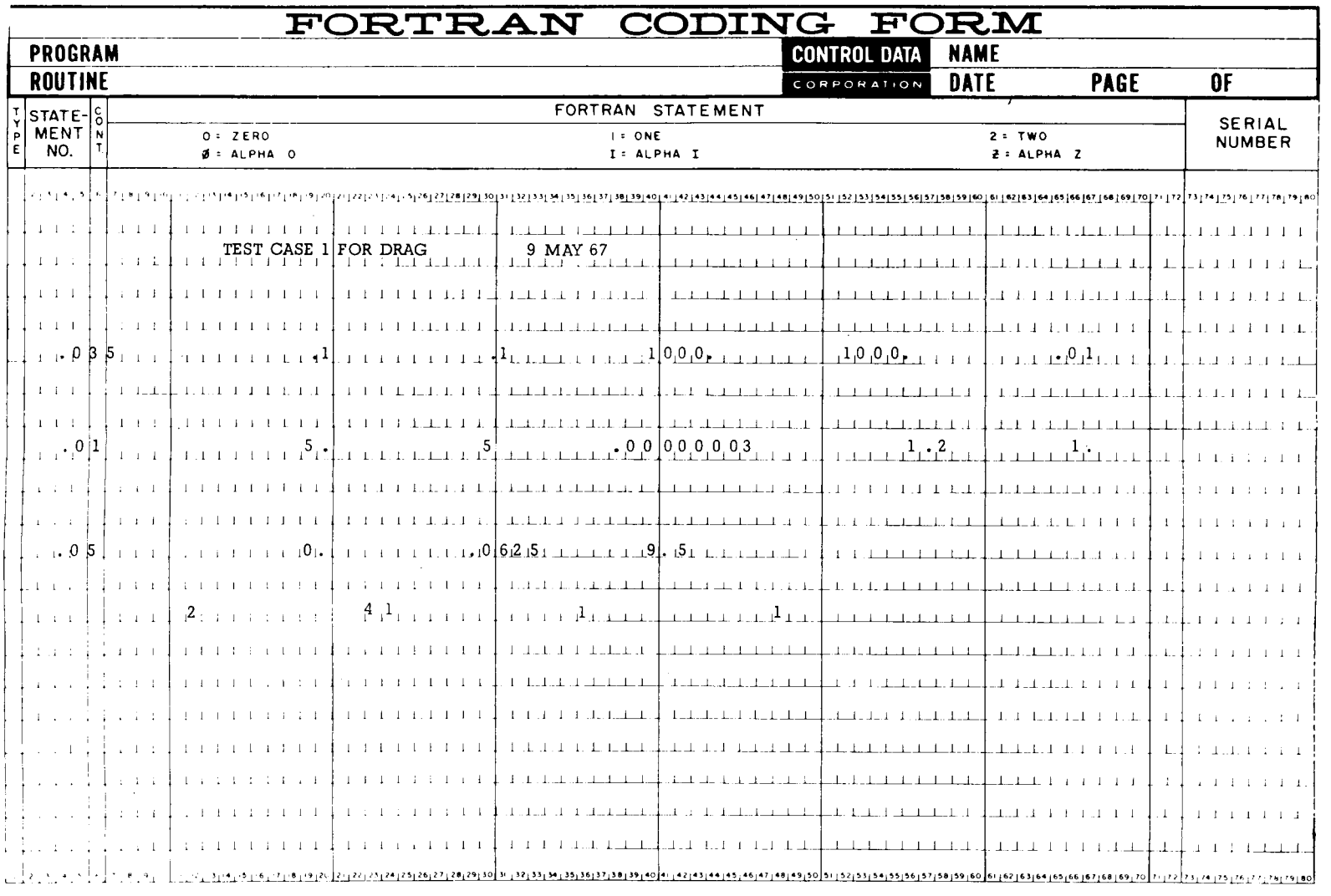

FIGURE D-5. SAMPLE INPUT

DYNAMIC SCIENCE BIPROPELLANT INSTABILITY PROGRAM

TEST CASE 1 FOR DRAG 9 MAY 67

INITIAL AMPLITUDE OF PRESSURE DISTURBANCE, AP = .035000

	STABILITY PARAMETERS	
	FUEL	OXIDIZER
BURNING-RATE PARAMETER, L	.100	.100
RE SUB D	1000	1000
RELATIVE VELOCITY, DELTA V	.0100	.0100
DRAG PARAMETER, D	5.00	5.00

J = 3.00000E-08
GAMMA = 1.2000
SCHMIDT NO. = 1.0000
V SUB Z = .050000

INITIAL TIME = 0.
FINAL TIME = 9.500000

TIME STEP = .062500
THETA STEP = .157080
TIME STEP/THETA STEP = .397887

Figure D-6. Sample Output.

2 41 2 2

TIME= 0. (PMAX-PMIN)/PAVE= .07000 IT= 0

AXIAL DERIVATIVES FOR V,RHO, AND T .....
1.1881234E-01 -8.2316833E-03 -1.5182166E-03

P	RHO	T	V THETA	W FUEL	W Ox,
1.00000	1.00000	1.00000	0.	1.00000	1.00000
1.01082	1.00900	1.00179	0.	1.00219	1.00219
1.02057	1.01711	1.00340	0.	1.00415	1.00415
1.02832	1.02354	1.00466	0.	1.00570	1.00570
1.03329	1.02766	1.00547	0.	1.00669	1.00669
1.03500	1.02908	1.00575	0.	1.00703	1.00703
1.03329	1.02766	1.00547	0.	1.00669	1.00669
1.02832	1.02354	1.00466	0.	1.00570	1.00570
1.02057	1.01711	1.00340	0.	1.00415	1.00415
1.01082	1.00900	1.00179	0.	1.00219	1.00219
1.00000	1.00000	1.00000	0.	1.00000	1.00000
.98918	.99098	.99819	0.	.99780	.99780
.97943	.98283	.99654	0.	.99580	.99580
.97168	.97635	.99522	0.	.99421	.99421
.96671	.97218	.99437	0.	.99318	.99318
.96500	.97075	.99408	0.	.99283	.99283
.96671	.97218	.99437	0.	.99318	.99318
.97168	.97635	.99522	0.	.99421	.99421
.97943	.98283	.99654	0.	.99580	.99580
.98918	.99098	.99819	0.	.99780	.99780
1.00000	1.00000	1.00000	0.	1.00000	1.00000

TIME= .12500 (PMAX-PMIN)/PAVE= .06841 IT= 2

AXIAL DERIVATIVES FOR V,RHO, AND T .....
1.1969334E-01 -8.2521907E-03 -1.5611059E-03

P	RHO	T	V THETA	W FUEL	W OX.
1.00005	1.00004	1.00001	-3.55243E-03	1.01469	1.01469
1.01061	1.00886	1.00173	-3.34710E-03	1.01531	1.01531
1.02012	1.01679	1.00328	-2.82405E-03	1.01358	1.01358
1.02765	1.02306	1.00449	-2.03903E-03	1.01062	1.01062
1.03249	1.02708	1.00526	-1.06796E-03	1.00795	1.00795
1.03415	1.02846	1.00553	1.17181E-11	1.00688	1.00688
1.03249	1.02708	1.00526	1.06796E-03	1.00795	1.00795
1.02765	1.02306	1.00449	2.03903E-03	1.01062	1.01062
1.02012	1.01679	1.00328	2.82405E-03	1.01358	1.01358
1.01061	1.00886	1.00173	3.34710E-03	1.01531	1.01531
1.00005	1.00004	1.00001	3.55243E-03	1.01469	1.01469
.98947	.99119	.99826	3.41138E-03	1.01138	1.01138
.97991	.98318	.99667	2.92822E-03	1.00592	1.00592
.97231	.97680	.99540	2.14343E-03	.99975	.99975
.96742	.97270	.99458	1.13262E-03	.99484	.99484
.96574	.97128	.99429	-1.30576E-11	.99296	.99296
.96742	.97270	.99458	-1.13262E-03	.99484	.99484
.97231	.97680	.99540	-2.14343E-03	.99975	.99975
.97991	.98318	.99667	-2.92822E-03	1.00592	1.00592
.98947	.99119	.99826	-3.41138E-03	1.01138	1.01138
1.00005	1.00004	1.00001	-3.55243E-03	1.01469	1.01469

TIME= .25000 (PMAX-PMIN)/PAVE= .06580 IT= 2

AXIAL DERIVATIVES FOR V,RHO, AND T .....
1.2188717E-01 -8.3632163E-03 -1.6079408E-03

P	RHO	T	V THETA	W FUEL	W OX.
1.00033	1.00028	1.00005	-6.90492E-03	1.04991	1.04991
1.01043	1.00874	1.00168	-6.48913E-03	1.04702	1.04702
1.01944	1.01627	1.00312	-5.46453E-03	1.03707	1.03707
1.02651	1.02217	1.00424	-3.94065E-03	1.02345	1.02345
1.03100	1.02593	1.00495	-2.06312E-03	1.01144	1.01144
1.03255	1.02721	1.00519	6.46601E-11	1.00658	1.00658
1.03100	1.02593	1.00495	2.06312E-03	1.01144	1.01144
1.02651	1.02217	1.00424	3.94065E-03	1.02345	1.02345
1.01944	1.01627	1.00312	5.46453E-03	1.03707	1.03707
1.01043	1.00874	1.00168	6.48913E-03	1.04702	1.04702
1.00033	1.00028	1.00005	6.90492E-03	1.04991	1.04991
.99011	.99170	.99840	6.65196E-03	1.04448	1.04448
.98078	.98386	.99687	5.73114E-03	1.03159	1.03159
.97329	.97755	.99564	4.21170E-03	1.01456	1.01456
.96843	.97346	.99483	2.23332E-03	.99938	.99938
.96674	.97204	.99455	-7.38390E-11	.99315	.99315
.96843	.97346	.99483	-2.23332E-03	.99938	.99938
.97329	.97755	.99564	-4.21170E-03	1.01456	1.01456
.98078	.98386	.99687	-5.73114E-03	1.03159	1.03159
.99011	.99170	.99840	-6.65196E-03	1.04448	1.04448
1.00033	1.00028	1.00005	-6.90492E-03	1.04991	1.04991

TIME= .37500 (PMAX-PMIN)/PAVE= .06224 IT= 2

AXIAL DERIVATIVES FOR V,RHO, AND T .....
1.2465107E-01 -8.5214666E-03 -1.6485620E-03

P	RHO	T	V THETA	W FUEL	W OX.
1.00091	1.00076	1.00015	-9.97776E-03	1.09201	1.09201
1.01034	1.00869	1.00164	-9.32477E-03	1.08490	1.08490
1.01857	1.01560	1.00293	-7.81432E-03	1.06587	1.06587
1.02488	1.02089	1.00391	-5.61179E-03	1.03990	1.03990
1.02880	1.02417	1.00452	-2.92968E-03	1.01609	1.01609
1.03011	1.02527	1.00473	1.82117E-10	1.00611	1.00611
1.02880	1.02417	1.00452	2.92968E-03	1.01609	1.01609
1.02488	1.02089	1.00391	5.61179E-03	1.03990	1.03990
1.01857	1.01560	1.00293	7.81432E-03	1.06587	1.06587
1.01034	1.00869	1.00164	9.32477E-03	1.08490	1.08490
1.00091	1.00076	1.00015	9.97776E-03	1.09201	1.09201
.99116	.99255	.99860	9.67558E-03	1.08529	1.08529
.98207	.98489	.99713	8.40137E-03	1.06532	1.06532
.97459	.97858	.99592	6.22828E-03	1.03589	1.03589
.96962	.97439	.99511	3.32978E-03	1.00653	1.00653
.96787	.97291	.99482	-2.16664E-10	.99336	.99336
.96962	.97439	.99511	-3.32978E-03	1.00653	1.00653
.97459	.97858	.99592	-6.22828E-03	1.03589	1.03589
.98207	.98489	.99713	-8.40137E-03	1.06532	1.06532
.99116	.99255	.99860	-9.67558E-03	1.08529	1.08529
1.00091	1.00076	1.00015	-9.97776E-03	1.09201	1.09201

TIME= .50000 (PMAX-PMIN)/PAVE= .05780 IT= 2

AXIAL DERIVATIVES FOR V,RHO, AND T .....
1.2746190E-01 -8.6957537E-03 -1.6765105E-03

P	RHO	T	V THETA	W FUEL	W OX.
1.00173	1.00145	1.00028	-1.27023E-02	1.13261	1.13261
1.01031	1.00869	1.00161	-1.17676E-02	1.12077	1.12077
1.01753	1.01477	1.00271	-9.77872E-03	1.09316	1.09316
1.02281	1.01923	1.00352	-6.96377E-03	1.05572	1.05572
1.02592	1.02184	1.00399	-3.60946E-03	1.02059	1.02059
1.02692	1.02268	1.00414	3.77151E-10	1.00549	1.00549
1.02592	1.02184	1.00399	3.60946E-03	1.02059	1.02059
1.02281	1.01923	1.00352	6.96377E-03	1.05572	1.05572
1.01753	1.01477	1.00271	9.77872E-03	1.09316	1.09316
1.01031	1.00869	1.00161	1.17676E-02	1.12077	1.12077
1.00173	1.00145	1.00028	1.27023E-02	1.13261	1.13261
.99257	.99371	.99885	1.24406E-02	1.12629	1.12629
.98375	.98625	.99746	1.09330E-02	1.10167	1.10167
.97623	.97989	.99626	8.22389E-03	1.06152	1.06152
.97102	.97548	.99542	4.46352E-03	1.01634	1.01634
.96911	.97387	.99511	-4.79872E-10	.99360	.99360
.97102	.97548	.99542	-4.46353E-03	1.01634	1.01634
.97623	.97989	.99626	-8.22389E-03	1.06152	1.06152
.98375	.98625	.99746	-1.09330E-02	1.10167	1.10167
.99257	.99371	.99885	-1.24406E-02	1.12629	1.12629
1.00173	1.00145	1.00028	-1.27023E-02	1.13261	1.13261

TIME= 9.50000 (PMAX-PMIN)/PAVE= .04373 IT= 2

AXIAL DERIVATIVES FOR V,RHO, AND T .....

1.3743482E-01 -9.0753874E-03 -2.0145446E-03

P	RHO	T	V THETA	W FUEL	W OX.
.99990	.99982	1.00008	1.82863E-02	1.21593	1.21593
.99191	.99306	.99885	1.37004E-02	1.14500	1.14500
.98643	.98840	.99800	1.01051E-02	1.09026	1.09026
.98362	.98599	.99759	7.32700E-03	1.05141	1.05141
.98188	.98448	.99736	4.03209E-03	1.01474	1.01474
.99130	.98393	.99733	1.41005E-07	.99607	.99607
.98188	.98448	.99736	-4.03185E-03	1.01474	1.01474
.9836	.98599	.99759	-7.32682E-03	1.05140	1.05140
.98643	.98840	.99800	-1.01049E-02	1.09026	1.09026
.99191	.99306	.99885	-1.37003E-02	1.14500	1.14500
.9999	.99982	1.00008	-1.82862E-02	1.21593	1.21593
1.01121	1.00938	1.00181	-2.39064E-02	1.30052	1.30052
1.02276	1.01918	1.00351	-2.77195E-02	1.35685	1.35685
1.02461	1.02092	1.00361	-2.42285E-02	1.30954	1.30954
1.01029	1.00910	1.00118	-1.14598E-02	1.11629	1.11629
1.00202	1.00209	.99994	7.13034E-08	1.00051	1.00051
1.01029	1.00910	1.00118	1.14598E-02	1.11629	1.11629
1.02461	1.02092	1.00361	2.42282E-02	1.30954	1.30954
1.02276	1.01918	1.00351	2.77192E-02	1.35685	1.35685
1.01121	1.00938	1.00181	2.39063E-02	1.30052	1.30052
.9999	.99982	1.00008	1.82863E-02	1.21593	1.21593

PRESSURE HISTORY

TIME	(PMAX-PMIN)/PAVE	PRESSURE
0.	7.00000000E-02	1.03500000E+00
1.25000000E-01	6.84127453E-02	1.03415044E+00
2.50000000E-01	6.58042695E-02	1.03254511E+00
3.75000000E-01	6.22402873E-02	1.03011374E+00
5.00000000E-01	5.78040205E-02	1.02691696E+00
6.25000000E-01	5.25823984E-02	1.02310077E+00
7.50000000E-01	4.66500734E-02	1.01885264E+00
8.75000000E-01	4.01719183E-02	1.01436681E+00
1.00000000E+00	3.40023009E-02	1.00981998E+00
1.12500000E+00	2.81601874E-02	1.00535859E+00
1.25000000E+00	2.24360046E-02	1.00109674E+00
1.37500000E+00	1.68818813E-02	9.97121105E-01
1.50000000E+00	1.26483208E-02	9.93498188E-01
1.62500000E+00	1.64339496E-02	9.90280301E-01
1.75000000E+00	2.06794340E-02	9.87508609E-01
1.87500000E+00	2.78899751E-02	9.85213746E-01
2.00000000E+00	3.51720547E-02	9.83415200E-01
2.12500000E+00	4.16831064E-02	9.82120201E-01
2.25000000E+00	4.70449502E-02	9.81321733E-01
2.37500000E+00	5.11432380E-02	9.80993931E-01
2.50000000E+00	5.38691671E-02	9.81081731E-01
2.62500000E+00	5.51069351E-02	9.81482687E-01
2.75000000E+00	5.47529763E-02	9.82034220E-01
2.87500000E+00	5.27811300E-02	9.82548858E-01
3.00000000E+00	4.93371384E-02	9.82896546E-01
3.12500000E+00	4.47818166E-02	9.83039310E-01
3.25000000E+00	3.99075126E-02	9.83002455E-01
3.37500000E+00	3.51953332E-02	9.82841843E-01
3.50000000E+00	3.32096803E-02	9.82626968E-01
3.62500000E+00	3.21640696E-02	9.82435132E-01
3.75000000E+00	3.19604051E-02	9.82351712E-01
3.87500000E+00	3.13739798E-02	9.82473879E-01
4.00000000E+00	3.10666197E-02	9.82916089E-01
4.12500000E+00	3.00071057E-02	9.83816511E-01
4.25000000E+00	2.88511429E-02	9.85341275E-01
4.37500000E+00	2.66425477E-02	9.87680468E-01
4.50000000E+00	2.71918872E-02	9.91029577E-01
4.62500000E+00	2.91685054E-02	9.95553469E-01
4.75000000E+00	3.14345064E-02	1.00133256E+00
4.87500000E+00	3.38942771E-02	1.00830198E+00

5.00000000E+00	3.70642595E-02	1.01620855E+00
5.12500000E+00	4.27206650E-02	1.02459868E+00
5.25000000E+00	5.04973813E-02	1.03284152E+00
5.37500000E+00	5.74181914E-02	1.04018661E+00
5.50000000E+00	6.26421240E-02	1.04581223E+00
5.62500000E+00	6.50813739E-02	1.04885293E+00
5.75000000E+00	6.41313354E-02	1.04848157E+00
5.87500000E+00	5.96399130E-02	1.04430886E+00
6.00000000E+00	5.22804296E-02	1.03693964E+00
6.12500000E+00	4.37251449E-02	1.02783787E+00
6.25000000E+00	3.76968520E-02	1.01866983E+00
6.37500000E+00	3.70676228E-02	1.01069445E+00
6.50000000E+00	3.68970586E-02	1.00446574E+00
6.62500000E+00	3.80375376E-02	9.99880287E-01
6.75000000E+00	3.80826928E-02	9.96467639E-01
6.87500000E+00	3.77723947E-02	9.93752919E-01
7.00000000E+00	3.82983335E-02	9.91488652E-01
7.12500000E+00	3.75968586E-02	9.89645723E-01
7.25000000E+00	3.70679371E-02	9.88246806E-01
7.37500000E+00	3.52538588E-02	9.87212181E-01
7.50000000E+00	3.71695373E-02	9.86345956E-01
7.62500000E+00	3.88564336E-02	9.85438603E-01
7.75000000E+00	4.07566528E-02	9.84372063E-01
7.87500000E+00	4.32956793E-02	9.83182441E-01
8.00000000E+00	4.57496888E-02	9.82057931E-01
8.12500000E+00	4.96496422E-02	9.81226490E-01
8.25000000E+00	5.80937389E-02	9.80863170E-01
8.37500000E+00	6.70222664E-02	9.81037498E-01
8.50000000E+00	7.47608032E-02	9.81665318E-01
8.62500000E+00	7.91030738E-02	9.82535216E-01
8.75000000E+00	7.86678549E-02	9.83292291E-01
8.87500000E+00	7.28519190E-02	9.83587777E-01
9.00000000E+00	6.25577141E-02	9.83394489E-01
9.12500000E+00	5.02982030E-02	9.82899960E-01
9.25000000E+00	4.32966152E-02	9.82306890E-01
9.37500000E+00	4.37314727E-02	9.81753726E-01
9.50000000E+00	4.37329676E-02	9.81302052E-01

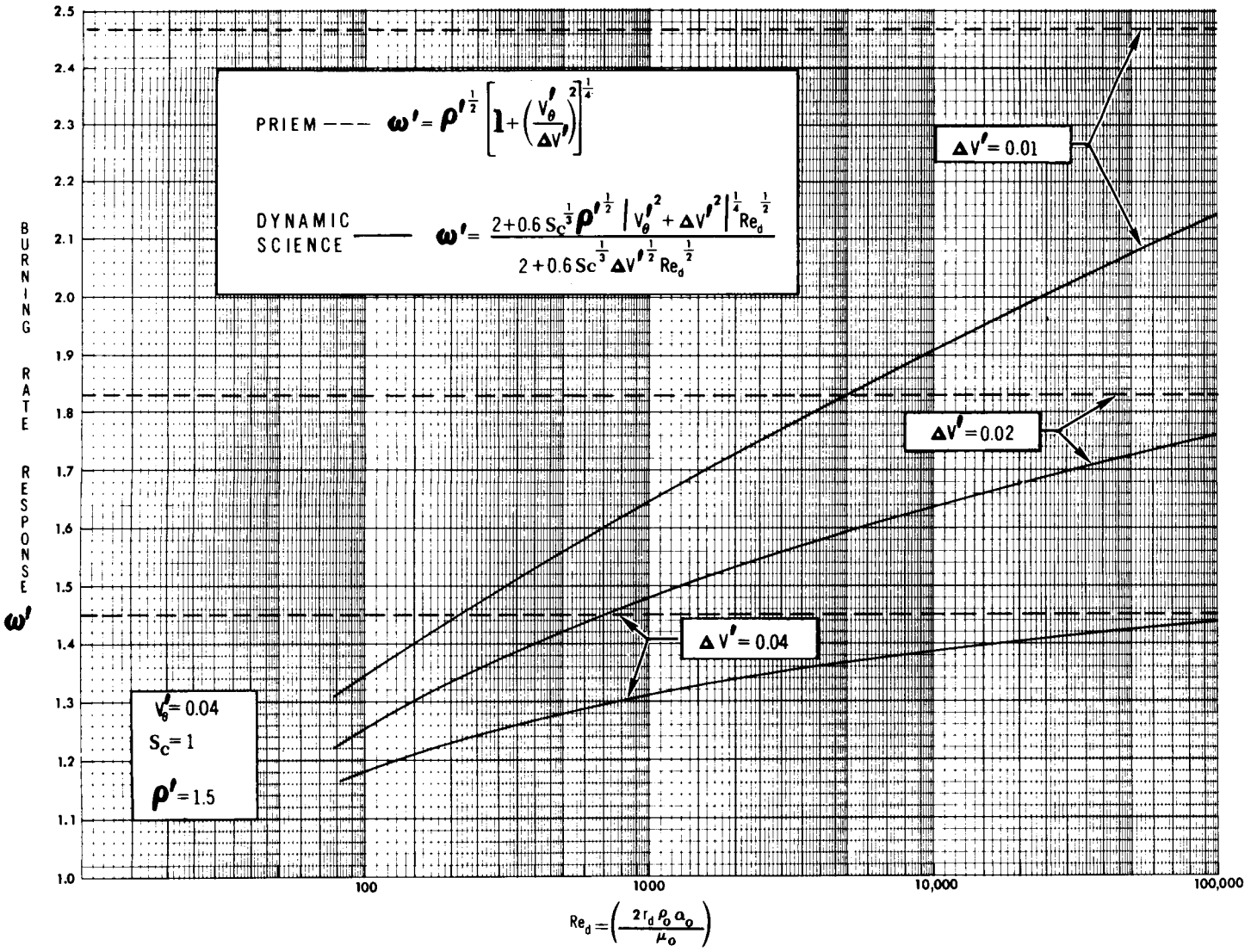

FIGURE (1) BURNING RATE RESPONSE DEPENDENCE ON Re_d

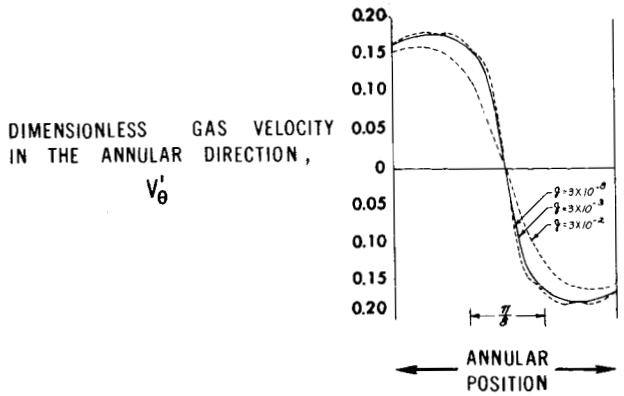

FIGURE 2a EFFECT OF THE VISCOUS DISSIPATION PARAMETER, ϑ , ON THE STEEPNESS OF THE DIMENSIONLESS GAS VELOCITY PROFILE.

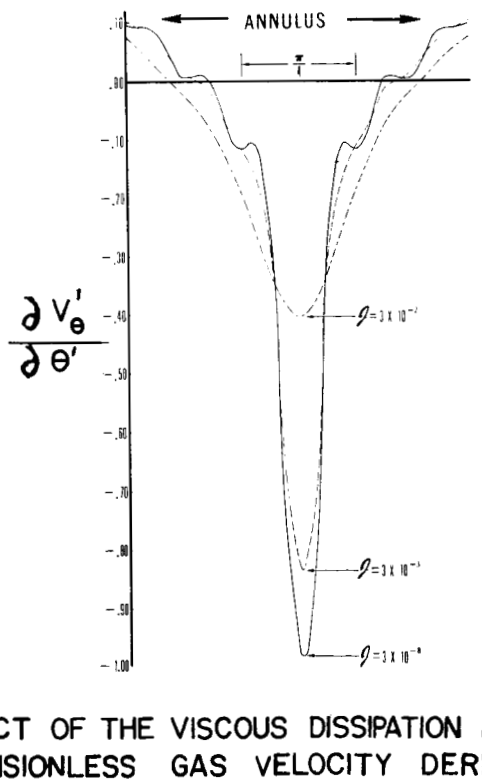

FIGURE 2b. EFFECT OF THE VISCOUS DISSIPATION PARAMETER, ϑ , ON THE DIMENSIONLESS GAS VELOCITY DERIVATIVE PROFILE.

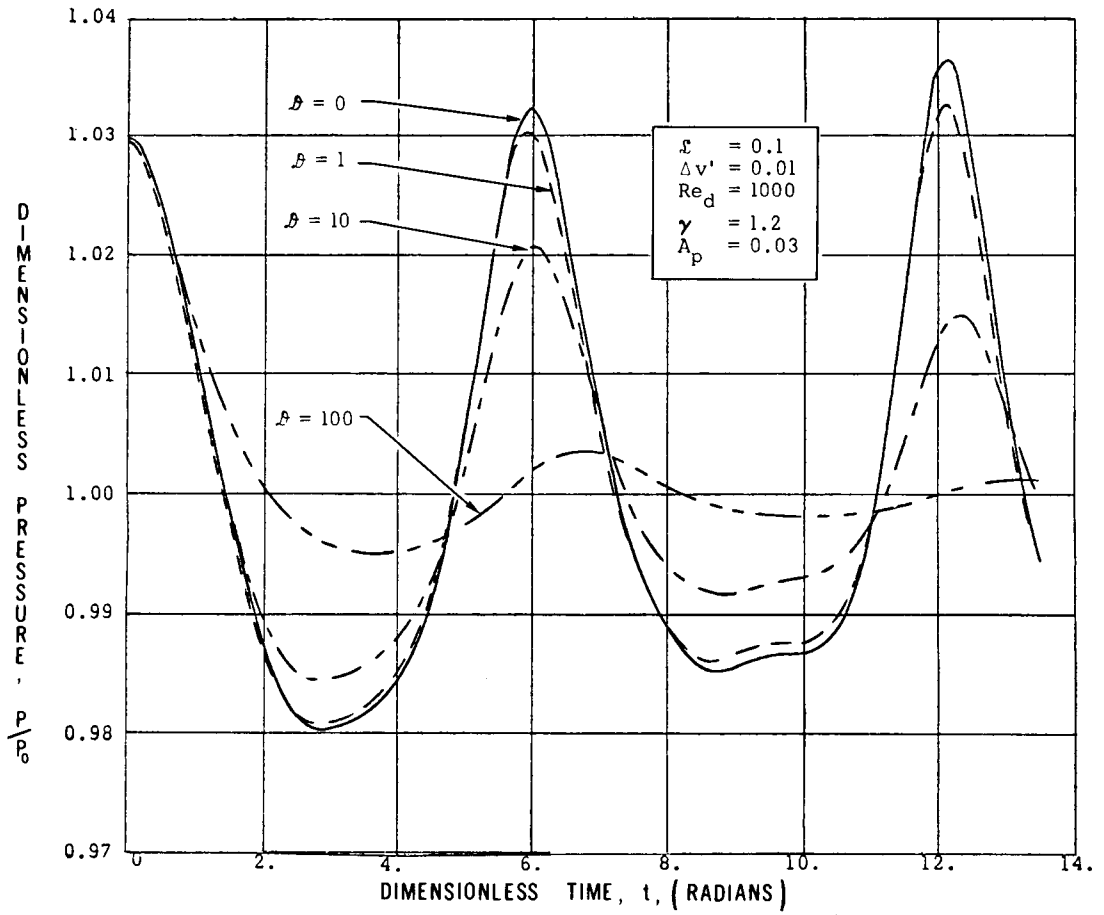

FIGURE 3 EFFECT OF DRAG PARAMETER ON PRESSURE HISTORY AT MAXIMUM PRESSURE NODE

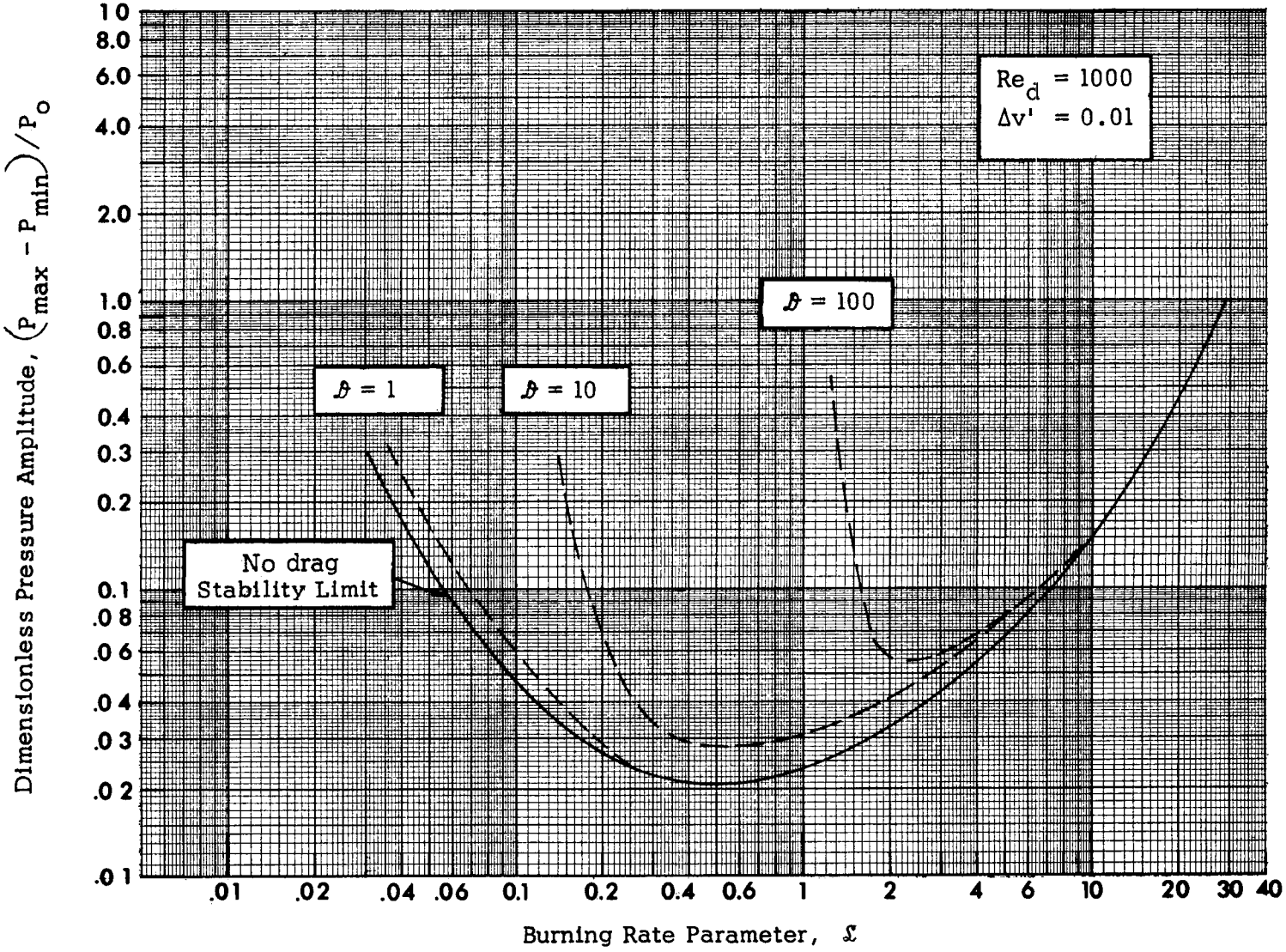

FIGURE 4 EFFECT OF DRAG PARAMETER ON STABILITY LIMITS

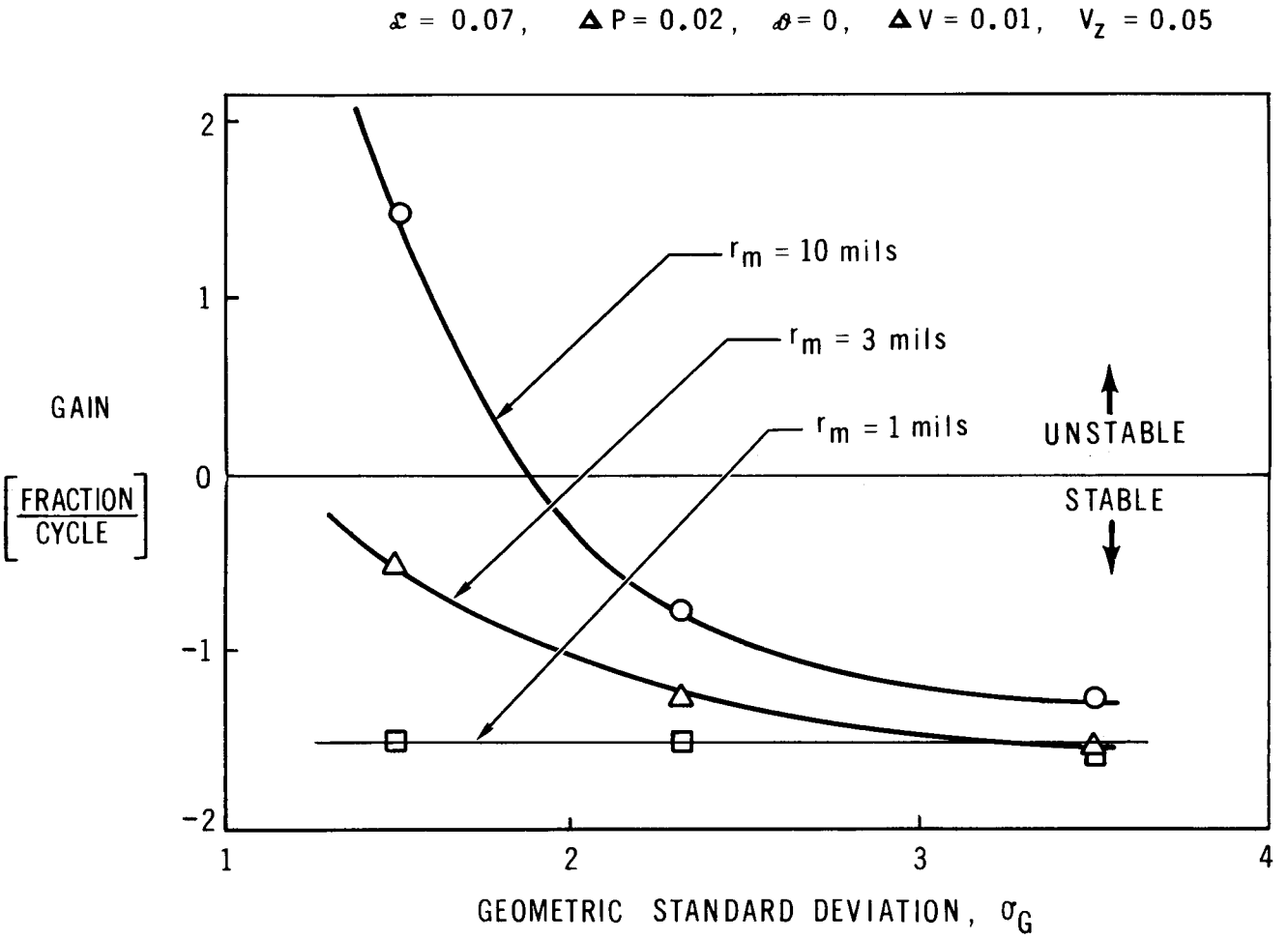

FIGURE 5. EFFECT OF MASS MEAN DROP RADIUS AND GEOMETRIC STANDARD DEVIATIONS ON STABILITY

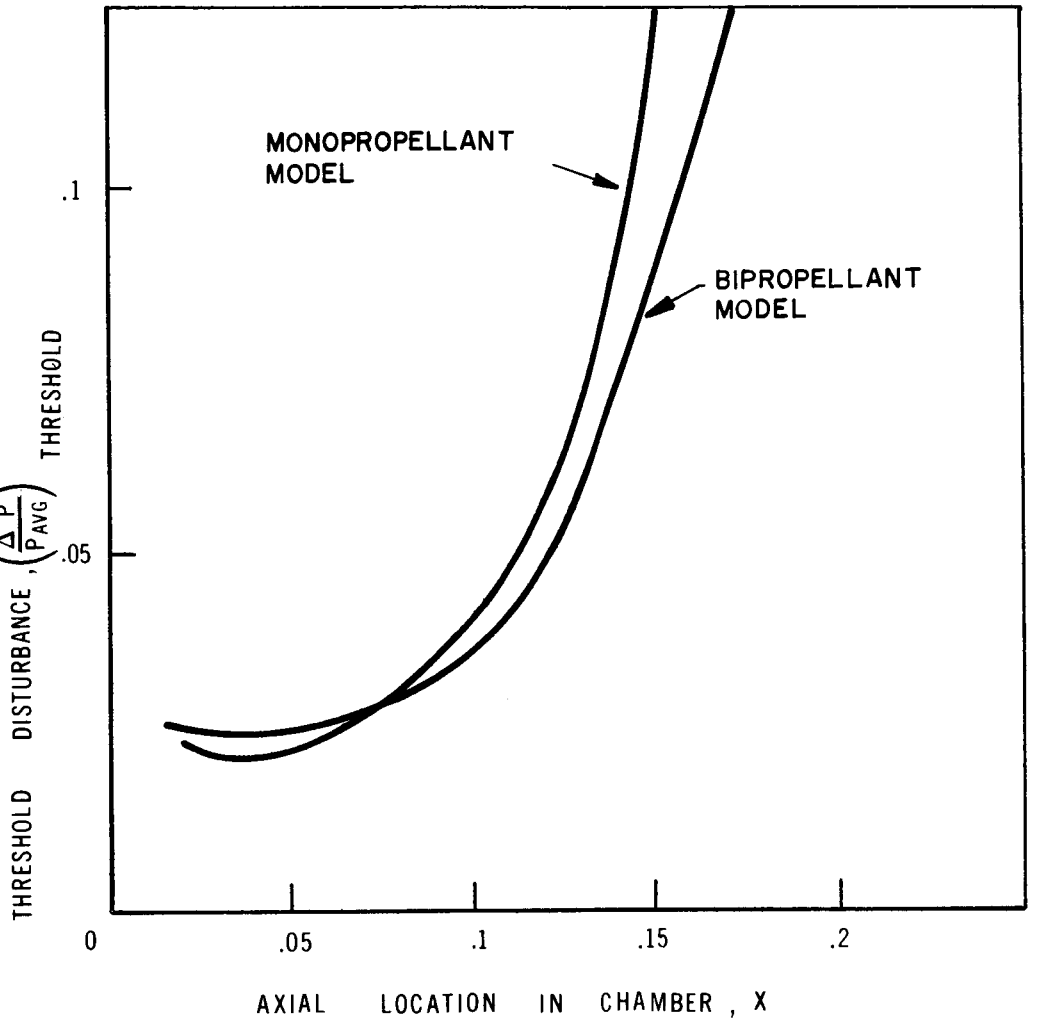

FIG. 6. STABILITY MAP : MONOPROPELLANT VS. BIPROPELLANT MODEL COMPARISON

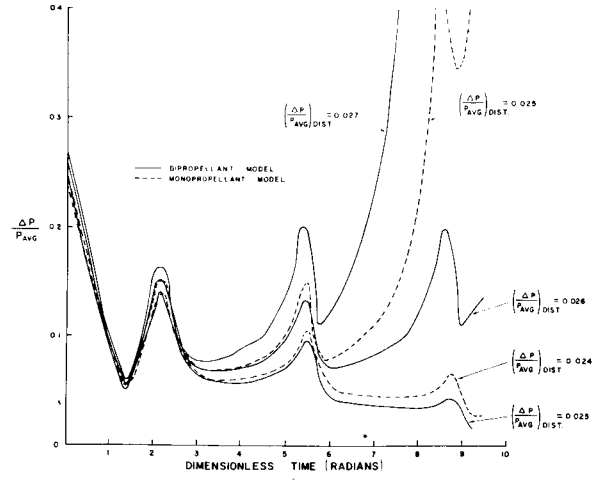

a) Axial Position of Annulus, x, = 0.02 in.

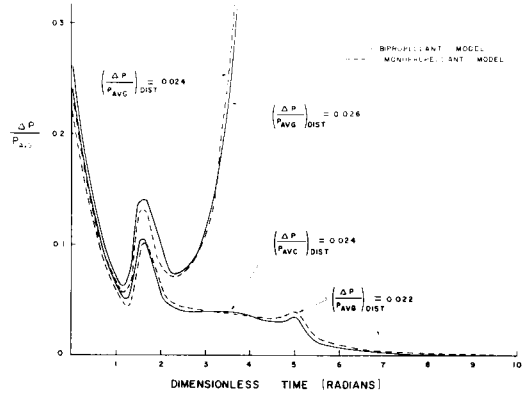

b) Axial Position of Annulus, x, = 0.05 in.

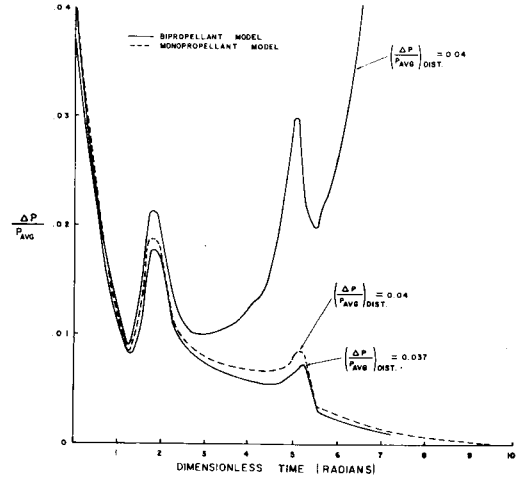

c) Axial Position of Annulus, x, = 0.10 in.

FIGURE 7. TIME RESPONSE OF SYSTEM TO VARIOUS INITIAL DISTURBANCES CLOSE TO THE THRESHOLD DISTURBANCE LEVEL.

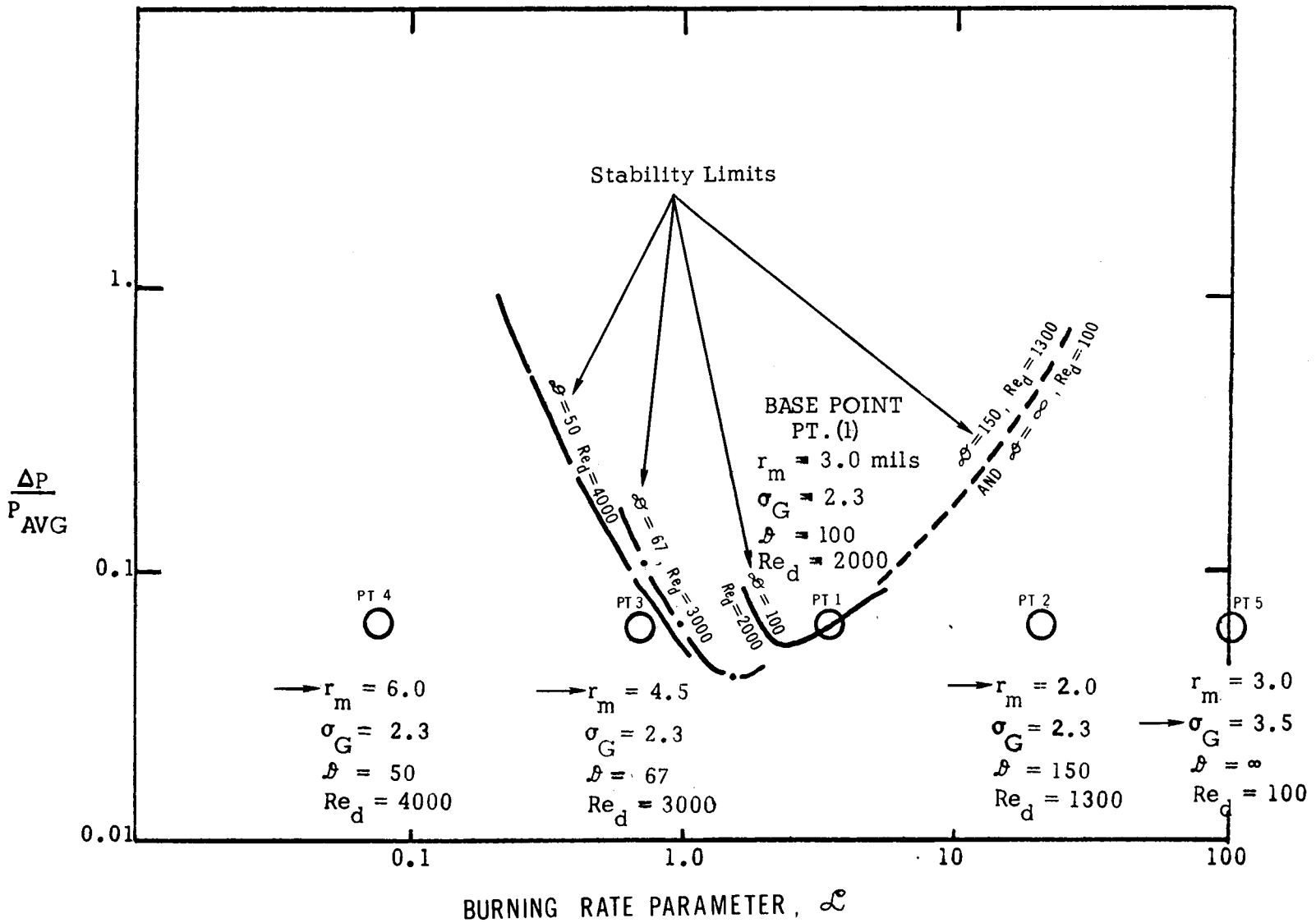

FIGURE 8. EFFECT OF DROP RADIUS AND DISTRIBUTION ON STABILITY
$Re_d = Re_d(r)$, $\mathcal{B} = \mathcal{B}(r)$, $\mathcal{L} = \mathcal{L}(r)$